

**INVESTIGATION INTO THE DEPHOSPHORIZATION OF
FERROMANGANESE ALLOYS FOR PRODUCTION OF ADVANCED
HIGH STRENGTH STEELS**

By

Mamaotseng Patricia Maphutha

Supervisor: Prof. Chris Pistorius

Co-supervisor: Dr. Joalet Steenkamp

A Dissertation submitted in partial fulfilment of the requirements for the degree
Masters of Engineering in the Department of Materials Science and Metallurgical Engineering
Faculty of Engineering, Built Environment and Information Technology
University of Pretoria, Pretoria.

October 2020

ACKNOWLEDGEMENT

I am very grateful to the people who have supported me throughout this research project:

- My supervisors, Prof Chris Pistorius and Dr Joalet Steenkamp for their guidance, patience and support.
- My family and friends for their endless encouragement and support.
- Mintek for the opportunity and funding.
- My colleagues for their support.
- Lastly, the Almighty God for giving me the strength to persevere.

ABSTRACT

The focus of the current study was to investigate dephosphorization of ferromanganese to produce a low P containing alloy that could effectively be used for the production of AHSS. The study involved conducting laboratory scale testwork to investigate dephosphorization of FeMn (HCFeMn and MCFeMn) alloys by CaO-based slag systems. Addition of Na₂O, BaO, and CaF₂ to MnO-CaO-SiO₂ slag was investigated to study the influence on dephosphorization. The effect of MnO-BaO-BaF₂ slag system without CaO was also investigated in a preliminary way. The testwork was carried out in a 25 kVA induction furnace at temperatures of 1350°C, 1400°C, and 1450°C at different retention times of 5 minutes, 30 minutes and 60 minutes. The analytical results of the product samples were used to evaluate the P-partition ratio.

In general, analysing the low P contents of the slags and alloys proved to be a challenge and at the lowest concentrations the uncertainty was large. The analytical results of the slags generally reported higher MnO-contents than was anticipated. This resulted in dilution of the other major slag components, i.e. SiO₂ and CaO. Low P₂O₅ contents were found in the slags, suggesting that the removal of P from the alloys was minimal. The alloy results reported C-pickup after the tests due to the dissolution of the graphite from the crucible. Loss of Mn from the alloys was also observed. The P-content of the alloys were generally higher than in the feed alloy.

The results generally showed the L_p remained small at <1 which is an indication that dephosphorization had not been achieved. The baseline slag comprising of 40%CaO-40%SiO₂-20%MnO reported relatively higher L_p values. Addition of Na₂O and CaF₂ did not show any added benefit. Substituting half of CaO by BaO, resulted in similar L_p values to those of the baseline slag under a few conditions, namely 1350°C and 1450°C at 30 minutes. The baseline slag was however not outperformed by the BaO-bearing slag under any of the other conditions. Increasing the temperature generally resulted in lower L_p values. This may be attributed to the exothermic nature of the phosphorus removal reaction which should be favourable at lower temperatures. Increasing the basicity (%CaO/%SiO₂ ratio) of the baseline slag showed an initial increase in L_p value for basicities of 0.7 to 0.9, thereafter a slight reduction in the L_p value was obtained. The latter results were not expected as higher basicity is anticipated to improve the P capacity of the slag. Increasing the basicity resulted in increased slag liquidus temperature of about 1500°C which negatively affected dephosphorization.

In summary, based on the L_p obtained, the conditions investigated with the CaO-based slags appeared to have been unfavourable for dephosphorization of FeMn alloys, as most of this impurity element remained in the alloy. The BaO-BaF₂-MnO slag showed potential to dephosphorise HCFeMn alloy, however the slag posed numerous challenges and the slag should be investigated further.

TABLE OF CONTENTS

ACKNOWLEDGEMENT	ii
ABSTRACT.....	i
TABLE OF CONTENTS.....	iii
LIST OF FIGURES	vi
LIST OF TABLES.....	vii
1 INTRODUCTION	1
1.1 Advanced High Strength Steels	1
1.2 Phosphorus in Steelmaking.....	2
1.3 Phosphorus in Ferromanganese Production.....	3
2 LITERATURE REVIEW	4
2.1 Dephosphorization Reactions	4
2.1.1 <i>Dephosphorization under oxidizing conditions using synthetic slag</i>	4
2.1.2 <i>Dephosphorization under reducing conditions using synthetic slags</i>	4
2.1.3 <i>Dephosphorization using hydrogen gas</i>	5
2.2 Dephosphorization parameters.....	6
2.2.1 <i>Phosphate Capacity of Slag</i>	6
2.2.2 <i>Phosphorus Partition Coefficient</i>	7
2.3 Dephosphorization of Fe.....	7
2.4 Dephosphorization of FeMn	9
2.5 Research aim, questions, and objectives	16
3 METHODOLOGY	17
3.1 Source and Prepare Feed Materials.....	17
3.1.1 <i>Industrial alloys</i>	17
3.1.2 <i>Synthetic slags</i>	18
3.2 Design Various Slag Systems to Dephosphorise FeMn Alloy.....	21
3.2.1 <i>Creating baseline CaO-based slag (Slag A)</i>	21
3.2.2 <i>Changing MnO (Slag B and Slag C)</i>	22
3.2.3 <i>Adding Na₂O-CaF₂ (Slag D, Slag E, and Slag F)</i>	22
3.2.4 <i>Adding BaO (Slag H)</i>	23
3.2.5 <i>Adding BaO-BaF₂ (Slag I)</i>	23
3.2.6 <i>Changing basicity of baseline CaO-based slag</i>	24
3.2.7 <i>Changing alloy composition</i>	24
3.3 Characterization of feed materials	24

3.4	Thermodynamic FactSage calculations.	24
3.4.1	<i>Effect of temperature on the percentage liquid alloy phase in the alloy systems</i>	26
3.4.2	<i>Effect of temperature on the percentage liquid slag phase in the different slag systems</i> 26	
3.4.3	<i>Phosphorus distribution ratio calculations</i>	26
3.5	Experimental Testwork.....	27
3.5.1	<i>Crucible selection</i>	27
3.5.2	<i>Drop-quench furnace-based experiments</i>	27
3.5.3	<i>Induction furnace-based experiments</i>	28
3.6	Characterization of product samples.....	31
3.6.1	<i>Macroscopic investigation</i>	31
3.6.2	<i>Bulk chemical compositions</i>	32
3.6.3	<i>Slag/alloy proportioning utilising X-ray tomography</i>	32
3.6.4	<i>Electron Microprobe analyses analysis</i>	33
3.6.5	<i>Elemental mass balance calculations</i>	34
3.6.6	<i>Phosphorous partition coefficient</i>	36
4	RESULTS	37
4.1	Characterised Feed Materials.....	37
4.2	Thermodynamic calculations	39
4.2.1	<i>Effect of temperature on the percentage liquid alloy phase in the alloy systems</i>	39
4.2.2	<i>Effect of temperature on the percentage liquid slag phase in the different slag systems</i> 39	
4.2.3	<i>Phosphorus partition coefficient calculations</i>	41
4.3	Characterization of product samples.....	43
4.3.1	<i>Macroscopic investigation</i>	43
4.3.2	<i>Bulk chemical compositions</i>	44
4.3.3	<i>Slag/alloy proportioning utilising X-ray tomography</i>	44
4.3.4	<i>Electron Microprobe analyses</i>	48
4.3.5	<i>Elemental mass balance calculations</i>	52
4.3.6	<i>Phosphorous partition coefficient</i>	61
4.3.7	<i>Degree of dephosphorization</i>	63
5	DISCUSSION	64
5.1	Phosphorus partition coefficient	65
5.1.1	<i>Effect of changing MnO content of base-line slag</i>	67
5.1.2	<i>Effect of adding Na₂O and CaF₂</i>	68
5.1.3	<i>Effect of adding BaO</i>	69

5.1.4	<i>Effect of changing basicity</i>	69
5.1.5	<i>Effect of changing temperature</i>	70
5.1.6	<i>Effect of changing initial alloy composition</i>	70
6	CONCLUSIONS AND RECOMMENDATIONS	73
6.1	Analytical results	73
6.2	P distribution ratio.....	73
6.3	Degree of dephosphorization	74
	REFERENCES	76
	APPENDIX A.....	82
	APPENDIX B	87
	APPENDIX C	96

LIST OF FIGURES

Figure 1: The effect of C on P slag/metal partition coefficient. Reproduced from (Bhardwaj, 2008).	9
Figure 2: Predominance area diagram of Ba-O-P and MnO systems at 1573 K (Chaudhary, et al., 2007).	12
Figure 3: Degree of dephosphorization ϵ_P % (line 1, 2) of HCFeMn and L_P (3-5) of BaO (1, 3, 5) and CaO (2, 4) slag contents. Reproduced from (Hara, et al., 1990).	14
Figure 4: Steps followed to prepare the HCFeMn alloy	18
Figure 5: Steps followed to prepare the synthetic	21
Figure 6: Liquidus isotherms for the system CaO – SiO ₂ – MnO showing the desired slag composition achievable with the addition of SiO ₂ .	23
Figure 7: Typical dimensions of the graphite crucibles used.	27
Figure 8: Schematic diagram of the induction furnace.	29
Figure 9: Schematic view of the 25 kW induction furnace setup.	30
Figure 10: Mass fraction of liquid as a function of temperature for HCFeMn and MCFeMn alloys.	39
Figure 11: Percentage liquid in the different slag compositions at various temperatures.	41
Figure 12: Predicted equilibrium P distribution coefficient for the different slags when reacted with the HCFeMn alloy. The dependent scale is log scale.	42
Figure 13: Predicted equilibrium P distribution coefficient for the different slags when reacted with the MCFeMn alloy. The dependent scale is log scale.	43
Figure 14: X-Ray Tomography scans with the summary of the volumes measured at the different segments.	47
Figure 15: Electron Backscattered images and analysis of A) alloy nugget at the bottom of the crucible B) alloy at the bottom of the crucible C) alloy at the alloy-slag interface for slag H-MCFeMn 1400°C, 30 minutes sample.	50
Figure 16: Electron Backscattered images and analysis of A) Slag at the alloy-slag interface, B) & C) low dense porous slag at the upper part of the crucible for slag H-MCFeMn 1400°C, 30 minutes sample.	51
Figure 17: C content of FeMn alloy as a function of temperatures.	52
Figure 18: Box plot of out/in apparent ratio for Mn, P and Si.	60
Figure 19: The average C accountabilities. Error bars indicate the 95% confidence levels on the mean.	60
Figure 20: Predicted oxygen partial of different slag/MCFeMn systems.	65
Figure 21: L_p values obtained at different temperatures for MCFeMn alloy; 30 minutes reaction time.	66
Figure 22: L_p values obtained at different temperatures for MCFeMn alloy; 60 minutes reaction time.	66
Figure 23: Effect of starting MnO content in the starting slag on L_p at 1450°C and 30 minutes retention time.	67
Figure 24: L_p versus the final MnO in slags at 1450°C and 30 minutes retention time	68
Figure 25: Comparison of phosphorus distribution between MCFeMn and HCFeMn and slag, found at 1350°C for 60 minutes reaction time	71
Figure 26: Comparison of phosphorus distribution between MCFeMn and HCFeMn and slag, for reaction at 1400°C for 30 minutes.	72

LIST OF TABLES

Table 1: Typical compositions of FeMn alloys (Olsen, et al., 2007) (mass %).....	2
Table 2: The purity levels of the respective powder used for producing HCFeMn master alloy	17
Table 3: Chemical compositions of the slag reagents used (mass %).....	19
Table 4: Different consumables used as well as their respective suppliers and prices	20
Table 5: Target chemical compositions of different slag systems.	21
Table 6: Typical compositions of HCFeMn and MCFeMn alloys (mass %) utilised in thermodynamic calculations (Olsen, et al., 2007).....	26
Table 7: Completed experimental tests	31
Table 8: Bulk chemical compositions of MCFeMn alloy	32
Table 9: EMPA elemental detection limit (% by mass).....	34
Table 10: Average bulk chemical composition of the industry MCFeMn alloy and HCFeMn master alloys used in the study (mass %)	37
Table 11: Bulk chemical compositions of the master slags (mass %)	38
Table 12: A summary of the calculated liquidus temperatures of the different slags	40
Table 13: A summary of the volumes obtained from the X-Ray tomography analysis, with the estimated masses assuming the phases to be dense	46
Table 14: The comparison between the average EMPA alloy chemistry and the bulk chemical composition of the alloy for slag H-MCFeMn 1400°C, 30 minutes sample.....	49
Table 15: The comparison between the average EMPA alloy chemistry and the bulk chemical composition of the slag for slag H-MCFeMn 1400°C, 30 minutes sample.	49
Table 16: Corrected bulk chemical composition of the alloys produced at different temperatures and retention times from MCFeMn dephosphorization reactions	54
Table 17: Corrected bulk chemical composition of the slags produced at different temperatures and retention times MCFeMn dephosphorization reactions	56
Table 18: Corrected bulk chemical composition of the alloys produced at different temperatures and retention times from HCFeMn dephosphorization reactions	57
Table 19: Corrected bulk chemical composition of the slags produced at different temperatures and retention times from HCFeMn dephosphorization reactions	58
Table 20: A summary of the L_p values obtained from the experiments	62
Table 21: Degree of dephosphorization obtained with MnO-BaO-BaF ₂ slag at 1400°C.	63
Table 22: Effect of %CaO/%SiO ₂ ratio on L_p at 1450°C and 30 minutes retention time.	70

1 INTRODUCTION

In the Kalahari Manganese Field (KMF), South Africa holds the largest land-based Mn resource constituting about 74% of the world's resource (USGS, 2020). South African reserves constitute about 32% of the world reserves (USGS, 2020). The bulk of the reserves currently mined in South Africa is exported for beneficiation overseas (Steenkamp, et al., June 2018). The National Development Plan 2030 is a plan for a future in which no person lives in poverty, where no one goes hungry, where there is work for all (National Planning Commission, 2030). Local beneficiation of South Africa's mineral riches is considered a vehicle to achieve this goal, especially where suitable capacity already exists, or where beneficiation is likely to lead to downstream manufacturing. Significant capacity exists for local beneficiation of the ore through the production of manganese ferroalloys and the production of niche products will be to the advantage of this sector (Steenkamp, et al., June 2018).

1.1 Advanced High Strength Steels

In the automotive industry the drive towards lightweight, high strength steel grades to mitigate the issues around the escalated energy crisis and environmental problems, is high. It was discovered that 10% weight reduction would lead to reduction in fuel consumption by between 3% and 7% (Demeri, 2013). This has led to the development of advanced high strength steels (AHSS) (Baluch, et al., 2014).

AHSS steels are a group of special steel grades that offer excellent strength that allow the use of thinner gauges to reduce the weight of vehicles. The AHSS are classified into six categories, namely Hot-formed (HF), Dual Phase (DP), Ferritic-Bainitic (FB), Complex-Phase (CP) Martensitic (MS), Transformation-Induced Plasticity (TRIP) and Twinning-induced Plasticity (TWIP) (Demeri, 2013).

As the Mn content in AHSS can be up to 25%, these steels could potentially be a significant market for manganese ferroalloys (Kolbeinsen & Safarian, 2013). The challenge lies in the maximum allowable P content in the steel, which is less than 0.05% (Arcelomittal, 2017), and the role FeMn alloys play in the steelmaking process.

1.2 Phosphorus in Steelmaking

The presence of P in high strength steels reduces toughness and may cause disintegration of material during fabrication and service. The properties of steels are sensitive to the chemical composition and grain structure. Grain boundaries typically enhance material strength and toughness, but elements such as P weaken the bonding forces. Steels with low P requirements include those vulnerable to embrittlement. These types of steels include mostly high-strength steels and low-alloy steels containing elements such as manganese (Mn), silicon (Si), titanium (Ti), niobium (Nb), vanadium (V), and chromium (Cr) (Bhadeshia & Suh, 2015). P in steel can enhance the properties (e.g. strengthen, corrosion resistance) but may also have negative impacts on other properties (e.g. toughness). The P content of the steel will be restricted due to the negative properties (Assis, et al., 2015). It is reported that intergranular embrittlement can occur in steels with P concentrations of 0.008% to 0.025% ((Mukherjee & Chatterjee, 1996; Wetlaufer & Kaspar, 2000).

During steelmaking, Mn is added as ferromanganese (FeMn) or silico-manganese (SiMn) alloys to the molten steel during the primary and/or secondary steelmaking step (Steenkamp & du Preez, 2015). Table 1 summarises the specifications of FeMn alloys (Olsen E. et al., 2007).

Table 1: Typical compositions of FeMn alloys (Olsen, et al., 2007) (mass %).

Alloy	Grades	Mn	C, max	Si	P,max	S, max
HCFeMn	Grade A	78.0-82.0	7.5	1.2	0.35	0.05
	Grade B	76.0-78.0	7.5	1.2	0.35	0.05
	Grade C	74.0-76.0	7.5	1.2	0.35	0.05
MCFeMn	Grade A	80.0-85.0	1.5	1.5	0.3	0.02
	Grade B	80.0-85.0	1.5	1.0	0.3	0.02
	Grade C	80.0-85.0	1.5	0.7	0.3	0.02
	Grade D	80.0-85.0	1.5	0.35	0.3	0.02
LCFeMn	Grade A	85.0-90.0	*	2.0	0.2	0.02
	Grade B	80.0-85.0	0.75	5.0-7.00	0.3	0.02

*: As specified

FeMn alloys are known as one of the major contributors of P contamination to steel (Chaudhary, et al., 2007). The FeMn alloys, used in the production of the AHSS steel grades,

are required to contain P below 200 ppm which is an order of magnitude below those specified in Table 1 (Karbowniczek, et al., 2014; Byung-Don You et al., 1999; Chaudhary et al., 2001). The removal of P from the alloys is thus necessary especially in the case of AHSS (Wetlaufer & Kaspar, 2000).

1.3 Phosphorus in Ferromanganese Production

During the carbothermic reduction process applied in FeMn production, the P in the slag is reduced to the alloy. In many instances, P originates from the Mn ores. As P is intimately associated with Fe and Mn in the ores, it is difficult to remove by mineral processing routes (Chaudhary and Goel, 2007). The P content in the ore is one of the important factors in the selection of Mn ore. South African Mn ores are generally low in P. The P present in the alloy, originates mainly from the carbonaceous reductants used (Olsen, et al., 2007). About 70-80% of P present in the reductant is reduced and reports to the alloy. The acceptable P content in the reductants is typically <0.02% (Subramanian & Harman, 1983).

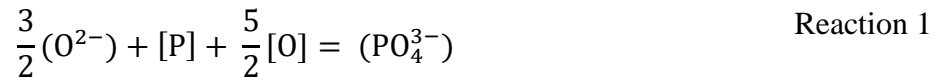
Even when carefully selecting ore and reductants, some P will report to the FeMn alloys. Dephosphorization of FeMn alloys under conditions similar to those used for dephosphorisation of steel, has not been favourable as substantial Mn losses were experienced. Significant amounts of Mn are oxidised to the slag as well as evaporates at high temperatures due to Mn's high vapour pressure (Chaudhary et al., 2007) (Chaudhary et al., 2001). New methods thus have to be developed to dephosphorise FeMn alloys.

2 LITERATURE REVIEW

2.1 Dephosphorization Reactions

2.1.1 *Dephosphorization under oxidizing conditions using synthetic slag*

Dephosphorization of molten alloy under oxidizing conditions can be described by the following ionic reaction (Chaudhary et al., 2007; Nasaralla, et al., 1991; Simeonov & Sano, 1985):



Where:

[X]: species dissolved in the alloy

(Y): species dissolved in the slag

Based on Reaction 1, it can be deduced that the removal of P from the alloy under these conditions can be aided by the following (Chaudhary, et al., 2007):

- Higher oxygen activity in the alloy
- High activity of basic oxide ($a_{\text{O}^{2-}}$) in the slag
- Low activity of the phosphate ($a_{\text{PO}_4^{3-}}$) in the slag

Highly basic slag contains more free oxygen ions (O^{2-}) and less bridging and terminal oxygen in the slag. Slag basicity can therefore be defined by the activity of oxygen ion in slags (Liu, et al., 1998). As indicated by Reaction 1, high concentrations of O^{2-} and therefore basic slags, are efficient for dephosphorization (Wagner, 1975).

2.1.2 *Dephosphorization under reducing conditions using synthetic slags*

Dephosphorization of ferromanganese can also be carried out with basic slag under reducing conditions to form a phosphide phase. The reaction is shown below (Chaudary & Goel, 2007):



Based on Reaction 2, it can be deduced that the removal of P from the alloy under these conditions can be aided by high activity of basic oxide ($a_{O^{2-}}$) in the slag. Relatively lower oxygen partial pressure is required for reducing conditions, CO gas is typically used. Metallics such as Ca, typically added as CaSi or CaC₂, would dissolve into the metal and react with P to form a phosphide phase. The reducing reaction occurs through the reaction between CaO in the flux and Si in the melt (for SiMn alloy), and also through the transfer of Ca from the CaSi introduced into the melt. The reactions below show examples of dephosphorization under reducing condition (Karbowniczek, et al., 2014):



The reaction product from Reaction 2 is phosphide which in the presence of atmospheric moisture produces toxic phosphene. Dephosphorization of FeMn alloy under reducing conditions is therefore not desirable (Chaudary & Goel, 2007).

2.1.3 Dephosphorization using hydrogen gas

P removal in vapour form as phosphine gas by the reaction of P with hydrogen dissolved in metal can occur considering the following reaction (Chaudary & Goel, 2007):



The reaction product phosphine would not be environmentally tolerable when released into the atmosphere (Chaudary & Goel, 2007).

Based on Reaction 6, it can be deduced that the removal of P from the alloy under these conditions can be aided by higher hydrogen activity in the alloy.

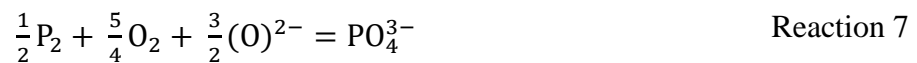
Dephosphorization under gaseous conditions may also result in loss of Mn which has a higher vapour pressure than P. Application of the technique is deemed undesirable for dephosphorization of FeMn alloys (Chaudary & Goel, 2007).

From the abovementioned reaction mechanisms, dephosphorization of liquid FeMn alloy by basic slags for selective removal of P over Mn under oxidizing conditions is deemed the most viable (Chaudary & Goel, 2007). Several alternative process routes have been investigated for dephosphorization of FeMn alloys using various basic flux systems under oxidizing conditions (You et al., 1999; Chaudhary et al., 2007; Chaudhary & Goel, 2007).

2.2 Dephosphorization parameters

2.2.1 Phosphate Capacity of Slag

The capability of a slag to contain phosphate ions (PO_4^{3-}) can be defined by the phosphate capacity of the slag ($C_{\text{PO}_4^{3-}}$) (Muraki, et al., 1966; Wagner, 1975). Equation 1 defines the $C_{\text{PO}_4^{3-}}$ for Reaction 7:



$$C_{\text{PO}_4^{3-}} = \frac{w\%_{\text{PO}_4^{3-}}}{P_{\text{P}_2}^{1/2} \cdot P_{\text{O}_2}^{5/4}} = K_1 \frac{(a_{\text{O}^{2-}})^{3/2}}{f_{\text{PO}_4^{3-}}} \quad \text{Equation 1}$$

Where:

P_{P_2} : Partial pressure of P_2 in equilibrium with [P] in the alloy (compare Reaction 1)

P_{O_2} : Partial pressure of O_2 in equilibrium with [O] in the alloy (compare Reaction 1)

From Equation 1, $C_{\text{PO}_4^{3-}}$ increases with increasing slag basicity ($a_{\text{O}^{2-}}$), and is a function of slag chemistry as well as temperature (Muraki, et al., 1966).

The electronegativity of the cation (M^+) is used to define the basicity of an oxide; as the electronegativity decreases, the attraction between the cation and the oxide also decreases (Simeonov & Sano, 1985). Pauling (Pauling, 1960) gave 0.9, 0.9 and 1.5 as the electronegativity of Na^+ , Ba^+ , Mn^{2+} respectively. The electronegativities of Na and Ba are less than that of Ca (1.3), therefore it is expected that the phosphate capacity of slags containing the basic oxides (Na_2O and BaO) will be higher resulting in better dephosphorization (Simeonov & Sano, 1985).

The main drawback with the more basic compounds is that they are considered too expensive for commercial use, are aggressive towards refractory linings, and can be harmful to the environment. Therefore, even though studies illustrated that BaO-bearing slags have phosphate capacities several orders of magnitude higher than CaO-bearing slags, it is CaO-bearing slags that are used in steel refining (Bhardwaj, 2008) (Satyendra, 2013).

2.2.2 Phosphorus Partition Coefficient

The effectiveness of dephosphorization is typically expressed as the P-distribution ratio (L_p) between slag and metal phases and the degree of dephosphorization which is defined as the ratio of P concentrations removed from the metal to the initial P content in the metal. L_p and Degree of dephosphorization are defined by the following expressions (Karbowniczek, et al., 2014):

$$L_p = \frac{(\%P)_{slag}}{[\%P]_{alloy}} \quad \text{Equation 2}$$

$$\%Dephos = \frac{[\%P]_{initial} - [\%P]_{final}}{[\%P]_{initial}} \times 100 \quad \text{Equation 3}$$

2.3 Dephosphorization of Fe

Nassaralla and Fruehan (Nassaralla & Fruehan, 1992) investigated the effect of CaF₂ addition to CaO-Al₂O₃ binary system and addition of highly basic oxides BaO, Li₂O and Na₂O to the CaO-Al₂O₃-CaF₂ ternary system on the dephosphorization of C-saturated iron alloy. The experiments were carried out by equilibrating 2 g of Fe-C_{sat}-P with 2 g of flux in a graphite crucible at 1400°C, 1425°C and 1450°C under 1 atm of CO. The results showed that addition of CaF₂ to the binary system increased the L_p by a factor of 2.5. Additions of BaO to CaO-Al₂O₃-CaF₂ increased the L_p by a factor of 4.6. Li₂O addition resulted in an increase of the L_p by a factor of 14. Addition of Na₂O resulted in an increase of L_p by 15. The efficiency of the addition of the basic oxides to dephosphorise the C-saturated iron increased in the following order BaO < Li₂O < Na₂O.

Kor (Kor, 1977) studied the effect of addition of fluorspar (CaF₂) and other substitutes such as borate, Mn ore and ilmenite additions, to basic slags on P and S equilibrium distribution ratio

at 1500°C. A Fe-P master alloy was reacted with the slag in a vertical Mo wire-wound furnace using about 175 g of alloy and 35 g of slag. The results obtained illustrated that increasing the CaF₂ concentration in the slag from 1.5% to 15% reduced the P content in the alloy by a factor of three. The CaF₂ lowers the activity of P₂O₅ in the slag as suggested by formation of fluorapatite (CaF₂·9CaO·P₂O₅) in the solidified slag.

Van Niekerk and Dippenaar (Van Niekerk & Dippenaar, 1998) also studied the dephosphorization of carbon-saturated iron by lime-based slags containing Na₂O and CaF₂. The P-containing lime-based slags from CaF₂-CaO-Na₂O-SiO₂ systems and carbon saturated Fe were equilibrated in carbon crucibles at 1350°C under CO atmosphere (1 atm) in a silicon-carbide, resistance heated tube furnace. P was initially added in the metal as FeP and later in the slag as P₂O₅ for the equilibration tests to validate that equilibrium was reached during the testwork. The slag system investigated included the Na₂O-SiO₂, Na₂O-SiO₂-CaO and Na₂O-SiO₂-CaO-CaF₂ systems. The slag to alloy ratio was maintained at 0.5. The results confirmed that the addition of Na₂O increases the phosphate capacity of silicate and lime-based slags considerably. It was observed that CaF₂ increases the activity coefficient of P₂O₅ and thus decreases the phosphate capacity of lime-based slag systems that contain Na₂O. CaO-CaF₂-SiO₂-Na₂O systems have a low melting temperature, a high phosphate capacity and are suitable for dephosphorization of C-saturated iron at low temperatures, but the addition of CaF₂ to the system should be limited.

Simeonov and Sano (Simeonov & Sano, 1985) carried out investigation to study the equilibrium P distribution ratio between carbon-saturated iron with a high Mn content of 4.6%-5.5% and 0.025%-0.06% P. The lime-based slags contained MnO, Na₂O, BaO and the tests were conducted under reducing conditions using CO gas. The slag systems investigated included MnO-SiO₂-CaO-CaF₂, MnO-SiO₂-CaO-CaF₂-BaO and MnO-SiO₂-CaO-Na₂O. Two grams of slag comprising of 43%-60% CaO, 8%-13% SiO₂, 35%-40% CaF₂, 2%-6% MnO, 0.1%-2.6% Na₂O and 1%-8.3% BaO were equilibrated with two grams of the C-saturated iron for 24 hr. The results illustrated that the addition of Na₂O and BaO increased the phosphate capacity of MnO-SiO₂-CaO-CaF₂ slag system with Na₂O being more beneficial. The difference in the phosphate capacity among the slag systems was explained by the difference in the basicity of the respective oxides estimated by the electronegativity of the cations. Furthermore, the results obtained showed that the equilibrium P distribution decreases with increasing MnO content in the slag. Increasing the basicity resulted in increased P equilibrium distribution, increasing

CaF₂ addition to replace the CaO in the slag decreased the P distribution coefficient due to the negative influence of CaF₂ on the slag basicity, additions of BaO and Na₂O have a favourable effect on P removal and the dephosphorization reaction is exothermic as higher values of P distribution ratio were obtained at lower temperatures.

2.4 Dephosphorization of FeMn

FeMn alloys have lower melting points than steel and dephosphorization thereof can be carried at lower temperatures. The presence of C may enhance dephosphorization of FeMn and limits oxidation of Mn. This is because an increase in C alloy content, increases the P activity coefficient, while decreasing the Mn activity coefficient and does not decrease the oxygen potential if it is controlled by the Mn/MnO equilibrium. Figure 1 shows the effect of C on L_p (Bhardwaj, 2008).

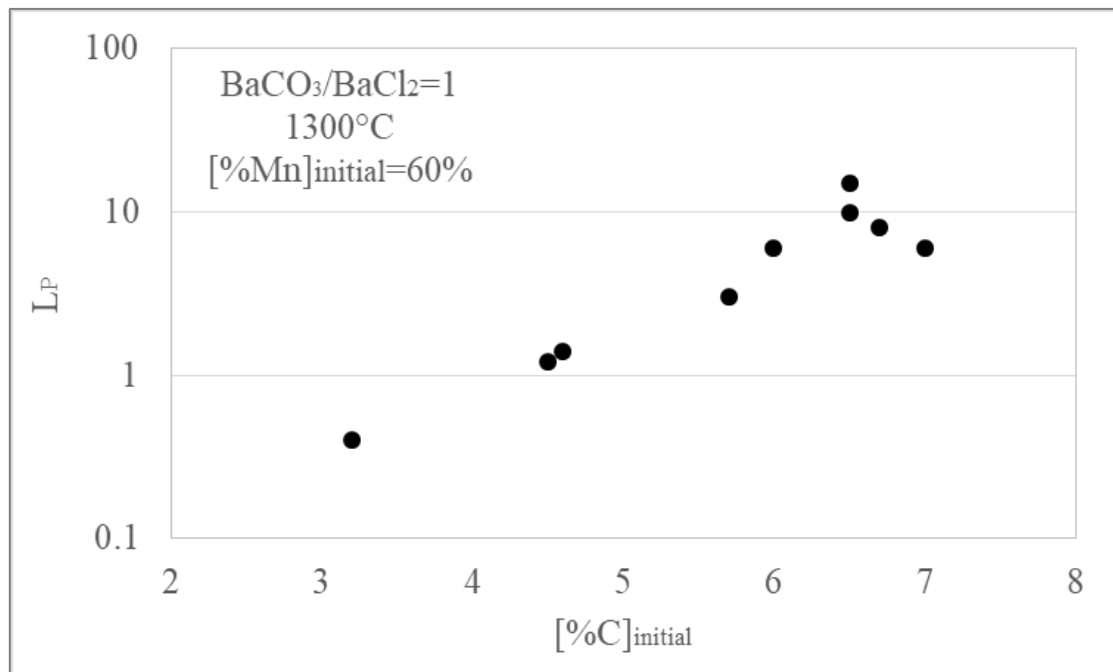
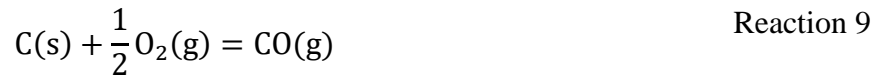


Figure 1: The effect of C on P slag/metal partition coefficient. Reproduced from (Bhardwaj, 2008).

The equilibrium P_{O_2} in the FeMn dephosphorization system is dependent on the following reactions (Yuanchi, et al., 1998):





Yuanchi , et al. (Yuanchi , et al., 1998), carried out experiments to investigate the effect of C and P_{O_2} on the dephosphorization of FeMn alloy. It was observed that there exists an optimum equilibrium, $[\text{C}]^*$, which corresponds to a maximum L_p and minimum L_{Mn} . When the dissolved C content is $< [\text{C}]^*$, the P_{O_2} of the system is controlled by the Mn-MnO equilibrium. With increasing $[\text{C}]$ concentration the activity of P increases and L_p will increase until $[\text{C}] = [\text{C}]^*$. When the dissolved C content is above $[\text{C}]^*$, P_{O_2} of the system is controlled by the C-CO equilibrium. The impact of P_{O_2} on L_p is larger than that of P activity, thus L_p decreases with increased dissolved C content.

Mn also has an effect on dephosphorization of FeMn alloys (Bhardwaj, 2008). The P activity coefficient decreases with increasing Mn content according to the expression below:

$$\log f_p = -0.0029[\% \text{Mn}] - \frac{386}{T} + 0.891 \quad \text{Equation 4}$$

Chaudhary and Goel (Chaudary & Goel, 2007) investigated the various dephosphorization approaches by different researchers. The results are summarized below:

- BaO-based fluxes are effective for dephosphorization of FeMn alloys as BaO has a high capacity for P. BaO is a stronger basic oxide than CaO (as discussed previously).
- Dephosphorization under oxidizing conditions is more effective in comparison to reducing conditions despite the fact that there may be Mn losses to slag. These advantages include:
 - Lower temperatures that favour removal of P under oxidizing conditions
 - Under reducing condition, dephosphorization is environmentally unfriendly (as discussed previously)
 - Higher flux consumption is required under reducing conditions
- Under oxidizing conditions, there is a narrow range of oxygen partial pressure below 3×10^{-17} atm in which it is thermodynamically feasible to dephosphorise selectively with minimum Mn-loss by reacting the alloy with a slag saturated in BaO and rich in MnO. The area is shown on Figure 2.

Chaudhary et al. (Chaudhary & Roy, 2001) carried out laboratory-scale testwork to minimize Mn loss and optimize flux consumption for dephosphorization of HCFeMn using BaCO₃-based fluxes. The tests were conducted in a high frequency induction furnace under oxidizing conditions and the parameters tested were as follows:

- Type of flux (BaCO₃, CaO, BaF₂, BaCl₂)
- Slag to metal mass ratio (1:2 to 1:25)
- Effect of temperature (1300-1500°C)
- Silicon addition in the alloy (0.6-1.6%)

The experimental results illustrated that addition of BaF₂ to the BaO-MnO system was the most effective for promoting dephosphorization: 68% P removal was achieved at 1380°C. The slag composition which resulted in the least Mn losses was found to lie in a range of 35-50% BaO, 20-25% MnO and 10-25% BaF₂. The degree of dephosphorization increased with an increase in the BaF₂ addition but no improvement was observed beyond 16-wt% addition. It was also noted that an increase in the MnO content of the slag would lower the BaF₂ content in the slag, resulting in less dephosphorization. Lastly, it was found that the Si content in the alloy had to be limited to 0.2% for effective dephosphorization.

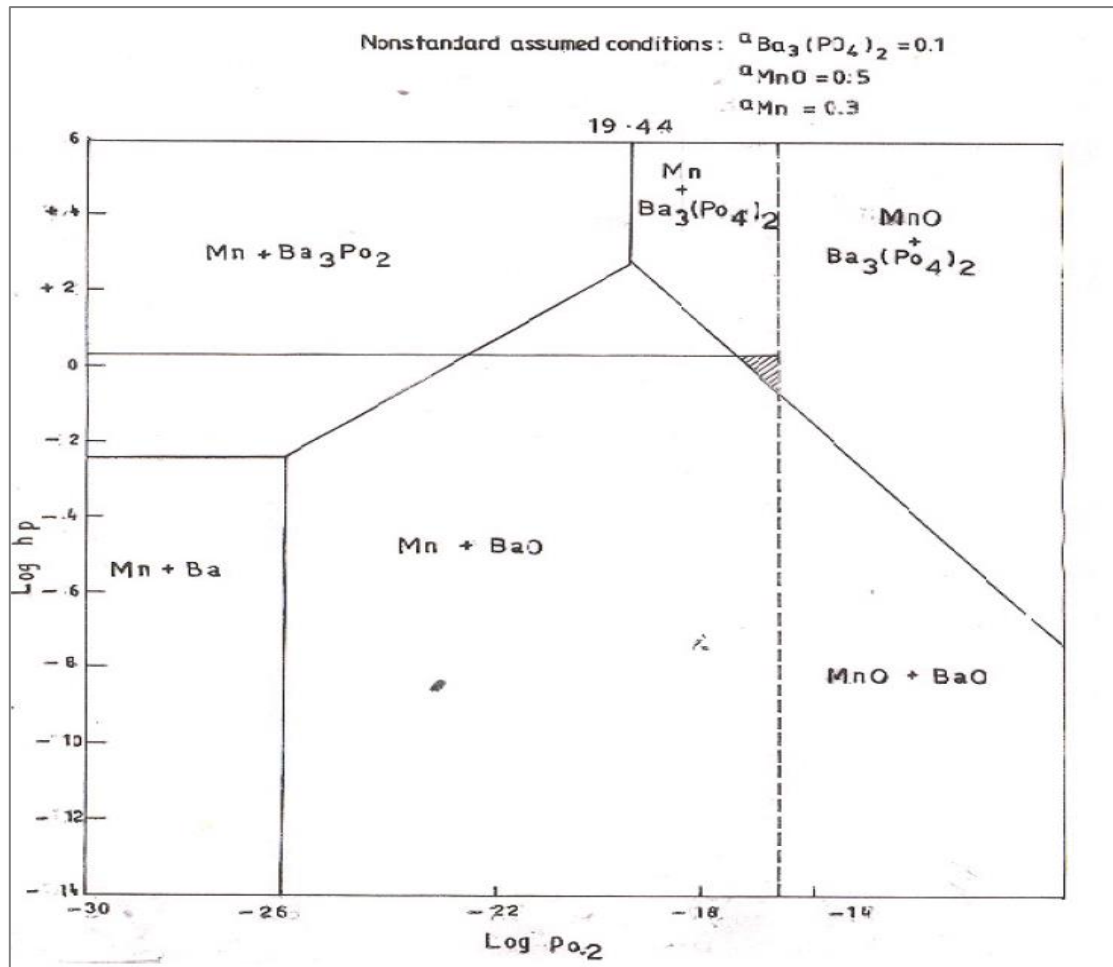


Figure 2: Predominance area diagram of Ba-O-P and MnO systems at 1573 K (Chaudhary, et al., 2007).

Chaudhary et al (Chaudhary, et al., 2007) further carried out a study to optimize the slag consumption as well as minimize the Mn loss using BaO based fluxes. BaO pellets were used, instead of BaCO₃ powder, to avoid the loss of flux as a dust during flux addition which occurred when powder was used. A plunging system was used to force the pellets to the bottom of the melt to reduce flux consumption and improve process kinetics (Chaudhary et al., 2007). The tests were also conducted under oxidizing conditions in a medium-frequency induction furnace at temperatures between 1300°C – 1500°C using a graphite crucible to achieve the required a_{Mn} of 0.3. A master alloy of composition (C-3.50%, Mn-67.60%, P-0.49%, Si-0.36%) was used during the study. The parameters tested were the MnO-BaO-BaF₂ flux compositions, quantity of flux, effect of temperature, the mode of addition, and residence time. The results can be summarized as follows:

- Melting of the BaO based flux was possible at 1350°C with MnO content of 10%, which resulted in 59% P removal and Mn loss of 2%. Increasing the MnO content in the slag resulted in poor P removal as the slag was not fully molten at 1350°C.
- Increasing the flux weight from 10% to 15% resulted in a slight improvement in the P removal from 59% to 61% at 1350°C. The Mn loss was 2% in both conditions.
- The implementation of a plunging system helped in reducing flux consumption to less than 5%. The results were achieved within a testing period of 10 minutes.
- The degree of dephosphorization reached the maximum at 1400°C with 63% P removal achieved. It was expected that an increase in temperature will reduce P removal in view of a lower value of the equilibrium constant (K) at higher temperatures.

Karbowniczek et al (Karbowniczek, et al., 2014) studied the dephosphorization of HCFeMn using a mixture of CaO-CaF₂ based fluxes. It was reported that the major drawback with the barium-based process was the high cost involved when sourcing barium compounds. Calcium compounds are more readily available and CaO-CaF₂ slags containing CaSi and CaC₂ were mainly investigated. The experimental testwork was conducted in an induction furnace with a capacity of 20kg at temperatures around 1450°C. Argon gas was injected into the molten bath during the process and was used to stir the metal bath. The dephosphorization efficiency obtained from the study ranged between 21% and 42%.

Dashevski, et al. (Dashevski, et al., 1998) studied dephosphorization of FeMn alloy with CaO and BaO slag mixtures in a high-frequency induction furnace at 1400°C under Ar atmosphere. The CaO slags mixtures comprised (30-40%) CaO - (50%-60% CaF₂) - (0-20%) CaCl₂ and the BaO bearing slag mixture comprised (26%-34%) BaO – (30%-40%) CaO-(15%-35%) MnO. The degree of dephosphorization and L_P achieved with the BaO slags were better by a factor of 2-3 when compared to CaO-slag mixtures. Figure 3 shows a summary of the results obtained from the study.

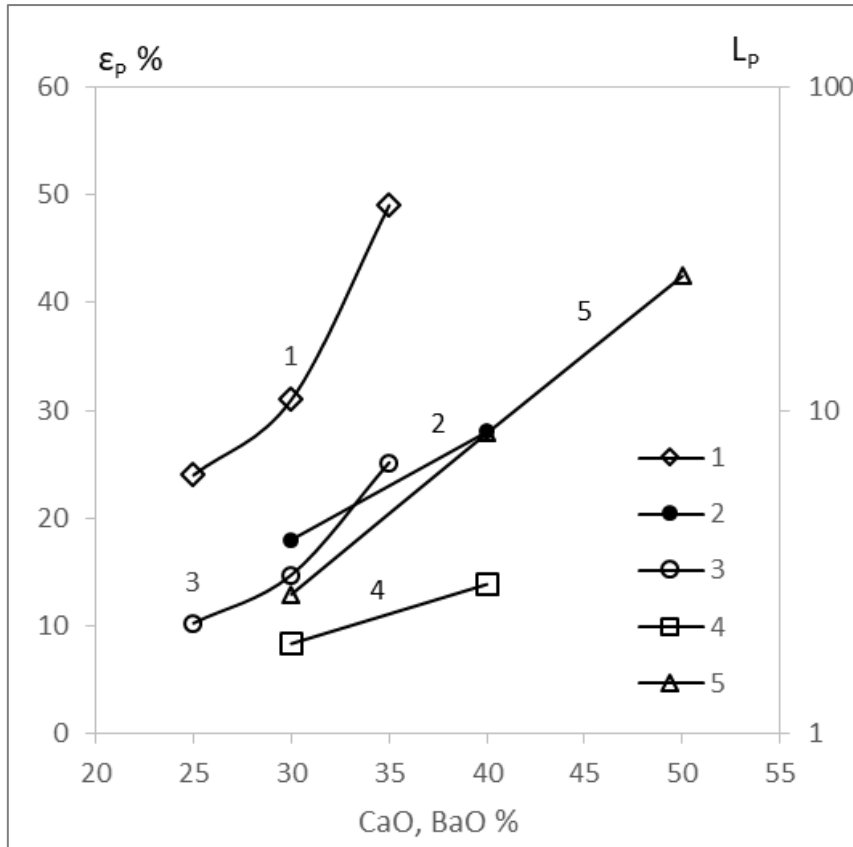


Figure 3: Degree of dephosphorization ϵ_p % (line 1, 2) of HCFeMn and L_p (3-5) of BaO (1, 3, 5) and CaO (2, 4) slag contents. Reproduced from (Hara, et al., 1990).

Lee and Kauser (Lee & Kauser, 1988) patented a method for the dephosphorization of HCFeMn by first desiliconizing the alloy to below 0.6% and then removing the P with BaCO_3 or BaO under oxidizing conditions. The tests were carried out in an induction furnace using 300 g BaCO_3 as a flux. It was observed that BaCO_3 was preferred over BaO as flux. The BaCO_3 decomposes to form CO_2 which behaves as an oxidizing agent to react with P and the BaO allows the dissolution of P into the slag. It was found that the best dephosphorization was obtained when the molten alloy has a Si content of <0.6%. Si content has direct impact on the oxygen potential of the melt and P can be removed under moderate oxidizing conditions with an initial Si content not more 0.6%.

Fujita, et al (Fujita, et al., 1988) also investigated the dephosphorization of Mn alloy (5%-60% Mn, 0.1%-0.2% P) with fluxes containing various carbonate basic fluxes, namely Li_2CO_3 , Na_2CO_3 , CaCO_2 and BaCO_3 , at an experimental scale of 70 kg using a flux to metal (weight) ratio of 0.04. The results showed that dephosphorization with CaCO_3 flux was hardly possible. Dephosphorization with fluxes containing Na_2CO_3 and Li_2CO_3 was also low. The rate of

dephosphorization with BaCO₃-based flux was relatively high with no occurrence of rephosphorization. The favourable conditions for dephosphorization were, i) low temperatures, ii) [%C] lower than the saturation value, iii) lower SiO₂ slag content to keep %BaO high.

Liu, et al (Liu, et al., 1998) studied the effect of different additives (CaO, MgO, SiO₂, CaF₂ and Al₂O₃) in BaO-BaF₂-MnO slags on the L_P and L_{Mn} (Mn partition ratio) between the slags and FeMn alloy at 1300°C in graphite crucibles. It was found that replacement of BaO with CaO or MgO resulted in a decrease in the P capacity and an increase in Mn capacity. Replacing BaF₂ with CaF₂ or SiO₂ resulted in poor dephosphorization ability and more losses of Mn to the slag. Addition of CaF₂ reduced the activity of BaO which reduced the benefit of BaO on dephosphorization.

Watanabe, et al (Watanabe, et al., 1993), investigated dephosphorization of C-saturated Fe-Mn alloy by BaO-MnO, BaO-MnO-BaF₂ and BaO-CaO-MnO fluxes at 1300°C and 1400°C. The tests were conducted under CO gas atmosphere, using 6 g flux and 2.5 g alloy. The alloy contained 9 to 92 % Mn and the MnO content ranged between 3%-31% for BaO-MnO system and between 11%-23% for BaO-MnO-BaF₂ system. The results indicated that the phosphate capacities of BaO-MnO and BaO-BaF₂ fluxes were larger than those of CaO-bearing fluxes. Dephosphorization by the BaO-MnO flux was possible for crude steel containing higher Mn content and may not be applicable for conventional HCFEMn. The L_P increased with an increase in the %BaO in the slag. Addition of BaF₂ to the slag improved the solubility of BaO and increased the L_P at lower Mn alloy contents.

In view of the above studies on dephosphorization of FeMn alloys, the BaO fluxes are reported to be effective. The drawback with applying BaO slag systems in the South African context is the scarcity and high cost of barium-based raw materials. Currently the basic oxide, together with BaF₂ flux, are sourced mainly from the U.S and this results in high cost implications. The use of BaO may therefore result in tech-economically unfeasible process in the South African context. Calcium and other basic reagents are more available, cheap and have been used for dephosphorization of iron. The current study focuses on the use of CaO in conjunction with other basic reagents to investigate if the removal of P from South African FeMn alloys can be improved by the various slag mixtures.

2.5 Research aim, questions, and objectives

The study aimed at investigating the use of CaO-bearing, synthetic slag systems – similar to the systems used in dephosphorization of iron – for the dephosphorization of FeMn alloys commercially produced in South Africa. Creating a CaO-based synthetic slag as baseline, the research questions are: what is the effect on dephosphorization of industrial FeMn alloys produced in South Africa when:

- Changing the MnO content?
- Adding Na₂O and CaF₂?
- Adding BaO and BaF₂?
- Changing basicity (%CaO/%SiO₂ ratio)?
- Changing temperature?
- Changing the composition of the alloy?

To obtain answers to these questions, the research objectives are to:

- Design various slag systems to dephosphorise FeMn alloys
- Source and prepare feed materials
- Characterise feed materials
- Conduct thermodynamic calculations using FactSage to:
 - Determine the effect of temperature on the percentage liquid alloy phase in the alloy system
 - Determine the effect of temperature on the percentage liquid slag phase in the slag systems
 - Calculate the phosphorus partition coefficient
- Conduct experimental testwork to evaluate the potential of each condition to dephosphorise FeMn alloys
- Characterise products
 - Determine the P-content of the alloys and slags
 - Determine the mass of alloy and the mass of slag formed
- Calculate the phosphorous partition coefficient and degree of dephosphorization

3 METHODOLOGY

3.1 Source and Prepare Feed Materials

3.1.1 Industrial alloys

Two FeMn alloys were utilised for the dephosphorization experiments, namely MCFeMn and HCFeMn alloys. MCFeMn formed the basis for the experiments. HCFeMn was only utilised in a few cases merely to investigate experimentally which of the two alloys would be easier to dephosphorise.

The MCFeMn was sourced from an industrial producer in South Africa. The alloy is typically tapped from a convertor, solidified, crushed and sized into different size fractions. The alloy used for the current study was the size fraction -50 +35 mm. At Mintek the sampled alloy was crushed, milled to -100 μm and split to obtain representative sub-samples for analysis and for experimental testwork.

A master alloy of HCFeMn was produced from laboratory-grade reagents obtained from different suppliers. The target composition was selected to match those produced in industry. The respective pure elements were blended, charged into a graphite crucible and melted at 1450°C in an induction furnace for a period of one hour (1hr) under an inert atmosphere using high purity Argon (99.999%) gas. Iron phosphide (Fe_2P) was used as a source of P and graphite powder was used as the source of C. Table 2 summarises the purity levels of each of the reagents as specified by the suppliers.

Table 2: The purity levels of the respective powder used for producing HCFeMn master alloy

Powders	Mn	Fe	Si	C	Fe_2P
Manganese	>99.0%				
Iron		>97.0%			
Silicon			99.0%		
Graphite				>99.9%	
Iron phosphide					99.5%

Among the elements used, Fe has the highest melting temperature of approximately 1536°C. The addition of carbon to the alloy reduces the melting point as do other impurities: about 3%

C reduces the melting point to 1350°C. The FACTSage calculations confirmed that the HCFeMn has a liquidus temperature of 1330°C. It was therefore assumed that producing the master alloy at 1450°C would result in sufficient superheat to allow adequate melting of the respective elements. Figure 4 indicates the steps followed to prepare the master alloy.



Figure 4: Steps followed to prepare the HCFeMn alloy

It is important to note an industrial HCFeMn alloy was used at the latter stages of the project, due to shortage of the pure elements to produce excess master alloy. A significant number of repeat tests were conducted during the initial stages of the project which lead to depletion of the master alloy and pure element. Unavailability of funds during the third year of the project, to source excess pure elements also influenced the decision to use the readily available industrial HCFeMn alloy.

3.1.2 Synthetic slags

The slag reagents used for the study were sourced from the commercial suppliers Sigma Aldrich and ACE chemicals. Analytical grade CaO, SiO₂, MnO₂, CaF₂, BaCO₃, Na₂CO₃, and BaF₂ were used. Table 3 summarises the chemical composition of the respective reagents used, with the manufacturer-stated minimum purity levels of the reagents. Analysis of the respective reagent showed that P, S and Fe were the major impurities in all the reagents used. MnO₂ comprise significant amount of Fe, P and S. Lime and silica also contain relatively high S and Fe contents. Contamination of the master slags by the impurities was therefore unavoidable as highly pure slag reagents are not readily available.

Table 3: Chemical compositions of the slag reagents used (mass %)

Composition	Manganese dioxide	Calcium dioxide	Silica	Barium carbonate	Sodium carbonate	Calcium fluoride	Barium fluoride
MnO ₂	90.0						
Al ₂ O ₃			0.80			0.38	
SiO ₂			98.50				
CaO		96.00 [#]	0.10				
Fe	10.4	0.097	0.32	0.02	0.014	0.29	
BaCO ₃				99.8			
Na ₂ CO ₃			0.10		99.0		
CaF ₂						>95	
BaF ₂							99.99
MgO	0.91	1.05	0.12		0.13	0.95	
LOI	0.30	3.5 [#]		0.2		≤1.0	
Insoluble matter	0.01	0.50			0.01		
P	0..25	0.006	0.008	<0.005	<0.005	0.012	not analysed
S	0.13	0.21	0.017	0.019	0.10	0.054	not analysed

*Can vary depending on storage conditions

Table 4 summarises the suppliers of the respective reagents used as well as the prices. It can be seen that the costs of BaO and BaF₂ are higher than the other slag reagents. Extrapolating from the cost of laboratory chemicals to industrial scale, it seems clear that the use of Ba-containing reagents would be expensive. However cheaper slag material may be used at industrial scale.

Table 4: Different consumables used as well as their respective suppliers and prices

ITEM	SUPPLIER	Price per 500 g
Synthetic fluxes		
CaO	ASSOCIATED CHEMICAL	R 165
MnO ₂	ACE (PTY) LTD	R 60
SiO ₂	ACE (PTY) LTD	R 40
Na ₂ CO ₃	ACE (PTY) LTD	R 102
BaCO ₃	Industrial analytical	R 1 650
CaF ₂	ACE (PTY) LTD	R 275
BaF ₂	MERCK	R 1 620/50g
Pure metals		
Fe	MERCK	R 1 610
Mn	MERCK	R 1 144
Si	Industrial analytical	R 7 725
Fe ₂ P	Industrial analytical	R13 375/10g
C	N/A	

Different synthetic slags were prepared for the completion of the testwork. Figure 5 presents the steps followed to prepare the respective slags. The slag components, i.e. CaO, SiO₂, Na₂CO₃, and BaCO₃ were calcined separately at 1000°C for 2 hrs in air to remove volatile matter. Decomposition of the carbonaceous matter for Na₂CO₃ and BaCO₃ was however not successful at 1000°C. The calcined materials were then weighed and blended in a ring mill to generate a homogeneous mixture and charged into a graphite crucible. The crucible charges were subsequently heated at 10°C/min to 1600°C and maintained at the temperature for 1 hour in an induction furnace under inert atmosphere using Ar gas.

The molten materials were allowed to cool to room temperature under an inert atmosphere. The slags were subsequently retrieved from the crucibles, crushed, milled, and decarburized at 1200°C for 2 hrs in air using alumina crucibles to burn off the residual carbon. The MnO₂ reagent was not added during the melting stage of the synthetic slags to avoid reaction with the graphite crucibles. The component was incorporated after the decarburizing stage. BaCO₃, was also only added to the decarburized slags. Inclusion of the component during the melting stage

resulted in erosion of the graphite crucibles. Figure 5 shows the steps followed to produce the different slags.



Figure 5: Steps followed to prepare the synthetic

3.2 Design Various Slag Systems to Dephosphorise FeMn Alloy

Table 5 summarizes the different slag compositions investigated. The motivations for each composition are discussed in the sub-sections below.

Table 5: Target chemical compositions of different slag systems.

Slag label	Slag systems							Total
	MnO	CaO	SiO ₂	CaF ₂	Na ₂ O	BaO	BaF ₂	
A	20.0	40.0	40.0					100.0
B	25.0	37.5	37.5					100.0
C	15.0	42.5	42.5					100.0
D	20.0	40.0	20.0		20.0			100.0
E	20.0	20.0	40.0		20.0			100.0
F	20.0	20.0	40.0	7.5	12.5			100.0
H	20.0	20.0	40.0			20.0		100.0
I	20.0					60.0	20.0	100.0
Basicity 0.7	20.0	34.0	46.0					100.0
Basicity 1.3	20.0	46.0	34.0					100.0

3.2.1 Creating baseline CaO-based slag (Slag A)

In the current study, the slag system comprising 20% MnO-40% CaO-40% SiO₂ was adopted as a baseline slag. The basic oxide CaO was selected to provide the free oxygen (O²⁻) when dissolved in the liquid slag (refer to Reaction 1). MnO was added to provide the oxidizing condition in the system. . The acidic SiO₂ was selected as a flux to reduce the melting point of the high-melting, basic MnO-CaO binary system. Figure 6 presents the MnO-SiO₂-CaO phase diagram showing the fluxing strategy chosen and the expected change in slag liquidus

temperature if 40% SiO₂ addition is made to the slag. As shown on the figure, the baseline slag has a liquidus temperature of 1320°C.

3.2.2 Changing MnO (Slag B and Slag C)

The amount of MnO in the slags used for dephosphorization of C-saturated iron as well as HCFeMn, was reported to have an influence on the phosphate capacities of the slags (Simeonov & Sano, 1985; Chaudary & Goel, 2007). The effect of MnO on the equilibrium P distribution was investigated in the current study by varying the MnO content in the slag while maintaining the basicity (%CaO/%SiO₂) constant. The MnO content was varied between 15-25% at 5% intervals.

3.2.3 Adding Na₂O-CaF₂ (Slag D, Slag E, and Slag F)

Addition of Na₂O has proven, from literature, to enhance the ability of CaO-based slags to dephosphorise liquid iron (Van Niekerk & Dippenaar, 1998; Nassaralla & Fruehan, 1992). CaF₂ on the other hand, is added during hot metal treatment to maintain the fluidity of lime-based slags. Both additives were reported to have an influence on phosphate capacities of basic slags (Fujita, et al., 1988) and are therefore investigated in the current study. CaO was partially replaced with Na₂O and CaF₂, while the MnO content was maintained constant.

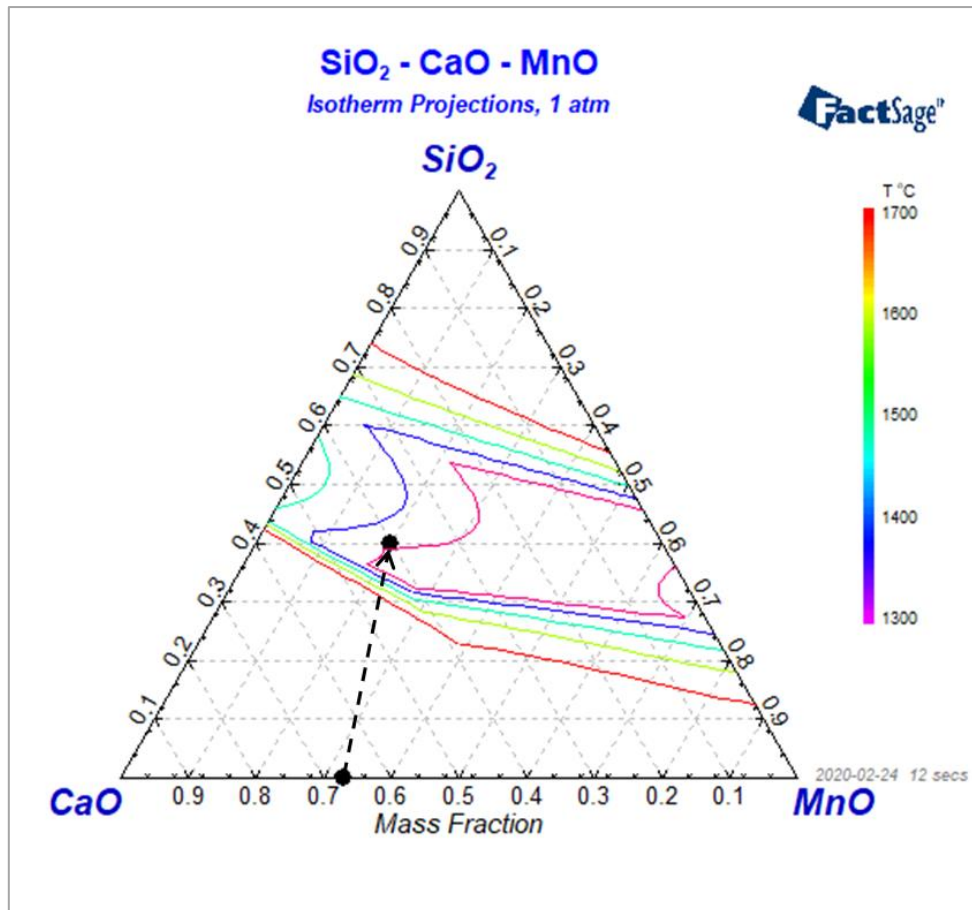


Figure 6: Liquidus isotherms for the system CaO – SiO₂ – MnO showing the desired slag composition achievable with the addition of SiO₂.

3.2.4 Adding BaO (Slag H)

From literature (Chaudary P.N et al., 2001), the BaO-BaF₂-MnO slag system was found to be effective for dephosphorization of FeMn alloys as well as liquid iron when BaO was used. The effect of BaO addition was investigated in the current study by replacing a fraction of CaO with BaO.

3.2.5 Adding BaO-BaF₂ (Slag I)

Replacing both the lime and silica by BaO and BaF₂ flux was also investigated. The slag system was reported by Chaudhary to be effective for dephosphorization of high carbon FeMn alloy (Chaudary, et al., 2008; Fujita, et al., 1988; Dashevski, et al., 1998). The slag was only investigated during the initial stages of the testwork, due to a number of challenges encountered when using the slag (slag reacting with graphite crucible, depletion of BaF₂ due to a significant number of attempted repeat tests), the slag could not be used at the later stages of the testwork.

3.2.6 Changing basicity of baseline CaO-based slag

The effect of changes in basicity, %CaO/%SiO₂, on the P partition coefficient was also investigated. The basicities investigated were 0.7, 0.9 and 1.3 using the baseline slag A while maintaining the MnO content constant as shown on Table 5.

3.2.7 Changing alloy composition

From literature (Fujita, et al., 1988; Watanabe, et al., 1993), it was observed that Mn has a detrimental effect on dephosphorization of C-saturated FeMn alloys, as increased Mn content decreases the activity coefficient of P. The synthetic slags were used with the HCFeMn at two different temperatures of 1350°C (30 minutes) and 1400°C (60 minutes). The results obtained were compared to those obtained with MCFeMn under the same conditions. The use of the MnO-BaO-BaF₂ slag (slag I) was also investigated at 1400°C, using the HCFeMn master alloy. Due to the shortage of BaF₂ the tests were only conducted at 1400°C for 5 minutes and 60 minutes.

3.3 Characterization of feed materials

The bulk chemical compositions of the feed materials were determined by Inductively Coupled Plasma-Optical Emission Spectroscopy (ICP-OES) technique. C and S were analysed by combustion method (LECO). P was analysed using wet chemical analysis by ICP.

With ICP-OES a known mass of the pulverised sample was fused using a strong oxidising agent, such as sodium peroxide. The molten material was digested in HCl/HNO₃ acid and the solution was assayed by ICP-OES. The method has the lowest detection limit of 0.005%.

With LECO (combustion) analyses, samples were heated in a combustion furnace, in oxygen. S and C were oxidised and detected as SO₂ and CO₂ by an infrared detector.

3.4 Thermodynamic FactSage calculations.

FactSage™ version 7.3 was utilised. The package is a fully integrated thermodynamic database computing system developed since 1976 by a joint research project between McGill University and École Polytechnique de Montréal (Canada). FactSage provides access to a number of

databases including pure substances, oxides, solutions, and alloy databases. The tool is widely used to study the thermochemistry for different chemical and metallurgical processes (Bale C.W et al., 2016).

The calculations were conducted in the Equilib module. In all calculations, the pure substance database (FactPS), which is suitable for pure solids, liquids, and gases, was utilised. As solution databases, FToxid was utilised to describe the slag system and FSstel the alloy system. FToxid includes a wide range of components such as Al₂O₃, CaO, FeO, Fe₂O₃, MnO, Na₂O, and SiO₂. Furthermore FToxid covers several solid solution database which include those listed below: (Bale, et al., 2016):

- Corundum: Al₂O₃-Cr₂O₃-Fe₂O₃;
- Wollastonite: CaSiO₃ (+FeSiO₃, MnSiO₃, MgSiO₃);
- Olivine: [Ca²⁺, Fe²⁺, Mg²⁺, Mn²⁺]^{M2}(Ca²⁺, Co²⁺, Fe²⁺, Mg²⁺, Mn²⁺, Ni²⁺, Zn²⁺)^{M1}SiO₄, where M1 and M2 represent the respective site fractions
- α-Ca₂SiO₄: α-Ca₂SiO₄ (+Fe₂SiO₄, Mn₂SiO₄, Mg₂SiO₄);
- Monoxide: CaO-FeO-MgO-MnO;
- α-Ca₂SiO₄: α-Ca₂SiO₄ (+Fe₂SiO₄, Mg₂SiO₄, Mn₂SiO₄);

FSstel is a steel database covering a wide range of compositions related to steelmaking processes (Bale, et al., 2016). Although thermodynamic data exist for HCFemn, it does not contain equilibrium data on P (Tang & Olsen, 2006). FSstel was proven in the past to represent equilibrium conditions in SiMn production, and as it contained data on P, was selected for the calculations presented here (Steenkamp, et al., 2015).

As pure species, all liquid and solid were selected except the Mn phosphide phases. As pure ideal gas species, only O₂ and Ar were selected. For solution systems, all solution phases were selected, except in cases where more than one option existed. Solution phases that were suppressed were SlagD Slag?, MeO_B, MeP_? cPyrB, and cPyr?. SlagA model was selected over Slag? model because SlagA provides much more reasonable L_P values for steelmaking than does Slag?. Slag? overestimates P removal. An example showing the L_P obtained from the slag models is presented in Appendix A. Since MeO_B, does not include BaO as solute, this solution phase was not selected. MeP_? cPyrB, and cPyr? were not selected because more than one option existed.

The calculations were done to investigate the liquidus temperature of the slags and alloys as well as the L_P between slag and alloy.

3.4.1 *Effect of temperature on the percentage liquid alloy phase in the alloy systems*

The liquidus temperature of the alloys were determined. The typical HCFeMn and MCFeMn compositions obtained from literature (see Table 6) were utilised.

Table 6: Typical compositions of HCFeMn and MCFeMn alloys (mass %) utilised in thermodynamic calculations (Olsen, et al., 2007).

Alloy	Mn	C	Si	P	Fe
HCFeMn	78.00	7.50	0.30	0.18	14.00
MCFeMn	80.00	1.50	0.60	0.20	17.70

3.4.2 *Effect of temperature on the percentage liquid slag phase in the different slag systems*

The equilibrium calculations were done to determine the liquidus temperatures. The slag systems in Table 5 were utilised.

3.4.3 *Phosphorus distribution ratio calculations*

The slag systems in Table 5 and alloys indicated in Table 6 were utilised. To determine the L_P for the different slag-alloy systems 100 g of alloy was reacted with 10 g of slag i.e. the slag-to-alloy mass ratio was maintained constant at 0.1. A small amount of Ar (0.01 g) was also added to allow for reactions to converge (Steenkamp, et al., 2015). The temperature range considered as 1300°C - 1700°C at 50°C intervals.

The results obtained from the equilibrium calculations were used to calculate the L_P , defined by the equation below:

$$L_P = \frac{\text{Wt\%P_FToxid_SLAGA}}{\text{Wt\%P_FSstel_Liqu}} \quad \text{Equation 5}$$

3.5 Experimental Testwork

3.5.1 Crucible selection

During the current study, graphite crucibles were selected. To avoid attack of the crucible by the different slag systems investigated, a graphite crucible was deemed suitable for the experimental testwork. The crucibles were also selected with the intention of maintaining the slag chemistries during the tests without interference by the crucible. The crucibles were sourced from Carboquip, a South African supplier. Figure 7 shows the dimensions of the crucibles used.

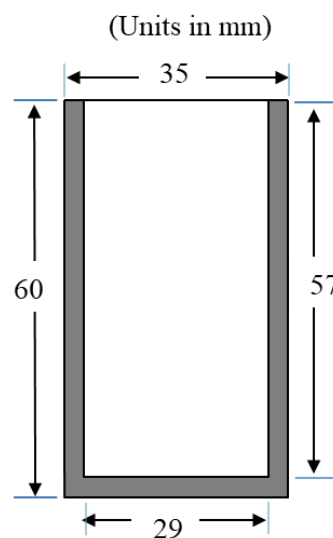


Figure 7: Typical dimensions of the graphite crucibles used

3.5.2 Drop-quench furnace-based experiments

Equilibration testwork was initially considered to study the dephosphorization of the produced HCFEMn master alloy. The tests were conducted in a drop-quench furnace during which a number of challenges were encountered. The challenges included BaO-containing slags reacting with the graphite crucible, subsequently resulting in damage to the alumina furnace tube. In some instances, the supporting (Mo) wire reacted with the gas/fumes produced from the decomposition of BaCO_3 , leading to unintended self-quenching. Ca-based raw materials did not behave aggressively towards graphite crucibles. The experimental setup used and the pictures of the damaged setup are included in Appendix A. It was then decided to carry out the experiments in an induction furnace. The results showing the L_P obtained from the few

completed tests are included in Appendix A Table A1, from the results low $L_p < 1$ were obtained.

3.5.3 Induction furnace-based experiments

The dephosphorization tests were conducted in a 25 kW induction furnace. The furnace operates by radiation heating from a graphite susceptor heated by magnetic induction created by a water-cooled copper coil. The furnace power is switched on by using an on/off button on the control panel. The power was adjusted manually; the temperature was controlled by manually increasing the power setpoint at an interval of 30 minutes until the target temperature was reached. As it is generally difficult to maintain a constant furnace temperature; a range of ten degrees above and ten degrees below the target temperature was maintained. Increasing the power setpoint at an interval of 30 minutes is the standard approach to insure that the operation temperature is not excessively exceeded. An extraction hood is mounted above the furnace to extract and direct any gasses generated from the experiment to a baghouse.

Figure 8 present the schematic diagram of the induction furnace and Figure 9 presents the induction furnace setup.

All tests applied the same test preparation method which entailed weighing the required amounts of the slag and alloy, followed by mixing of the feed charges in a ring mill for about 30 seconds to produce a homogenous mixture. About 10 g of both the starting alloy and slag was used for the experiment, the actual masses used are shown in Appendix B, Table B1. The actual slag masses were higher than 10 g because of the lower purity levels of the reagents used, i.e. MnO_2 , Na_2CO_3 and $BaCO_3$. The samples masses were used in order to generate sufficient product samples for chemical analysis and to avoid depletion of the master slags. The uniform charge was then packed into the graphite crucible. Packing was done such that a dense, compact solid charge was formed to promote interaction of solid particles in the crucible.

The charged crucibles were weighed and inserted into the furnace chamber. The furnace chamber was covered with high temperature, refractory blankets (Fiberfrax) to prevent air ingress and preserve heat in the chamber. An alumina tube was used to deliver Argon gas into the furnace chamber to create an inert environment throughout the duration of each test. An alumina sheath was used to encase the B-therocouple used to control and monitor the sample temperature.

The furnace was heated gradually by incremental power input adjustments until a target test temperature was reached; the typical heating rate was 8-10°C/min under inert atmosphere. The Ar gas line was purged through a gas flowmeter that was calibrated by the supplier, HM FloConsult, at 1 bar and 20°C. The flow rate was maintained at around 2 L/min throughout the test durations. Calibration of the B-type thermocouple utilised was also done prior to the testwork to ensure that accurate process temperature was recorded.

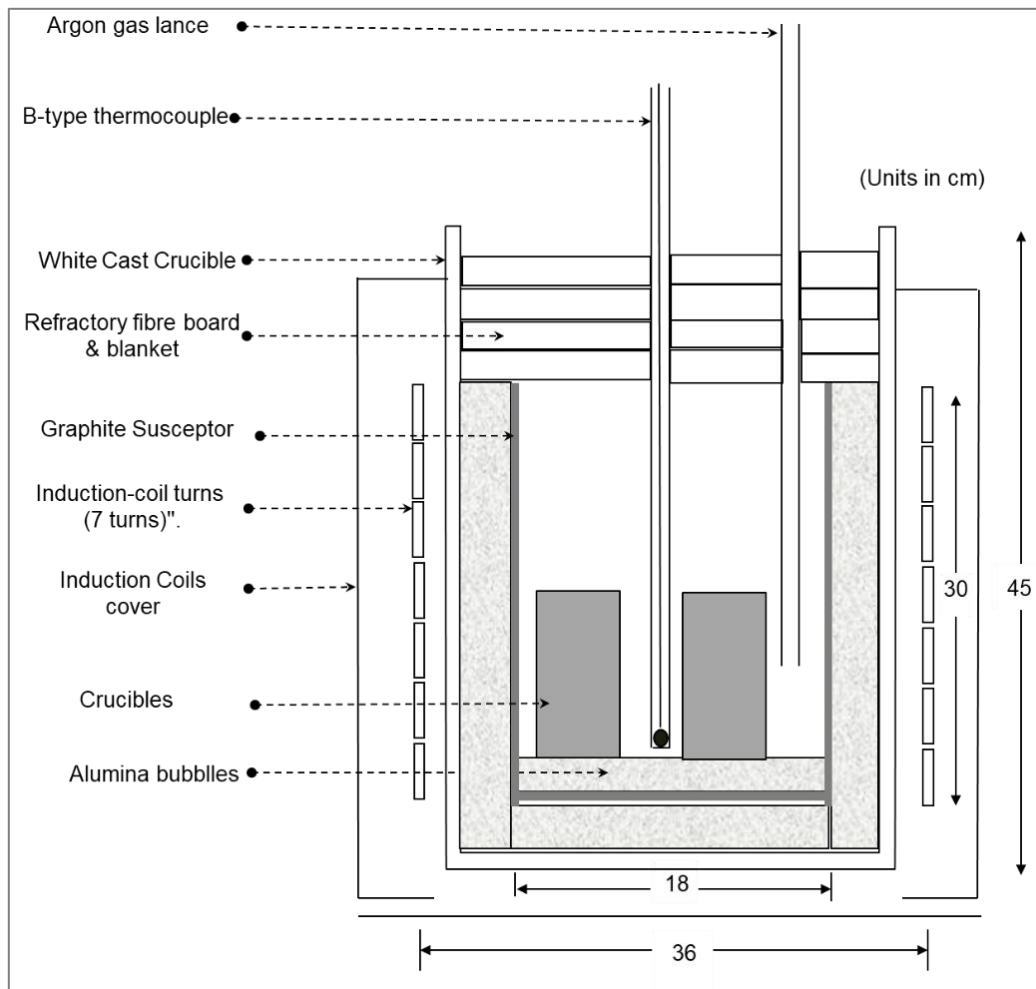


Figure 8: Schematic diagram of the induction furnace.

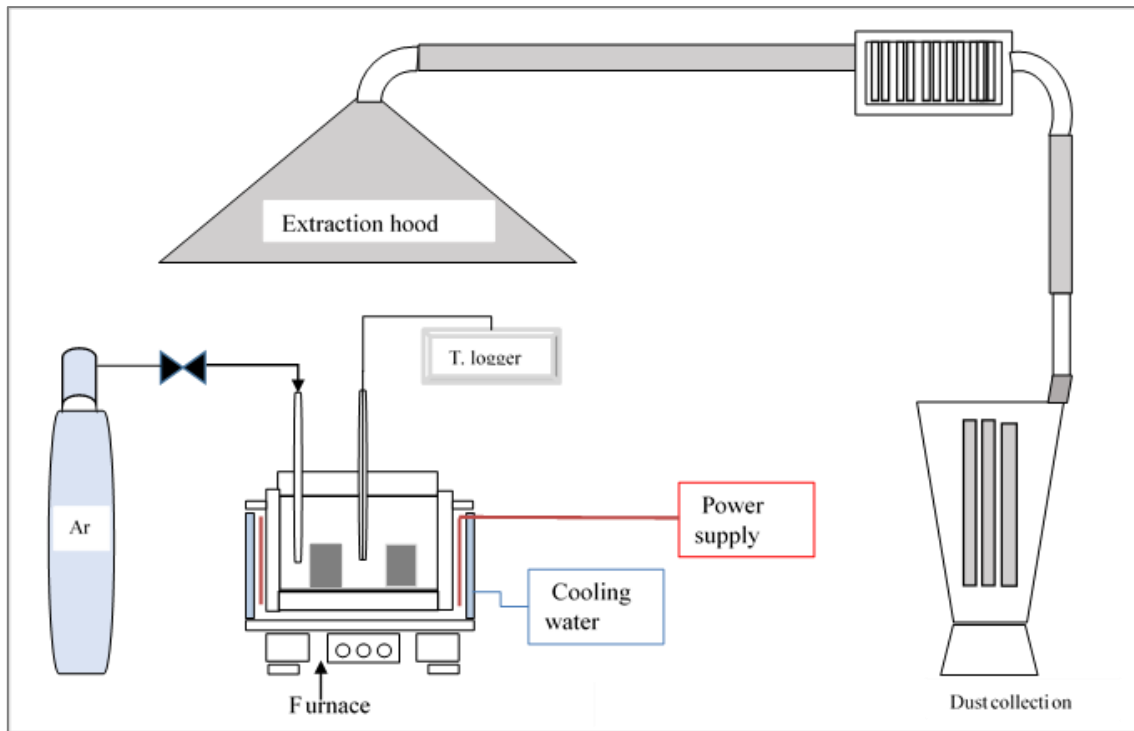


Figure 9: Schematic view of the 25 kW induction furnace setup.

Initially, molten slag and alloy samples were taken at different time intervals from the crucibles, using a silica tube connected to a rubber pipet filler. After collecting the sample, the silica tube was immediately quenched in water and cracked to separate and collect samples for chemical analysis. The challenges encountered with this procedure was that in most cases slag could not be collected from the crucibles due to the small amounts, tube melting during sampling and separating the slag from the glass. This procedure was not encouraging and discontinued. The results showing the final P contents of the sampled alloys are included in Appendix A Table A2; from the results suggest that dephosphorization was only possible with BaO-based slag (Slag I).

The tests were then carried out at different retention times without intermediate sampling. Table 7 summarises the test matrix followed. Testwork using Slag D was unsuccessful because the slag has a high liquidus temperature of about 1800°C; separation of slag-alloy was not achieved at the experimental temperatures. The slag was therefore not investigated further. Slag I was aggressive towards the graphite crucible during the experiment. Crucible erosion occurred during the tests and the crucible contents leaked from the crucible.

Table 7: Completed experimental tests

Slag	Alloy	Target Basicity*	Sampling times (min)	Temperature (°C)
Slag A	MCFeMn	1	5,30, 60	1350, 1400,1450
Slag A	MCFeMn	1.3 0.7	30	1450
Slag A, E, F, H	HCFeMn	1	60	1350
	Industrial alloy		30	1400
Slag B	MCFeMn	1	30	1450
Slag C	MCFeMn	1	30	1450
Slag E	MCFeMn	1	5,30, 60	1350, 1400,1450
Slag F	MCFeMn	1	5,30, 60	1350, 1400,1450
Slag H	MCFeMn	1	5,30, 60	1350, 1400,1450

* %CaO/%SiO₂

Upon completion of each test, the furnace power was switched off, the refractory blankets slightly moved to make way for the removal of the graphite crucibles from the furnace chamber. Steel tongs were used to remove the hot crucibles from the furnace for quenching. The crucibles were immediately quenched in a water-and-ice bath to ensure immediate cooling of the molten slag and alloy. Quenching was done to maintain the phase chemistry in both the slag and alloy at the specific test conditions. The quenched crucibles were then dried at 105°C overnight in a drying oven.

3.6 Characterization of product samples

3.6.1 Macroscopic investigation

The dried sample was weighed and broken to retrieve the slag and alloy. The alloy and slag samples were separated manually, weighed and pulverized for analysis.

In general, separation of the quenched slag and alloy was incomplete and alloy globules were often found entrained in the slag. This created difficulties in quantifying the mass of the alloy products. Weighing of the product slags was also challenging as a fraction of the slag was attached to the crucible wall and occasionally, a fraction of the slag spilled from the crucible during quenching.

3.6.2 Bulk chemical compositions

The analyses of the low P contents in the slags and alloys proved to be a challenge and at the low concentrations the uncertainties were large. The analytical results obtained from the in-house laboratory were not repeatable, due to the very low P-content of the samples, which led to inconclusive test results. Outsourcing of the P analysis to an external laboratory was done. The analysis of the other elements was also done at the external laboratory.

In order to address the issue of repeatability at the external laboratory, four sub-samples of the MCFeMn alloy were analysed using the ICP technique. Table 8 presents the chemical compositions of the samples. Included are the statistical results obtained from the analyses. The results show a small variation in the P contents from the four samples.

Table 8: Bulk chemical compositions of MCFeMn alloy

Element	1	2	3	4	Average	Standard deviation
C	1.540	1.600	1.540	1.540	1.550	0.030
Mn	78.80	77.70	79.60	78.70	78.700	0.779
S	0.009	≤ 0.005	0.013	0.009	0.010	0.002
P	0.073	0.067	≤ 0.005	0.067	0.069	0.003
Si	0.42	0.44	0.42	0.45	0.433	0.015
Fe	18.80	19.90	17.90	17.90	18.625	0.950

3.6.3 Slag/alloy proportioning utilising X-ray tomography

The X-ray tomography (XRT) analysis was done to determine the volume of the slag and alloy in the crucible. From the measured volumes, the respective slag and alloy masses were calculated. The analysis was done to address the challenges related to weighing of the final product samples. A comparison was made between the XRT measured masses and the masses calculated from the elemental mass balance. As a result of XRT equipment failure, only one sample was analysed namely slag H-MCFeMn sample tested for 30 minutes reaction time.

The X-Ray Tomography (XRT) analysis was performed by Mintek's Minerals Processing (MNL) department. The sample, still in-situ in its crucible, was scanned using X-ray computed

tomography on a Zeiss X-ray microscope (XRM) scanner. The XRT data was visualised and processed using the Volume Graphics Studio Max 2.2 package (VG Studio). In order to extract accurate volumes for the three target phases, a region growing tool was utilised to generate an extracted volume within a particular grey-value interval. The tool uses a flooding algorithm that expands the graphical selection (a user-defined sphere) from a seed point (centroid of sphere) in x, y, and z directions. The user defines a tolerance for the region growth to isolate desired grey level ranges. This is an iterative process and once all the desired target (metal for example) is included in the region, and all the undesired targets (slag/air) are excluded, the region of interest is extracted as solid from which volume and surface areas may be calculated.

3.6.4 Electron Microprobe analyses analysis

In order to address the uncertainties issues related to the analysis of product samples, Electron Microprobe analysis (EMPA) was done and the results were compared to the bulk chemical results.

For EMPA, a crucible containing slag and metal was impregnated with resin and then cut in half (long axis) to give two halves showing a full section from base to rim. Randomly selected particles of the major measurable phases in each of the samples were analysed with a JEOL JXA-8230 electron probe microanalyser using wavelength-dispersive spectrometry (WDS). The system was calibrated with pure oxide and silicate standards. Analyses were performed at an accelerating voltage of 20 kV, with a beam current of 30nA, and a 5 μ m spot size. Counting times of 10 seconds on peak, and 5 seconds on each of the two background positions adjacent to the peak, were used. Matrix correction was automatically done by the PRZ procedure in the JEOL quantitative analysis software. The analytes included Si, C, Ca, P, S, Ba, Fe, Mn, Ti and Al. The first run analysed the metal and dense slag at the bottom of the crucible as well as metal droplets on the walls of the crucible, and the porous slag. The minimum detection limits for the analysis are specified in Table 9.

Table 9: EMPA elemental detection limit (% by mass).

Element	Si	Ca	C	P	S	Ba	Mn
Detection Limits Slag Run with Al coating	0.02	0.02	0.05	0.01	0.01	0.01	0.01
Detection Limits Alloy Run with Al coating	0.01	0.16	0.17	0.03	0.03	0.09	0.26

3.6.5 *Elemental mass balance calculations*

The analytical results of alloy samples showed the effect of entrainment of slag in the alloy, indicated by Ca being reported as part of the alloy analysis. Conditions in these tests were not sufficiently reducing to result in dissolved calcium in the alloy, so any analysed Ca must indicate that some slag was included in the alloy analysis. A similar effect was observed with certain slag compositions indicating high Fe contents. Conditions were not sufficiently oxidising to form significant FeO, so Fe reported in the slag analysis reflected alloy entrainment. The EMPA results of the few analysed samples also confirmed that the slags did not contain any FeO. Due to the difficulties associated with quantifying the final alloy and slag masses, the Fe and Ca contents were used to predict the masses of the alloy and slag.

During the mass balance calculation, the assumptions made were that:

- There was no Ca in the product alloy
- There was no Fe in the product slag
- Both elements were conserved

The two elements were then used to calculate the product alloy and slag masses. The calculated product masses were then used to correct the compositions of the alloys and slags. Correcting the compositions entailed recalculating the compositions to remove the entrained phases.

Correcting the bulk chemical compositions of the slags entailed the following:

1. Using the chemical composition of the associated slag and the Ca alloy content to calculate the amount of slag entrained in the alloy as follows:

$$Mass_{entrainedslag} = \frac{(\%Ca_{alloy} \times mass_{alloy})}{(\%Ca_{slag})} \quad \text{Equation 6}$$

2. Using the calculated entrained slag mass, the mass of the respective elements, i , was then calculated:

$$Mass_{i,entrainedslag} = \%m(i)_{slag} \times mass_{entrainedslag} \quad \text{Equation 7}$$

3. Thereafter the mass of each element in the alloy was corrected by subtracting the entrained elemental mass from the initial elemental mass in the alloy:

$$Mass_{i,correctedmass} = Mass_{i,alloy} - Mass_{i,entrainedslag} \quad \text{Equation 8}$$

4. The corrected alloy composition was subsequently calculated:

$$\%m(i)_{correctedalloy} = \frac{mass_{i,correctedmass}}{mass_{alloy}} \quad \text{Equation 9}$$

The elemental mass balance calculations made use of the elemental accountability technique, which refers to the percentage of each element in the feed materials that is recovered as product. The elemental accountability is generally affected by errors in analyses and masses of raw materials and product samples. In general, it is evaluated on major elements present in the slag and metal. In the current study the elements of interest were P, Fe, Mn, Ca, Si and C.

Due to the low the P concentrations, the accountability calculations were susceptible to large errors. The tests were thus generally affected by the uncertainties in analyses of the product samples and the final product masses. The calculated product masses and the corrected compositions were then used to calculate the accountability of a given element i was calculated as follows:

$$\% \text{ Accountability}, i = \frac{m_{i,alloyproduct} + m_{i,slagproduct}}{m_{i,alloyfeed} + m_{i,slagfeed}} \times 100 \quad \text{Equation 10}$$

Where m denotes the mass of the element

3.6.6 Phosphorous partition coefficient

The P-content in the slag and alloy samples obtained from the corrected analysis were used to calculate L_p and degree of dephosphorization for the different experimental conditions based on Equation 2 and Equation 3.

4 RESULTS

4.1 Characterised Feed Materials

Table 10 summarises the average chemical composition of the MCFeMn alloy and HCFeMn master alloy. The presence of S in the HCFeMn alloy was not expected, as high purity reagents were used to produce the master alloy. Analytical uncertainties may have been the attributing factor to sulphur detection in the master alloy.

Table 10: Average bulk chemical composition of the industry MCFeMn alloy and HCFeMn master alloys used in the study (mass %).

Element	Industry MCFeMn	Industry HCFeMn	HCFeMn master alloy
Mn	78.70	75.80	75.40
Fe	18.62	17.00	15.30
Si	0.43	0.33	0.18
C	1.56	6.77	8.30
P	0.069	0.061	0.082
S	0.010	0.014	0.014
Total	99.17	99.90	99.93

Table 11 presents the chemical composition of the prepared master slags. The results indicate that FeO, MgO, S, P, Al₂O₃ were the major impurity in the master slags. As previously indicated in Table 3, the slag reagent used comprised significant amount of the impurities, The target MnO, SiO₂ and CaO contents in the master slags were not entirely accomplished; this was mainly attributed to the FeO content in the slag. The FeO impurity was introduced mainly by the MnO₂ reagent. The total chemical compositions of the slags are also generally lower than 100%, this was attributed to the expression of Mn as MnO instead of MnO₂ and the presence of carbonaceous matter introduced by BaCO₃ and Na₂CO₃. These slags were utilised in the dephosphorization tests.

Table 11: Bulk chemical compositions of the master slags (mass %)

	S	P ₂ O ₅	Al ₂ O ₃	SiO ₂	CaO	MnO	FeO	BaO	MgO	Na ₂ O	CaF ₂	Total
Target				40.00	40.00	20.00						
Slag A	0.03	0.18	0.74	40.30	35.00	16.90	3.72		0.60			97.46
Target				40.00	20.00	20.00				20.00		
Slag E	0.01	0.13	0.49	36.90	16.92	15.60	3.37		0.39	15.99		89.78
Target				40.00	20.00	20.00				12.50	7.50	
Slag F	<0.005	0.25	0.55	36.65	18.04	16.40	3.43		0.44	11.60	5.16	92.46
Target				40.00	20.00	20.00		20.00				
Slag H	<0.005	0.12	0.61	40.30	19.12	17.20	3.90	14.31	0.45			95.98
Target				37.5	37.5	25.00						
Slag B	<0.005	0.12	0.30	36.00	34.00	22.90	4.42		1.0			99.88
Target				42.50	42.50	15.00						
Slag C	<0.005	0.12	0.31	42.00	40.50	12.80	2.73		1.05			99.51
Target				34.00	47.00	20.00						
Basicity 1.3	<0.005	0.12	0.28	31.00	40.50	17.50	2.7		0.95			93.11
Target				47.00	34.00	20.0						
Basicity 0.7	<0.005	0.13	0.26	44.70	30.97	16.5	3.572		0.49			97.06

4.2 Thermodynamic calculations

4.2.1 Effect of temperature on the percentage liquid alloy phase in the alloy systems

Figure 10 indicates the percentage liquid in the HCFeMn and MCFeMn alloys at various temperatures. Upon heating the liquid alloy phase increases and become fully liquid at about 1225°C and 1291°C for MCFeMn and HCFeMn respectively.

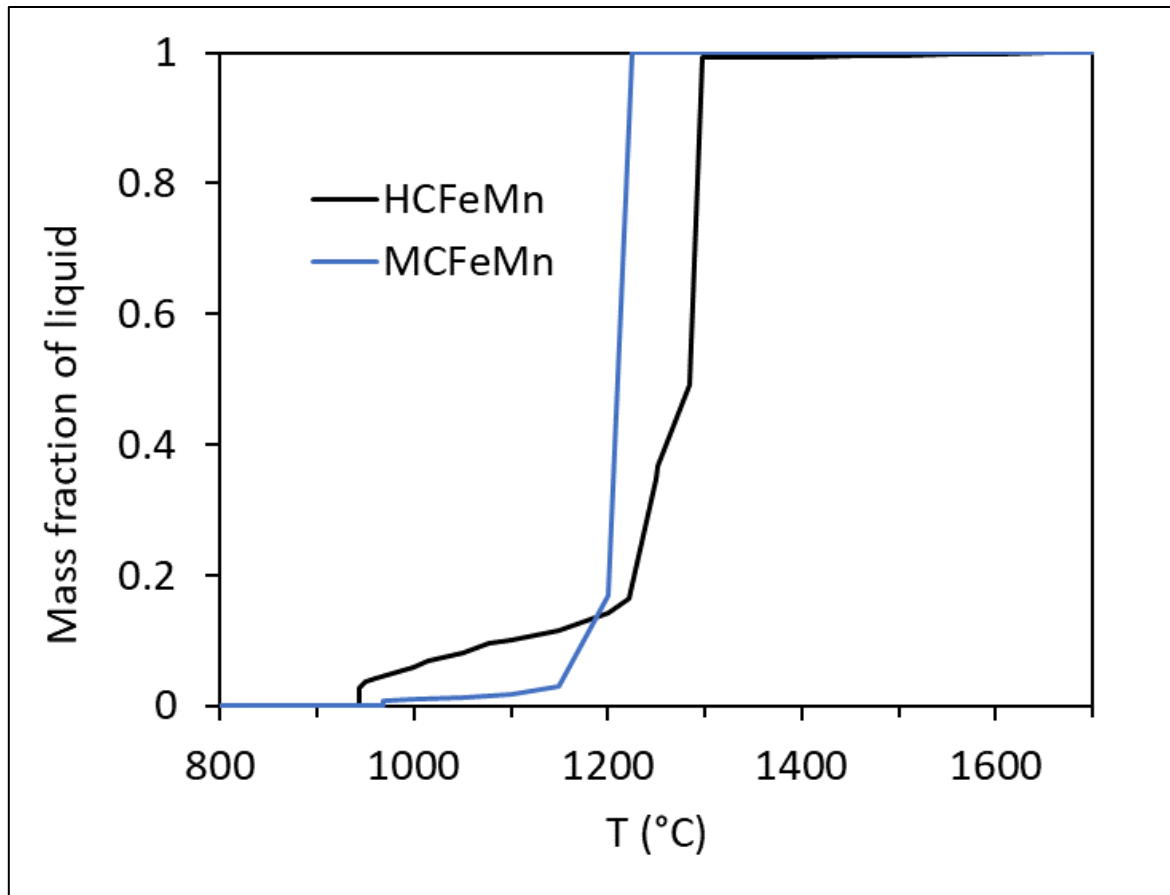


Figure 10: Mass fraction of liquid as a function of temperature for HCFeMn and MCFeMn alloys.

4.2.2 Effect of temperature on the percentage liquid slag phase in the different slag systems

Figure 11 summarizes the calculated proportion of liquid slag as a function of temperature for the different slags investigated.

Table 12 shows the summary of the liquidus temperatures of the respective slags. The results show that all the slag systems, except for Slag D and Slag B1.3, are fully molten at temperatures

$\leq 1391^{\circ}\text{C}$. The increased liquidus temperatures in both the slags was due to the effect of reduced silica content of the slag.

The results for Slags A, B and C show that increasing the MnO content while maintaining the basicity (%CaO/%SiO₂) constant, reduced the predicted liquidus temperature of the slag.

Replacing calcium oxide (in Slag A) with sodium oxide (Na₂O) (Slag E) significantly lowered the liquidus temperature of the slag. However, reducing the SiO₂ concentration (slag D) content resulted in increased liquidus temperature. Because of the higher basicity of this slag, some lime (solid solution based on CaO) is stable up to 1800 °C (the liquidus temperature of this slag). However, the slag is predicted to be 88% liquid (balance CaO solid solution) at 1218 °C.

The results show that the predicted liquidus temperature of the slag was reduced to 1266°C by replacing calcium oxide (Slag A) with barium oxide (Slag H). When adding BaF₂ (Slag I) the liquidus temperature was reduced to 1251°C. Based on the calculation results, no immiscible slag phases formed.

Table 12: A summary of the calculated liquidus temperatures of the different slags

Slag	Composition	Liquidus Temp. (°C)
Slag A	20%MnO, 40%CaO,40%SiO ₂	1327
Slag B	25%MnO, 37.5%CaO, 37.5%SiO ₂	1288
Slag C	15%MnO, 42.5%CaO, 42.5%SiO ₂	1391
Slag D	20%MnO, 40%CaO, 20%SiO ₂ -20%Na ₂ O	1800
Slag E	20%MnO, 20%CaO, 40%SiO ₂ , 20%Na ₂ O	1156
Slag F	20%MnO, 20%CaO, 40%SiO ₂ , 12%Na ₂ O-7.5%CaF ₂	1121
Slag H	20%MnO, 20%CaO, 40%SiO ₂ , 20%BaO	1266
Slag I	20%MnO, 60%BaO, 20BaF ₂	1251
SlagA basicity0.7 'Slag0.7'	20%MnO, 3.4%CaO, 46%SiO ₂	1385
SlagA basicity1.3 'Slag1.3'	20%MnO, 46%CaO, 34%SiO ₂	1640

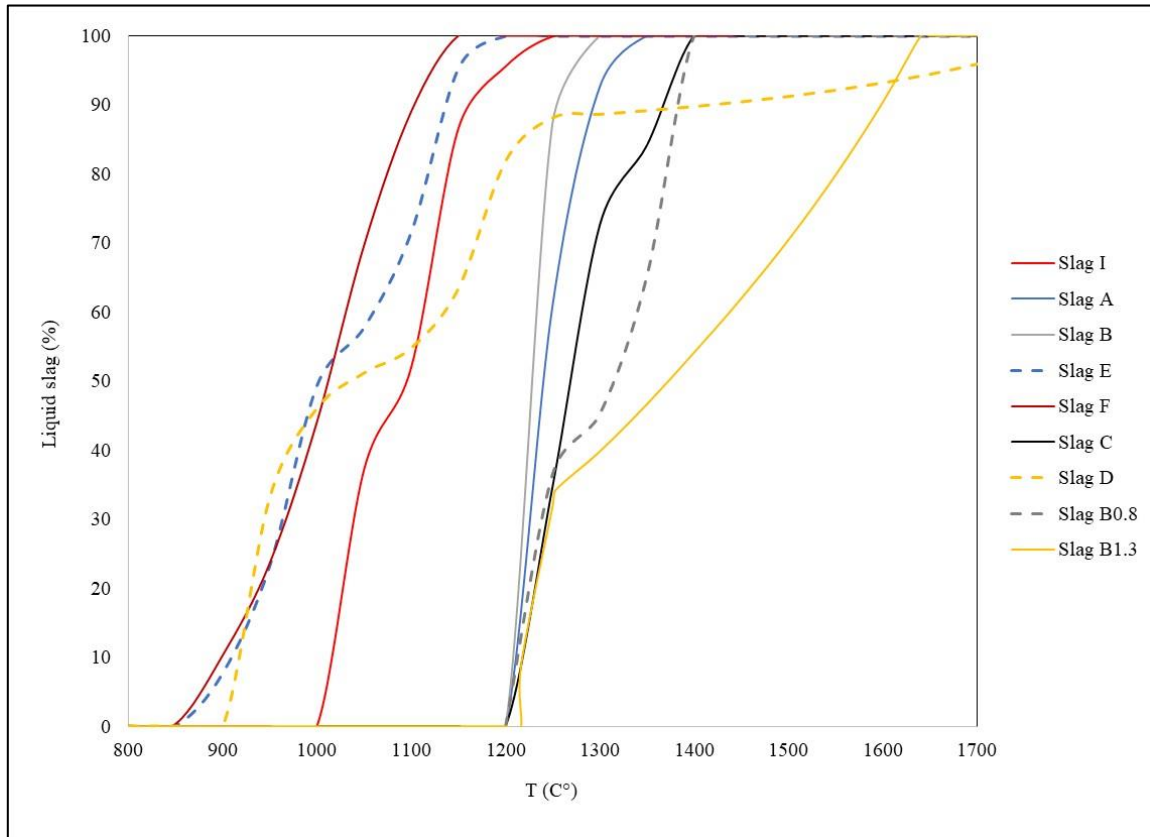


Figure 11: Percentage liquid in the different slag compositions at various temperatures

4.2.3 Phosphorus partition coefficient calculations

L_p was calculated as indicated in Equation 5. For slags system that are partially molten (Slag D and Slag B1.3) throughout the investigated temperature range, L_p was calculated for the liquid portion of the slag. The L_p values obtained from the thermodynamic calculations are presented in Figure 12 for HCFeMn and Figure 13 for MCFeMn. The calculations generally predict that dephosphorization of both alloys will not be possible with the CaO slags as the L_p achieved were well below 1. The results generally showed an increase in L_p from most of the slag-alloy systems as temperature is increased, which is unexpected.

Addition of BaO in conjunction with CaO, presented a detrimental effect with lower predicted partition coefficient obtained as indicated by slag H. Replacing both CaO and SiO₂ with BaO and BaF₂ flux, slag I resulted in higher L_p values, above 1. The predictions by FactSage, in relation to the BaO-BaF₂-MnO slag system, agree with the observations made by various researchers (Fujita, et al., 1988; Liu, et al., 1998; Chaudhary, et al., 2007; Dashevski, et al.,

1998). The effect of temperature on L_P for slag I is small compared to the opposite effect for most of the other slags.

Comparing the results obtained from the two alloys, the prediction by FactSage show that the BaO-based slag will not dephosphorise the MCFeMn alloy and lower L_P values were obtained with MCFeMn alloy. The L_P predictions for CaO-based slags were very low and not in agreement with thermodynamic analysis and findings in literature that L_P decrease as temperature is increased. Based on the results, it appears that FactSage does not accurately predict dephosphorization ratios for FeMn calculations. Experimental testwork was then necessary to compare the results to those predicted by FactSage.

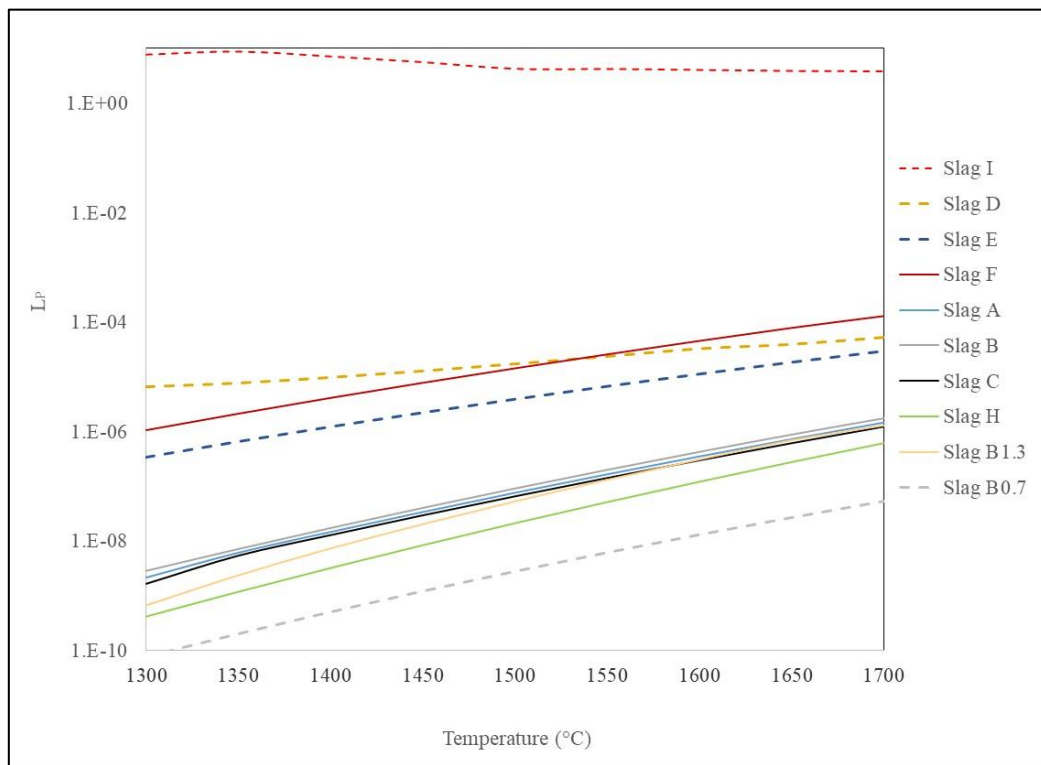


Figure 12: Predicted equilibrium P distribution coefficient for the different slags when reacted with the HCFeMn alloy. The dependent scale is log scale.

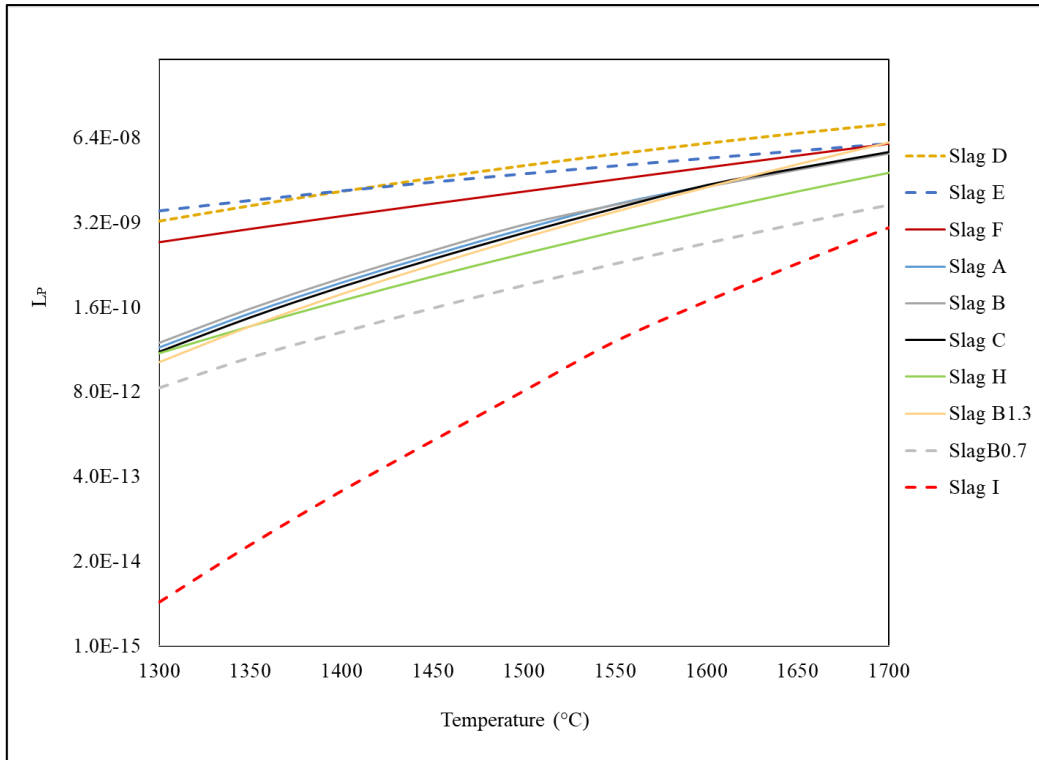


Figure 13: Predicted equilibrium P distribution coefficient for the different slags when reacted with the MCFeMn alloy. The dependent scale is log scale.

4.3 Characterization of product samples

4.3.1 Macroscopic investigation

Visual inspection showed that the slags were a dark colour varying between green and grey. The BaO-containing slags generally had a different colour and texture. In each sample, two different slag regions were observed: the first slag was dense and porous with a glassy brownish colour and was found surrounded by the alloy at the base of the crucible. The second slag region was porous and creamy-white in colour and located above slag 1, mostly at the top of the crucible, coating the crucible inner wall. The formation of the two slag phases may be attributed to the possible variation in the cooling rate of the slag during quenching. During quenching it was observed that the BaO and Na₂O slags foamed and a fraction escaped the crucible. Slag foaming could result in possible reduction of Na₂CO₃ and BaCO₃ by C (from the crucible) generating gas.

The alloys generated from the tests generally had similar appearance. Alloy globules were concentrated at the base of the crucible. In samples obtained at the lower temperature, alloy globules were entrained in the slag. The non-entrained alloy droplets were attached to the

crucibles and this created challenges with separating the graphite from the alloy. Because of the relatively small size of the alloys, shaving off the graphite was also a challenge. The typical appearances of the product samples are shown in Appendix B, Figure B1.

4.3.2 Bulk chemical compositions

The analytical results of the alloys and slags are reported in Table B2 and Table B3 in Appendix B. The 5 minutes retention time at 1350°C was not sufficient to allow separation of the alloy from the slag. Small alloy globules (about 2 mm in size) were entrained in the slag and were difficult to separate. Analysis of the samples could not be completed due to the inability to separate the product samples. As mentioned earlier, the analytical results of alloy samples generally reported Ca as part of the alloy analysis. The slag compositions indicated high Fe contents. Conditions in these tests were not sufficiently reducing to result in dissolved calcium in the alloy, so any analysed Ca must indicate that some slag was included in the alloy analysis. Furthermore the conditions were not sufficiently oxidising to form significant FeO, so Fe reported in the slag analysis reflected alloy entrainment. There was also no indication of FeO in the slags by the micro-probe analysis. The difficulties encountered in sufficiently separating the product samples had a negative impact on the compositions of the product samples and also on L_p calculations. This then required characterization of the product samples by EMPA to assess the effect of the slag/alloy entrainment on the P analysis and conduct mass balance to correct the compositions of the product samples.

4.3.3 Slag/alloy proportioning utilising X-ray tomography

Figure 14 shows the 3D images. Included is the summary of the volumes defined from the respective segments. The analysis was only completed on one sample, namely slagH+MCFeMn tested at 1400°C for a retention time of 30 minutes. Due to non-availability of the instrument, more samples could not be analysed. The 3D image stack was imported into VG Studio and subsequently processed in four parts. The lower comprising mostly metal (slices 50 through 145). The next level comprised mostly the denser slag (slices 146 through 250), with a combined dense and porous slag mix in slices 251 through 668. The uppermost segment was predominantly air from slice 669 through 1014. In all four segments the crucible was removed graphically using the region growing function in the software.

The following challenges were however encountered:

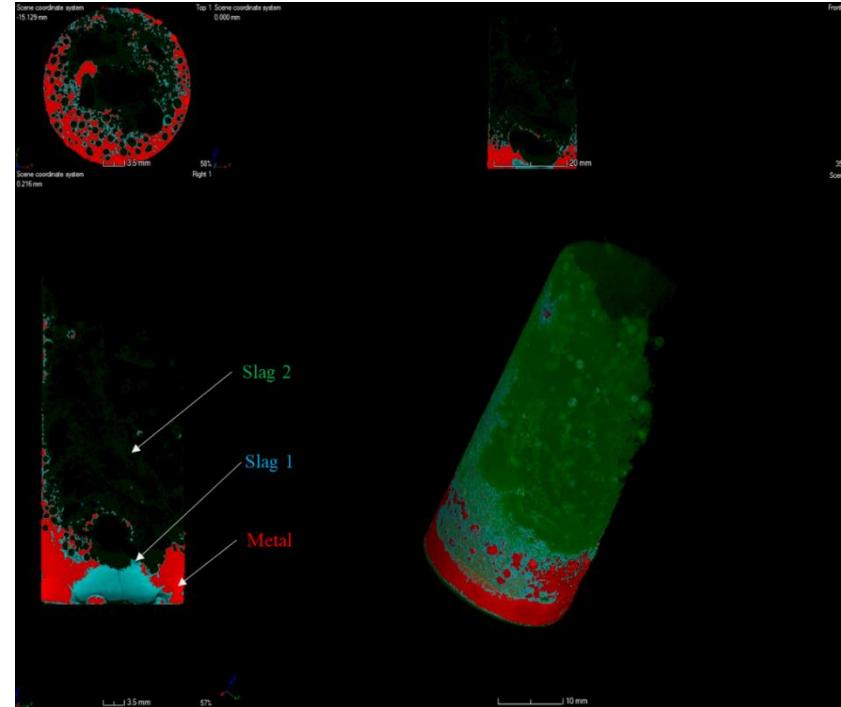
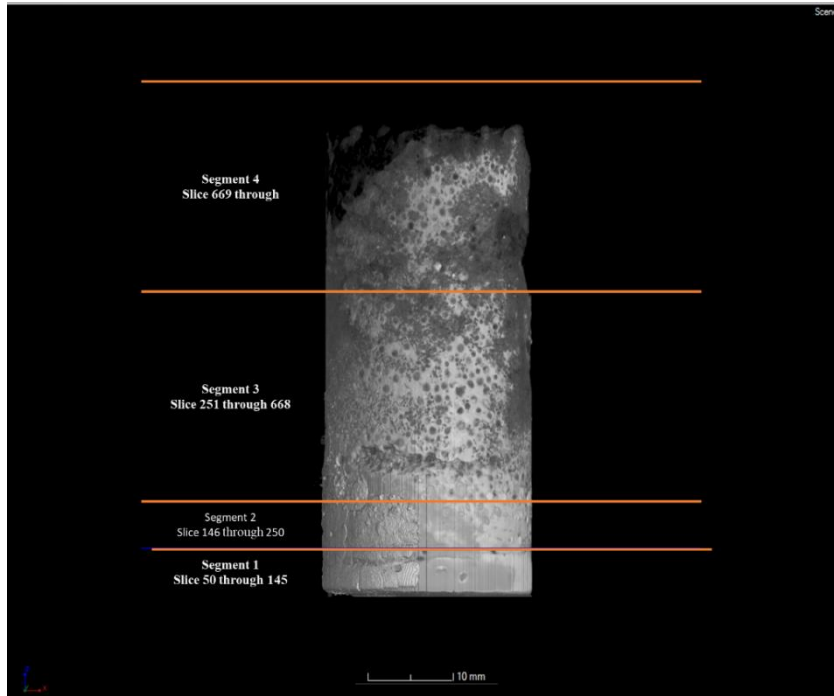
- The sample size limited the resolution. The best possible resolution was 15 $\mu\text{m}/\text{voxel}$, if the sample was scanned in vertical segments. Vertical segment stacking had challenges.
- The sample density was high. The use of a very long exposure to get sufficient X-ray transmission was then considered.
- The density contrast between the porous slag in the top and the metal at the bottom was very wide. It was not possible to balance the grey levels across independently scanned vertical segments.
- The scan time was over 30 hours for a good quality scan.
- As a compromise, the whole crucible was scanned in one run. With consideration for preserving the detector, a lower power x-ray setting with a lower than ideal exposure time was used.
- The data was compressed resulting in a pixel resolution of 56 μm .
- The low power and the low exposure resulted in beam hardening artefacts (in other words the grey levels are in a wide range across the metal for example), and there are grey level overlaps between different phases.

Table 13 shows the summary of the respective volumes of the crucible contents, i.e. alloy, less-dense slag 1 and denser slag 2. Based on the results, the volume occupied by the alloy was measured as 1.372 mm^3 , that of the lower-density slag 1 was 3.103 mm^3 without pores and that of slag 2 was 3.507 mm^3 . The reported slag volumes were larger than anticipated, as discussed below.

Based on the bulk analyses of the alloy and the combined slag, the density of the respective products were estimated from literature, as 7.3 g/cm^3 for the alloy and 3.1 g/cm^3 for the slag (Eramet, 2013) (Mills & Keene, 1987). The measured volumes were then used to calculate the masses of the alloy and the combined slag. The calculated alloy mass was 10 g, agreeing with the mass actually used for the dephosphorization tests. However, the measured slag mass was much larger than anticipated at 20 g, the actual calculated mass was 16 g. The higher measured slag mass reflects the uncertainties of true volume measurement of the foamed slag.

Table 13: A summary of the volumes obtained from the X-Ray tomography analysis, with the estimated masses assuming the phases to be dense

Summary	volume (mm ³)	density (g/cm ³)	mass g
Total Metal	1,371.81	7.3	10.01
Total Slag 1	3,103.26	3.1	20.49
Total Slag 2	3,507.01		
Total solid volume	11781.423		



	mm ³			mm ³	
Segment 1	Total Volume (with voids)	2,150.690	Segment 3	Total Volume (with voids)	10,571.000
	Total Volume (solids)	2,132.960		Total Volume (solids)	3,777.670
	Metal Volume	1,338.510		Metal Volume	19.670
	Slag 1 Volume	794.451		Slag 1 Volume	2248.110
	Slag 2 Volume	0.000		Slag 2 Volume	387.600
Segment 2	Total Volume (with voids)	2,660.309	Segment 4	Total Volume (with voids)	8,217.830
	Total Volume (solids)	2,256.793		Total Volume (solids)	3,614.000
	Metal Volume	13.550		Metal Volume	0.084
	Slag 1 Volume	1,813.812		Slag 1 Volume	323.143
	Slag 2 Volume	660.766		Slag 2 Volume	2,458.798

Figure 14: X-Ray Tomography scans with the summary of the volumes measured at the different segments.

4.3.4 *Electron Microprobe analyses*

The sample from the X-Ray Tomography analysis was characterised by EMPA and a comparison between the EMPA results and the bulk chemical results was made.

Figure 15 and Figure 16 show some of the backscattered electron images and the elemental chemistry of the randomly picked areas of the alloy and slag respectively. Other images and analysis are included in Appendix C.

The general observation made from the results are as follows:

1. Infiltration of the alloy and slag into the crucible was observed
2. Two phases with different compositions were observed in the alloy. P was detected in the phase with relatively low C content.
3. The slag is made up of MnO-CaO-BaO silicate phase. The analysis of the different point appear to be somewhat similar. The slag is mainly comprised of MnO t at 39% followed by SiO₂ at 36%, then CaO at about 14% and BaO at 11%. The concentraton of P varied between 0.01-0.03% P₂O₅.
4. FeO was barely detected in the silicate phases. The results suggest that the Fe-oxide in the starting slags was reduced by the carbon, from the graphite crucible, during the experiments.

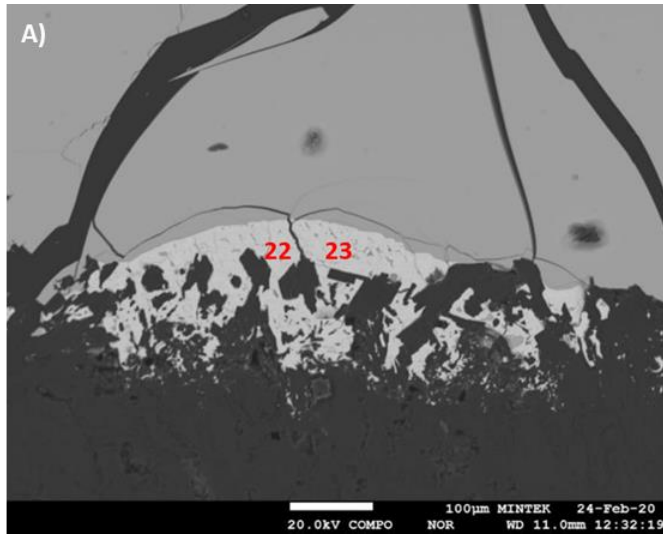
Table 14 and Table 15 represent the comparison between the bulk chemical analysis and the EMPA analysis for the alloy and slag respectively for slag H-MCFeMn sample. The alloy P content was higher from the EMPA analysis. This suggest that there was underestimation of the element during the bulk chemical analysis. The EMPA analysis showed no presence of Ca in the alloy. In terms of the slag analysis, the EMPA analysis showed near-zero FeO content in the slag. This supports the observation that separation of the slag and alloy was not done successfully during sample preparation for the bulk chemical analysis. Included in Table 14 and Table 15 are the original ICP-OES results, there was no significant difference between the original and corrected results.

Table 14: The comparison between the average EMPA alloy chemistry and the bulk chemical composition of the alloy for slag H-MCFeMn 1400°C, 30 minutes sample.

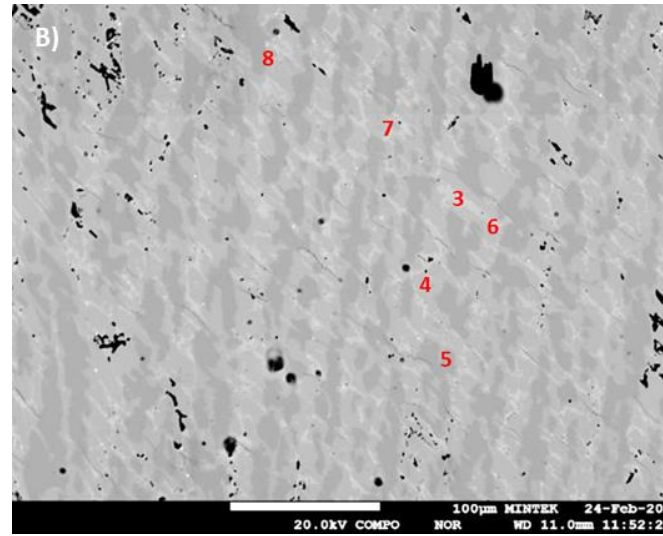
Alloys	C	S	P	Si	Ca	Mn	Fe	Total
EMPA (average)	8.38	0.00	0.25	0.54	0.00	64.14	27.37	100.99
Original ICP-OES	7.49	0.00	0.07	0.550	0.18	64.96	26.43	99.960
Corrected ICP-OES	7.48	0.00	0.07	0.27	0.00	64.47	26.43	98.73

Table 15: The comparison between the average EMPA alloy chemistry and the bulk chemical composition of the slag for slag H-MCFeMn 1400°C, 30 minutes sample.

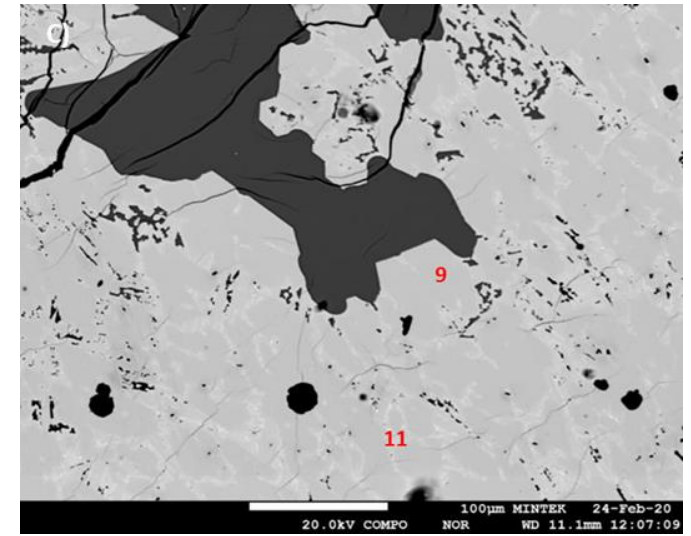
Slags	C	S	P ₂ O ₅	SiO ₂	CaO	MnO	FeO	BaO	Total
EPMA(average)		0.03	0.02	36.89	13.30	39.07	0.03	11.16	100.50
Original ICP-OES	0.460	0.05	0.02	30.30	14.70	39.00	0.10	10.00	95.43
Corrected ICP-OES	0.438	0.05	0.02	30.30	14.70	38.75	0.00	10.00	95.07



Position	C	Si	Mn	Fe	Total
23	9.51	0.02	69.70	20.66	99.89
22	9.34	0.03	70.76	20.65	100.78

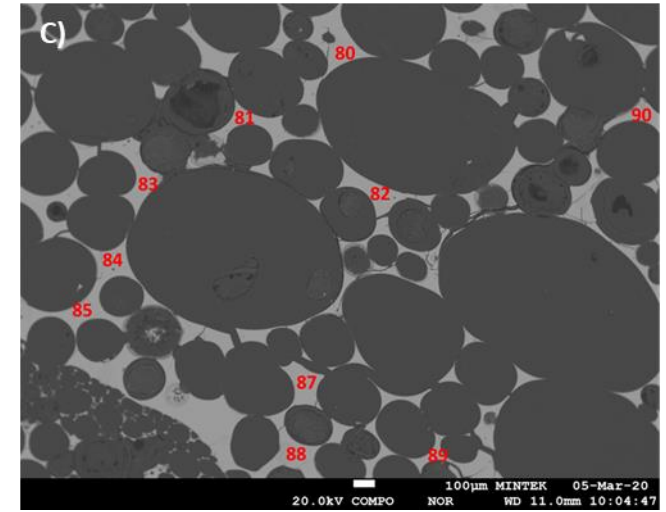
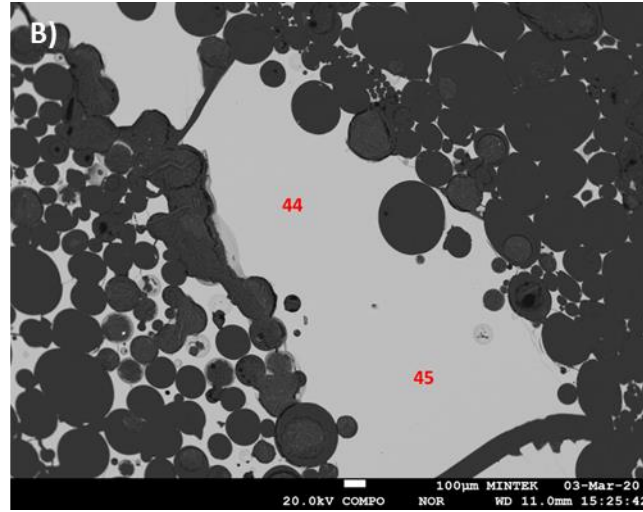
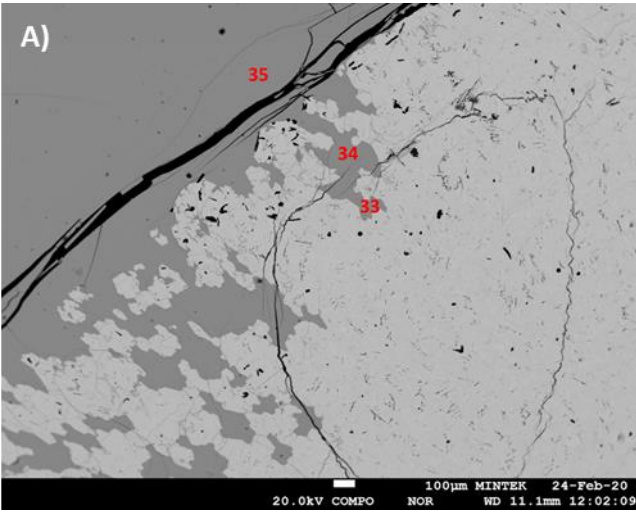


Point	C	P	Si	Mn	Fe	Total
3	8.08	0.33	0.41	62.44	28.47	99.74
4	8.74	-	-	64.49	26.44	99.68
5	10.41	-	0.02	68.64	21.23	100.30
6	5.29	0.66	1.83	59.86	30.87	98.52
7	7.76	0.35	0.49	64.05	26.71	99.37
8	10.24	-	-	69.81	20.96	101.00



Point	C	P	Si	Mn	Fe	Total
9	10.45	-	0.03	69.61	20.53	100.62
11	5.07	0.66	1.16	61.89	29.79	98.57

Figure 15: Electron Backscattered images and analysis of A) alloy nugget at the bottom of the crucible B) alloy at the bottom of the crucible C) alloy at the alloy-slag interface for slag H-MCFeMn 1400°C, 30 minutes sample.



Point	S	CaO	SiO ₂	MnO	FeO	BaO	Total
33	0.03	13.35	35.01	39.49	0.11	11.07	99.10
34	-	13.71	32.55	39.49	-	10.88	96.40
35	-	14.08	34.89	39.13	-	10.90	99.01

Point	S	P ₂ O ₅	CaO	SiO ₂	MnO	BaO	Total
44	0.03	0.02	13.41	36.27	39.22	11.18	100.18
45	-	-	14.03	34.80	39.29	10.95	99.08

Point	S	P ₂ O ₅	CaO	SiO ₂	MnO	BaO	Total
80	-	-	13.35	37.57	39.23	11.34	101.48
81	-	-	14.20	37.82	39.35	11.35	88.52
82	-	-	14.18	37.95	39.16	11.35	88.46
83	0.06	0.01	13.36	36.90	39.42	11.36	101.20
84	-	-	14.16	38.32	39.11	11.39	88.82
85	-	-	13.23	37.83	38.93	11.26	101.26
86	-	-	14.18	38.13	39.29	11.34	88.76
87	-	-	14.21	37.80	39.37	11.28	88.45
88	-	-	14.22	38.05	39.09	11.39	88.53
89	0.02	0.01	13.38	37.55	39.23	11.31	101.54
90	-	0.03	13.35	37.42	39.39	11.38	101.57

Figure 16: Electron Backscattered images and analysis of A) Slag at the alloy-slag interface, B) & C) low dense porous slag at the upper part of the crucible for slag H-MCFeMn 1400°C, 30 minutes sample.

4.3.5 Elemental mass balance calculations

Table 16 and Table 17 present the corrected chemical compositions of the alloys and slags respectively from the MCFeMn dephosphorization tests. Included also are the masses of the alloys and slags calculated from the Ca-Fe mass balance calculation. The analytical results of the alloy generally showed increased C contents between 5%-8%. The results suggest that there was dissolution of C from the graphite crucible as the alloy was undersaturated with carbon. Figure 17 shows the equilibrium C concentrations of FeMn alloy at different temperatures calculated from FactSage. For the temperatures investigated, i.e. 1350°C to 1450°C, the %C saturation is in a range of 7.04%-7.25%.

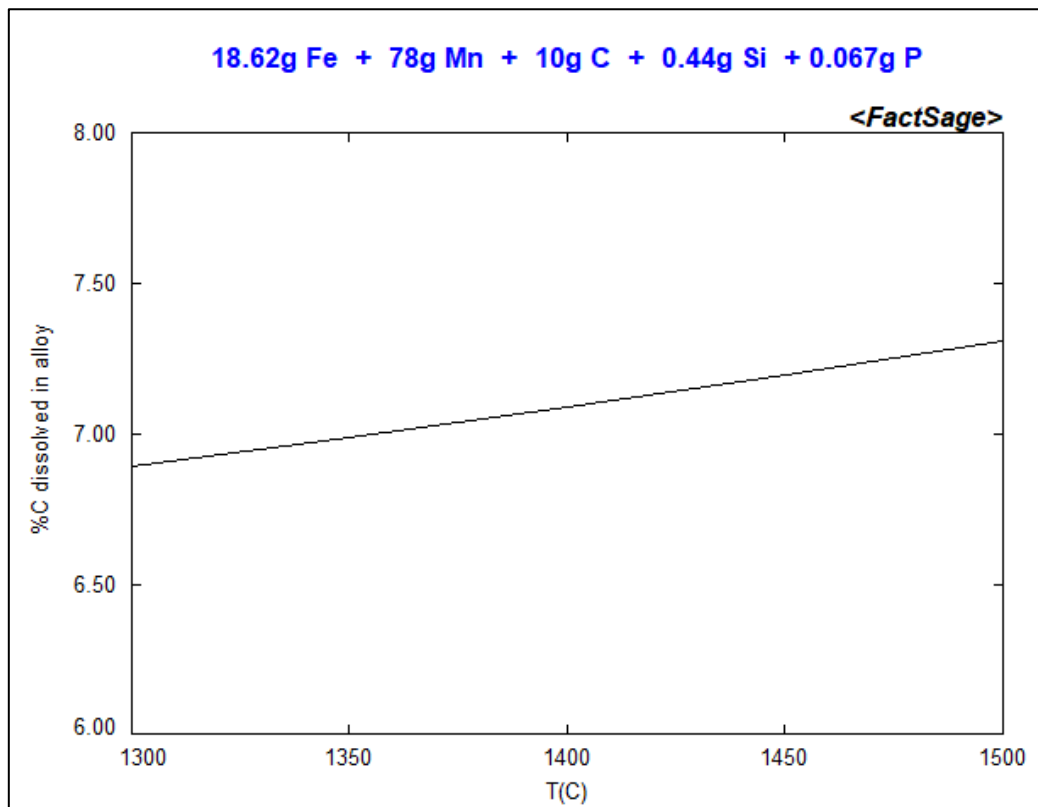


Figure 17: C content of FeMn alloy as a function of temperatures.

Observed also from the chemical compositions are the lower Mn and higher Fe contents, when compared to the starting alloy composition. This suggested that oxidation of Mn had occurred during the experiments. The P contents were apparently higher in most alloys than in the starting alloy. The higher P content may be attributed to factors such as the loss of Mn in the alloy which lead to increased P concentration and removal of P from the slag to the alloy as the starting slags contained P. The calculated alloy masses varied between 6 g and 10 g.

The analytical results of the slags show increased MnO contents in the slags showing the effect of Mn oxidation from the alloy. Low $P_2O_5 \leq 0.05\%$ contents were generally observed. It appears from the results that no significant dephosphorization was achieved. The calculated slag masses varied between 9 g and 20 g, higher than the starting mass.

Table 18 and Table 19 represent the corrected chemical compositions of the alloys and slags respectively from the HCFeMn dephosphorization tests. Comparing the compositions of the alloys to that of the starting alloy, an increase in the Fe content and reduction in the Mn contents were observed, similar to the MCFeMn alloy tests. The P contents in the reacted alloys were also generally higher than that of the starting alloy, containing 0.061%-0.097% P. As previously mentioned, the higher P content may be attributed to factors such as the loss of Mn in the alloy which lead to increased P concentration and removal of P from the slag to the alloy as the starting slags contained P. Based on the results, dephosphorization of the HCFeMn alloy was not possible under these conditions.

The analytical results of the slags report a higher MnO content in the slags in a range of 25%-39%, the initial concentration was about 20% or less. This resulted in dilution of the other major slag components (SiO_2 and CaO). Minor amounts of C were also analysed in most of the slags, likely originating from the graphite crucible. The loss of Mn is influenced by the oxygen partial pressure in the system. Factors that may have contributed to the loss of Mn include air ingress during the test, exposure of the alloys to oxygen during quenching and possibly the presence of CO_2 from $BaCO_3$ and MnO_2 (the source of MnO in the slags) increasing the oxygen partial in the system.

Table 16: Corrected bulk chemical composition of the alloys produced at different temperatures and retention times from MCFeMn dephosphorization reactions

T	time	Alloy	C	S	P	Al	Si	Mn	Fe	Total	Mass, g
Before reaction			1.600	0.010	0.069		0.440	78.700	18.620	99.47	10.00
1350°C	5 min	A-H									
	30 min	Alloy A	7.990	0.006	0.090	0.007	0.208	65.931	22.700	96.938	9.56
		Alloy E	3.840	0.010	0.053	0.094	3.698	47.854	22.100	77.651	9.81
		Alloy F	7.799	<0.005	0.104	0.014	0.129	58.894	26.400	93.343	8.19
		Alloy H	7.045	0.007	0.107	0.013	0.416	65.937	23.000	96.533	9.49
	60 min	Alloy A	5.691	<0.005	0.053	0.233	<0.005	65.785	24.000	95.763	9.00
		Alloy E	6.475	<0.005	0.054	<0.005	<0.005	60.715	23.162	90.406	9.36
		Alloy F	7.696	0.006	0.111	0.016	1.235	60.972	27.400	97.436	7.92
		Alloy H	6.686	0.008	0.090	<0.005	2.396	62.919	27.000	99.099	8.16

T	time	Alloy	C	S	P	Al	Si	Mn	Fe	Total	Mass, g	
1400°C	5 min	Alloy A										
		Alloy E	6.986	0.006	0.130	0.265	0.297	62.943	26.300	96.927	8.20	
		Alloy F	6.108	0.006	0.141	0.274	0.595	62.568	26.970	96.661	8.04	
		Alloy H	6.280	0.005	0.131	0.243	0.098	65.859	25.500	98.116	8.64	
	30 min	Alloy A										
		Alloy E	6.730	0.006	0.077	<0.005	<0.005	61.861	27.900	96.577	7.76	
		Alloy F	7.646	0.007	0.076	<0.005	<0.005	63.512	26.400	97.643	8.22	
		Alloy H	7.483	0.000	0.072	<0.005	0.270	64.472	26.430	98.727	8.38	
	60 min	Alloy A	6.890	<0.005	0.103	<0.005	0.327	66.272	25.700	99.294	8.44	
		Alloy E	5.440	<0.005	0.112	0.006	0.231	64.322	27.400	97.513	7.94	
		Alloy F	7.296	<0.005	0.140	<0.005	0.363	65.192	23.500	96.492	6.66	
		Alloy H	6.769	<0.005	0.117	<0.005	0.410	64.994	26.800	99.095	7.87	
1450°C	5 min	Alloy A	6.890	<0.005	0.096	<0.005	0.143	65.825	23.400	96.354	9.29	
		Alloy E										
		Alloy F	6.700	<0.005	0.119	0.012	0.181	60.596	26.600	94.215	8.22	
		Alloy H	6.494	<0.005	0.097	<0.005	0.279	64.483	24.000	95.356	9.04	
	30 min	Alloy A	6.854	<0.005	0.053	<0.005	<0.005	69.276	21.600	97.783	10.08	
		Alloy E	5.970	<0.005	0.090	<0.005	0.278	71.512	17.500	95.350	6.58	
		Alloy F	6.898	<0.005	0.078	<0.005	<0.005	63.193	27.500	97.672	7.94	
		Alloy H	6.538	<0.005	0.076	0.032	<0.005	64.419	26.650	97.706	8.28	
	60 min	Alloy A	7.890	<0.005	0.083	0.297	<0.005	67.857	22.600	98.730	9.53	
		Alloy E	6.888	0.005	0.093	<0.005	0.105	65.428	22.900	95.421	6.33	
		Alloy F	7.390	0.005	0.087	<0.005	<0.005	66.958	22.200	96.640	6.92	
		Alloy H	7.580	<0.005	0.095	0.036	<0.005	62.250	26.400	96.362	8.32	

Table 17: Corrected bulk chemical composition of the slags produced at different temperatures and retention times MCFeMn dephosphorization reactions

T. °C	Time		C	S	P ₂ O ₅	Al ₂ O ₃	SiO ₂	CaO	MnO	BaO	MgO	CaF ₂	Total	Mass, g	
1350	30 min	Slag A	0.000	0.038	0.105	0.420	30.589	25.900	37.345		0.400		94.79	14.4	
		Slag E	0.430	0.017	0.046	0.465	30.858	12.300	44.771		0.560		89.45	16.1	
		Slag F	0.000	0.021	0.042	0.569	28.277	14.210	43.014		0.350	3.533	90.135	14.6	
		Slag H	0.332	0.031	0.133	0.479	29.375	19.800	42.285	10.500	0.260		103.20	10.2	
	60 min	Slag A	0.874	0.029	0.107	0.229	30.600	25.900	37.466		0.400		95.605	13.9	
		Slag E	1.792	0.008	0.106	0.480	31.900	21.600	23.385		0.540		79.81	9.1	
		Slag F	1.091	0.000	0.212	0.606	35.840	18.870	10.867		1.150	3.235	82.268	11.9	
		Slag H	0.391	0.000	0.143	0.590	32.287	15.800	31.468	8.500	0.570		89.75	13.7	
1400	5 min	Slag A													
		Slag E	0.000	0.032	0.000	0.433	28.578	13.400	48.140		0.310		90.89	14.2	
		Slag F	0.159	0.030	0.000	0.405	28.060	13.542	42.286		0.350	2.665	87.524	19.8	
		Slag H	0.067	0.046	0.002	0.529	30.692	24.400	40.653	10.000	0.400		106.80	8.8	
	30 min	Slag A													
		Slag E	0.000	0.030	0.034	0.359	23.300	11.600	32.700		0.300		68.32	16.8	
		Slag F	0.134	0.035	0.017	0.450	28.000	13.655	37.720		0.320	3.491	83.833	15.6	
		Slag H	0.438	0.048	0.015	0.470	30.298	14.700	38.755	10.000	0.350		95.07	15.2	
	60 min	Slag A	0.027	0.034	0.094	0.850	30.494	20.900	39.528		0.860		92.787	17.8	
		Slag E	2.536	0.020	0.038	0.730	25.806	10.000	34.875		0.479		74.48	20.2	
		Slag F	0.454	0.029	0.000	0.640	29.158	12.388	47.456		0.600	2.503	93.239	17.3	
		Slag H	0.054	0.021	0.010	0.400	31.096	11.900	44.392	12.950	0.530		101.35	18.1	

T.°C	Time		C	S	P ₂ O ₅	Al ₂ O ₃	SiO ₂	CaO	MnO	BaO	MgO	CaF ₂	Total	mass	
1450	5 min	Slag A	0.000	0.066	0.030	0.520	31.477	26.500	30.738		0.450		89.78	14.2	
		Slag E													
		Slag F	0.000	0.038	0.014	0.479	30.585	17.900	42.162			0.360	3.831	92.18	15.2
			Slag H	0.831	0.031	0.014	0.480	31.496	14.900	37.334	12.200	0.620		97.91	13.0
	30 min	Slag A	0.153	0.037	0.030	0.590	35.500	25.800	32.346			0.480		94.93	14.8
		Slag E	0.175	0.042	0.005	0.429	26.538	12.067	46.601			0.280		86.13	16.9
		Slag F	0.099	0.047	0.000	0.560	33.098	15.289	47.728			0.390	3.082	100.30	14.9
		Slag H	0.143	0.042	0.041	0.680	31.100	13.900	42.612	11.20	0.382			100.52	15.6
	60 min	Slag A	0.000	0.069	0.040	0.669	29.700	26.050	34.841			0.460		91.83	13.6
		Slag E*	0.650	0.035	0.009	0.470	29.097	20.000	45.764			0.300		96.32	9.1
		Slag F	0.000	0.034	0.006	0.469	29.200	14.400	45.644			0.390	2.358	92.52	15.5
		Slag H	0.000	0.033	0.023	0.554	26.700	12.100	39.245	10.500	0.480			89.63	17.5

: Na₂O, not analysed

Table 18: Corrected bulk chemical composition of the alloys produced at different temperatures and retention times from industry HCFeMn dephosphorization reactions

T	Reaction time	Slag	C	S	P	Si	Mn	Fe	Mg	Total	Mass, g
Starting alloy			6.77	0.014	0.061	0.330	75.800	17.000		99.980	10.00
1350°C	60 min	Alloy A	6.988	0.006	0.075	0.140	68.296	21.700	<0.005	97.209	9.23
		Alloy E	7.360	0.007	0.110	0.310	61.300	26.900	0.006	95.993	6.99
		Alloy F	7.170	0.007	0.086	0.152	64.734	23.300	<0.005	95.452	8.60
		Alloy H	7.830	0.007	0.090	0.241	64.586	24.100	0.005	96.858	8.14
1400°C	30 min	Alloy A	7.388	0.008	0.061	0.499	64.939	22.100	0.012	95.007	10.79
		Alloy E	7.080	0.000	0.096	0.340	66.328	23.900	0.007	97.752	8.05
		Alloy F	7.508	0.000	0.091	0.337	65.281	23.000	0.008	96.225	8.20
		Alloy H	7.370	0.000	0.068	0.376	66.581	22.800	0.007	97.203	10.53

Table 19: Corrected bulk chemical composition of the slags produced at different temperatures and retention times from industry HCFeMn dephosphorization reactions

T.	time	Slag	C	S	P₂O₅	Al₂O₃	SiO₂	CaO	MnO	BaO	MgO	Total	Mass, g	
1350°C	60 min	Slag A	0.185	0.019	0.029	0.900	33.186	27.500	27.197		0.540	93.13	12.1	
		Slag E												
		Slag F	0.000	0.013	0.007	0.360	32.884	15.800	43.046			0.630	92.74	15.6
		Slag H	0.062	0.017	0.000	0.517	24.677	10.600	26.379	10.750		0.478	73.48	21.3
1400°C	30 min	Slag A	0.211	0.008	0.021	0.570	40.464	31.900	20.170		0.369	93.71	12.8	
		Slag E	0.292	0.011	0.000	0.480	32.982	14.700	43.006			0.420	91.89	16.9
		Slag F	0.215	0.021	0.053	0.420	32.857	17.100	39.099			0.439	90.20	16.6
		Slag H	1.673	0.021	0.013	0.460	32.188	14.500	46.740	14.070		0.530	110.19	17.4

Figure 18 presents the box plot for overall accountabilities of Mn, P and Si calculated from the mass balance calculations. The results indicate that the masses of Si and Mn in the product were overestimated and P was underestimated. The over accountability of Mn and Si may results from errors associated with the correcting the elemental composition in the two phases as well as analytical errors. Accountabilities of P are generally prone to large errors, due to their low concentration in the samples, and introduces large uncertainties in the analysis of the element. The low accountability might be attributed to the errors associated with the analysis of the element and errors associated with the correcting the elemental composition in the two phases.

Figure 19 shows the comparison between the overall accountability of C from the two alloys. The results show excessively high accountabilities from the tests with MCFeMn. The lower average accountability close to 100% was only obtained from tests done with HCFeMn alloy. The high accountabilities obtained with MCFeMn alloy are as a result of the dissolution of the graphite crucible into the alloy.

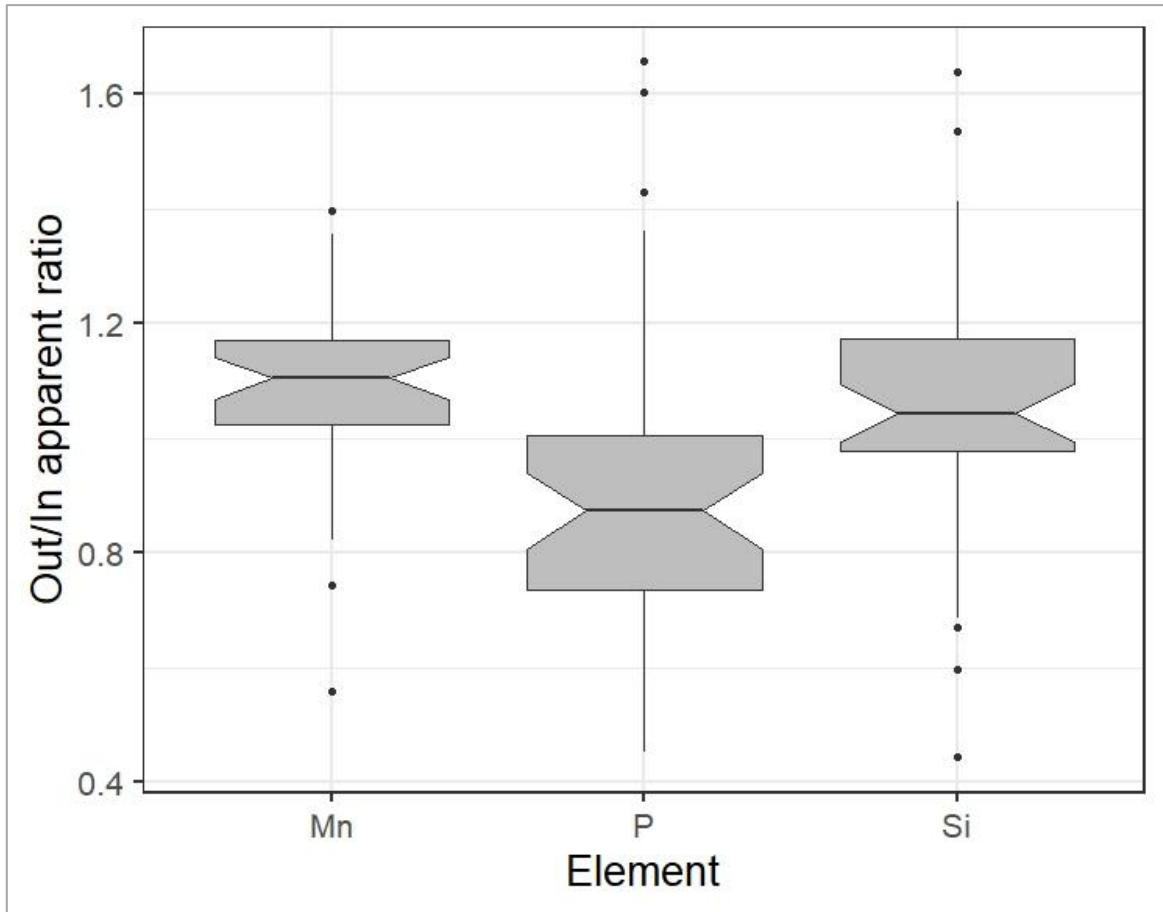


Figure 18: Box plot of out/in apparent ratio for Mn, P and Si.

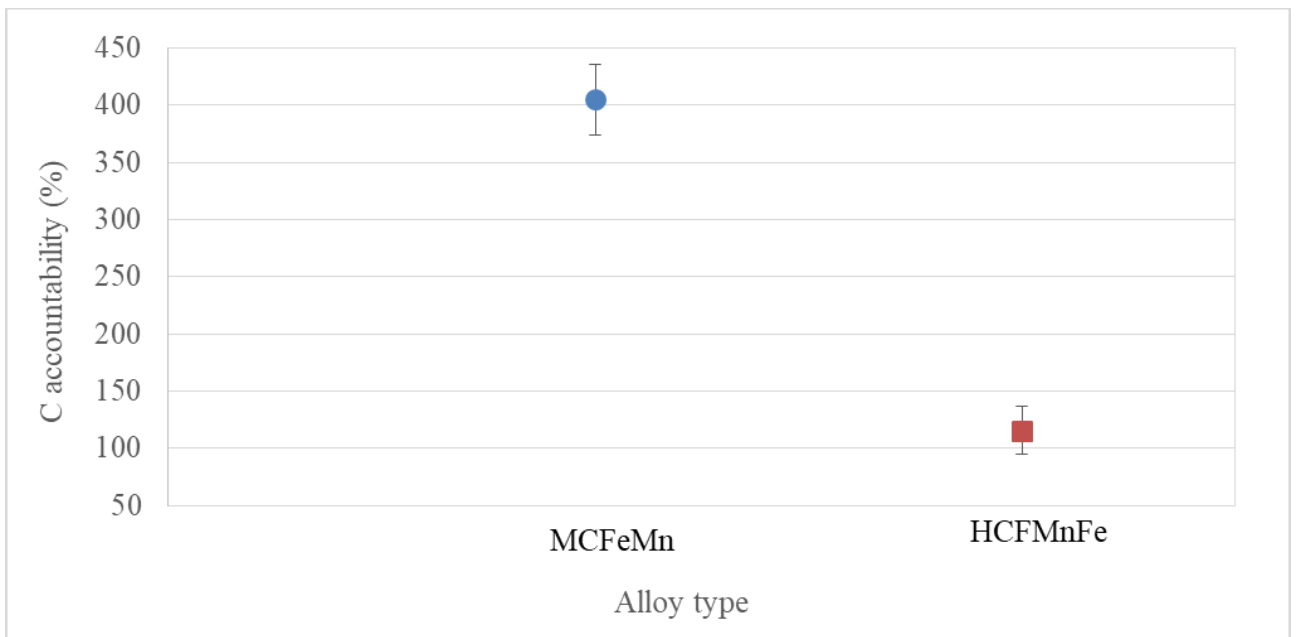


Figure 19: The average C accountabilities. Error bars indicate the 95% confidence levels on the mean.

4.3.6 Phosphorous partition coefficient

Table 20 presents a summary of the L_p values obtained from the experiment. The results generally show that the L_p remained small (<1), in line with the previous conclusion that a significant amount of P remained in the alloy and little or no dephosphorization occurred.

The results show that the baseline slag CaO-SiO₂-MnO slag (Slag A) appeared to yield relatively higher L_p values when compared to the other slags at the temperatures and reaction times investigated.

Table 20: A summary of the L_p values obtained from the experiments

Temperature, time		L_p
1350°C, 30 min	Alloy A	0.507
	Alloy E	0.385
	Alloy F	0.178
	Alloy H	0.542
1350°C, 1 hr	Alloy A	0.875
	Alloy E	0.862
	Alloy F	0.839
	Alloy H	0.693
1400°C 5 min	Alloy H	0.007
1400°C, 30 min	Alloy E	0.193
	Alloy F	0.098
	Alloy H	0.088
1400°C 60 min	Alloy A	0.401
	Alloy E	0.146
	Alloy H	0.036
1450°C 5 min	Alloy A	0.136
	Alloy F	0.053
	Alloy H	0.065
1450°C, 30 min	Alloy A	0.245
	Alloy E	0.024
	Alloy H	0.276
1450°C, 60 min	Alloy A	0.214
	Alloy E	0.040
	Alloy F	0.032
	Alloy H	0.104
Industry HCFeMn 1350°C, 1 hr	Alloy A	0.169
	Alloy F	0.033
Industry HCFeMn 1400°C, 30 min	Alloy A	0.153
	Alloy F	0.253
	Alloy H	0.082
MCFMN B 1450°C 30min	Slag B	0.147
MCFMN C 1450°C 30min	Slag C	0.101
MCFMN A basicity 1.3 1450°C 30min	Slag A	0.130

4.3.7 Degree of dephosphorization

Based on the analytical results and the low P accountabilities achieved, the degree of dephosphorization suffered large uncertainties. Based on the aforementioned challenges, no plausible conclusion could be made on the degree of dephosphorization achieved for the investigated industry alloys.

The preliminary results obtained from the sampling tests conducted at 1400°C, indicated on Table 21 have indicated that P removal from the HCFeMn master alloy was achieved with the Slag I (20%MnO-60%BaO-20%BaF₂) system. A summary of the other results is given in Appendix A, Table A2. The results showed that Slag I achieved 26% and 23% dephosphorization at 5 minutes and 60 minutes reaction times respectively. The sampling of the associated slags was unsuccessful. The use of this slag during the testwork posed numerous challenges and could not be investigated further. Dephosphorization of the master alloy with the other slag systems at the specified conditions was not possible. The use of the CaO free slag, i.e. using BaO solely as the basic oxide and BaF₂ as a flux thus appeared to be relatively effective for dephosphorization, however the results are not conclusive. Chaudhary, et al, (Chaudhary, et al., 2007) achieved 63% dephosphorization at 1400°C after 5 minutes using an alloy that comprised of C-3.50%, Mn-67.60%, P-0.49%, Si-0.36% and pre-calcined 64%BaO-24%BaF₂-12%MnO slag. The lower degree of dephosphorization achieved in the current study may be attributed to the difference in the master alloy.

Table 21: Degree of dephosphorization obtained with MnO-BaO-BaF₂ slag at 1400°C.

Time	Alloy	Slag	%P _{initial}	%P _{final}	Degree of dephosphorization
5 min	HCFeMn master alloy	20%MnO-60%BaO-20%BaF ₂	0.082	0.063	26.8%
60 min				0.060	23.2%

5 DISCUSSION

Based on the bulk chemical analysis the P contents of alloy products were generally higher than in the starting alloy. The higher P content may be attributed to the loss of Mn in the alloy which led to increased P alloy concentration. The starting slags also had P as an impurity, which may have led to reversion of P from the slag to the alloy. The slag analytical results showed a higher MnO content in the slags in a range of 25%-39%, the initial concentration was about 20% or less. This resulted in dilution of the other major slag components (SiO_2 and CaO) and possibly P. The loss of Mn is influenced by the oxygen partial pressure in the system. Factors that may have contributed to the loss of Mn include possible air ingress during tests and the exposure of the alloys to oxygen during quenching, as Mn has a high affinity for oxygen. Liu, et al (Liu, et al., 1995) observed the use of CaO , SiO_2 and CaF_2 to dephosphorise ferro-manganese melts resulted in increased Mn losses to the slag. Watanabe, et al (Watanabe, et al., 1993), reported that MnO in a basic slag acts as an acidic oxide which may consume the basic effect of the slag reducing the capacity of the slag to remove P from the alloy. The presence of MnO in the slag is important to provide the oxidizing atmosphere, however high MnO content can lead to low dephosphorization (Chaudhary & Roy, 2001).

Figure 20 shows the predicted oxygen potentials of the different systems with temperature, included is the P_{O_2} trends for C/CO equilibrium reactions which represents the reaction of C with any O_2 in the system that may result from air ingress. FactSage predicts that the P_{O_2} for the C/CO equilibrium reaction was higher than for the slag-alloy equilibrium reactions at temperatures lower than 1390°C for MCFeMn-SlagA/B/C and MCFeMn-Slag H systems. Oxidation of Mn may have occurred at temperature lower than 1390°C for the aforementioned slag-alloy systems. For slagF/E-MCFeMn systems, oxidation of Mn was feasible even at higher temperatures up to about 1440°C . The loss of Mn during the experiment may be attributed to air ingress during the experiment as well as exposure of the alloys to air during quenching.

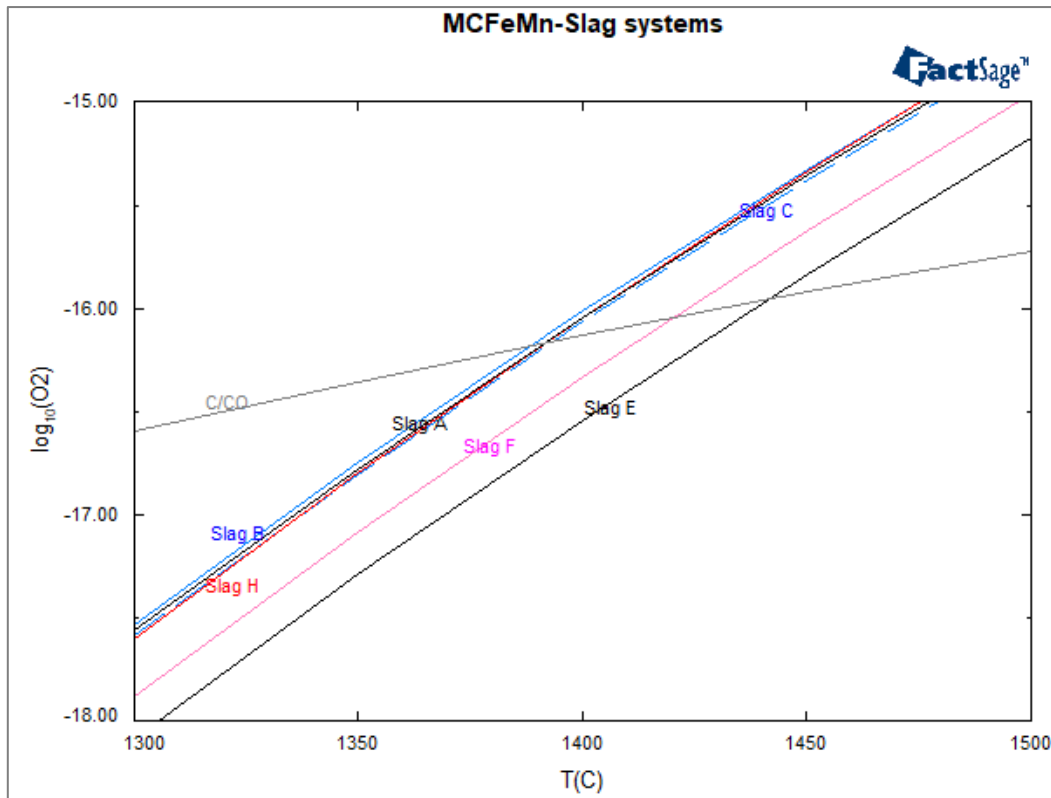


Figure 20: Predicted oxygen partial of different slag/MCFeMn systems.

5.1 Phosphorus partition coefficient

Figure 21 and Figure 22 show the L_p values obtained at different temperatures for reaction times of 30 minutes and 60 minutes, respectively. The results show that the baseline slag CaO-SiO₂-MnO slag (Slag A) appeared to yield relatively higher L_p values when compared to the other slags at the temperatures and reaction times investigated.

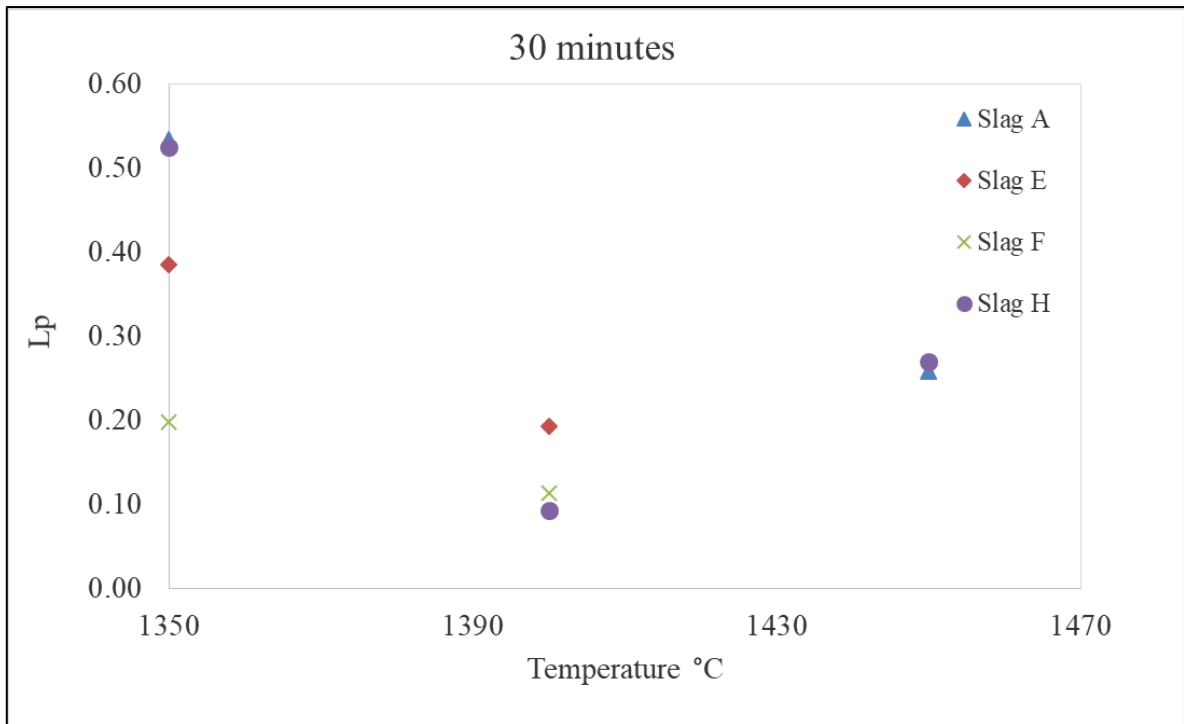


Figure 21: L_p values obtained at different temperatures for MCFeMn alloy; 30 minutes reaction time.

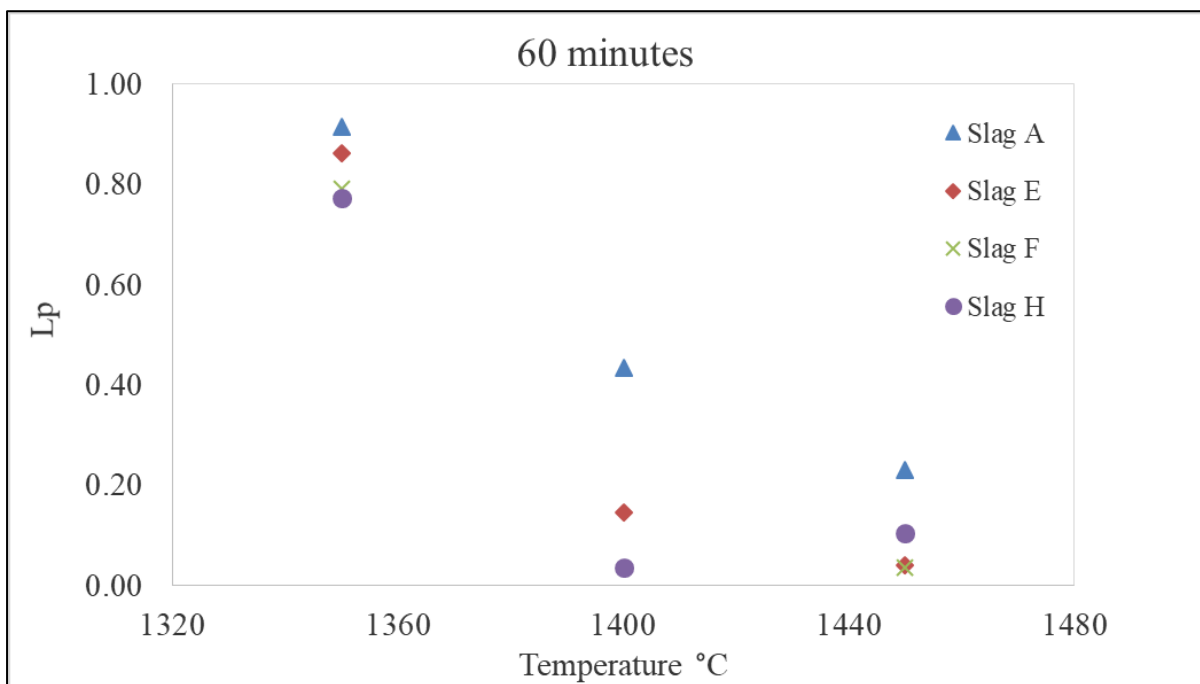


Figure 22: L_p values obtained at different temperatures for MCFeMn alloy; 60 minutes reaction time.

5.1.1 Effect of changing MnO content of base-line slag

Figure 23 shows the L_p obtained at the three initial MnO slag contents at 1450°C, 30 minutes reaction time. Figure 24 represents the L_p versus the final MnO slag contents, which show increased MnO contents in the final slags.

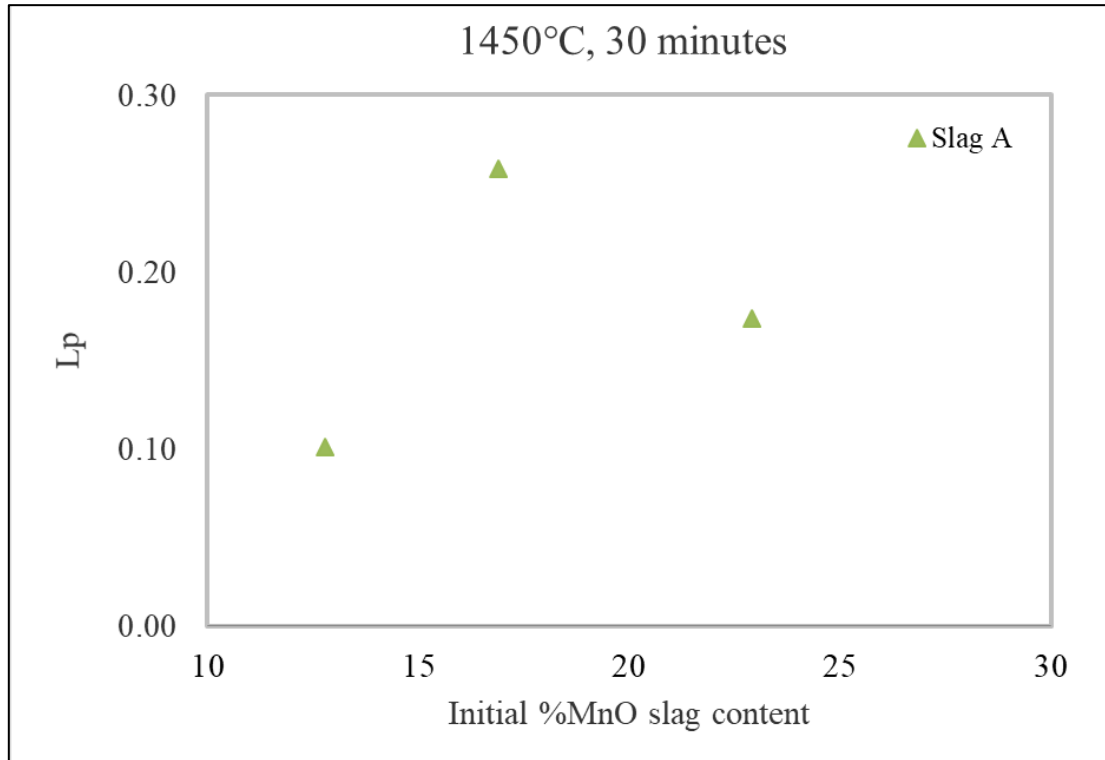


Figure 23: Effect of starting MnO content in the starting slag on L_p at 1450°C and 30 minutes retention time for MCFeMn alloy.

The L_p results show that there was an increase in L_p from 15% to 20% MnO, thereafter a reduction in the partition ratio was obtained. High amount of MnO may affect the activity of the basic oxides such as CaO and BaO in the slag and can reduce the capacity of the slag to absorb P. Chaudhary, et al (Chaudhary, et al., 2007) observed that an increase in the MnO content to above 20% in BaO slag system resulted in poor P removal. From the dephosphorization of HCFeMn studies done by Lui, et al (Liu, et al., 1995), it was observed that increased amount of MnO in slag had a negative influence on the phosphate capacity of BaO-MnO-BaCl₂ slag. It was therefore concluded from the investigations that the MnO content above a certain value is disadvantageous to capability of the slag to dephosphorise FeMn alloys. In the current study, the high MnO slag contents may have negatively affected the P capacity of the slags.

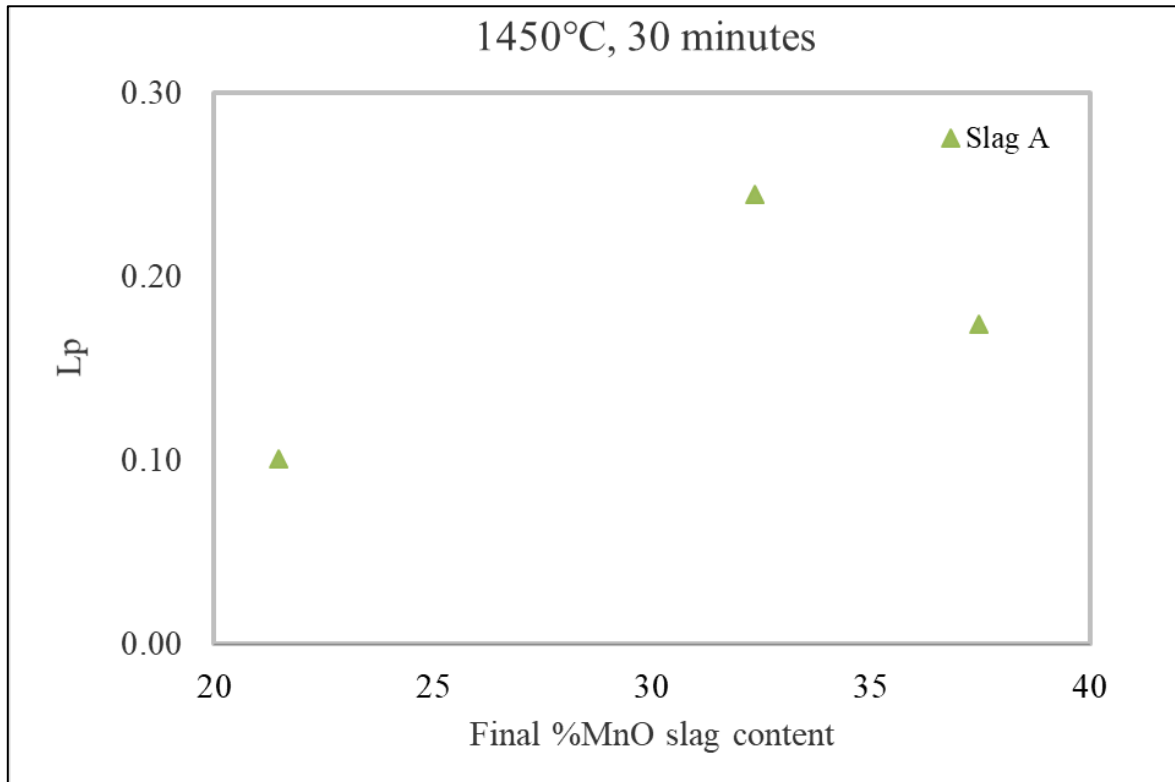


Figure 24: L_p versus the final MnO in slags at 1450°C and 30 minutes retention time for MCFeMn alloy.

5.1.2 Effect of adding Na_2O and CaF_2

Na_2O is a more basic oxide than CaO so it was expected that dephosphorization would be improved by Na_2O additions. The results represented in Figure 21 and Figure 22 generally show that addition of Na_2O indicated by Slag E generally did not show any added benefit as low L_p values were still obtained. From literature, addition of the compound to CaO -based slags improved dephosphorization of liquid iron, however at high temperatures Na_2O can be reduced by either C or Mn and produce CO/MnO ; the instability of Na_2O can therefore have a negative effect on dephosphorization of FeMn alloys due to loss of Mn (Tabuchi & Sano, 1985). In the current study the loss of Mn from the alloy was observed even with the Na_2O free slags, so it is not possible to conclude on the effect of Na_2O on Mn loss. Fujita, et al (Fujita, et al., 1988) also observed that low dephosphorization rates were achieved when using Na_2CO_3 flux on FeMn alloy.

The fluoride ion (F^-) from CaF_2/BaF_2 is reported to stabilize the phosphate ion (PO_4^{3-}) during the ionic dephosphorization reaction in molten slag under oxidizing conditions and thus contribute positively to dephosphorization (Liu, et al., 1998). However, Ca^{2+} binds fluoride ions much more strongly than Ba^{2+} does, because of the difference in the ionic radius of the two cations. Therefore, less free fluoride ions would be available when using CaF_2 to enhance dephosphorization (Liu, et al., 1998). Liu, et al observed that addition of CaF_2 to MnO-BaO- BaF_2 slag reduced L_p and increased the Mn capacity of the slag, i.e. Mn losses to the slag. In the current study the addition of CaF_2 (Slag F) showed no improvement in terms of L_p .

5.1.3 Effect of adding BaO

The use of BaO in conjunction with CaO (Slag H), also showed no improvement. Similar L_p values to those of Slag A were obtained under a few conditions, namely 1350°C and 1450°C at 30 minutes. Slag A was however not outperformed by slag H under any of the other conditions. Nasaralla, et al (Nasaralla, et al., 1991), investigated the use of BaO as an additive in CaO-based flux to dephosphorise Fe-C-P alloy. It was observed that small amount of BaO < 40% showed no effect on phosphate capacity of the slag. A larger increase in the phosphate capacity was only observed after increasing the BaO to above 40% in the CaO- CaF_2 slag. The researchers also later observed L_p significantly increased, by a factor of 4.6, when a high BaO content of 30% was used in CaO- Al_2O_3 - CaF_2 slag system (Nassaralla & Fruehan, 1992). During the current study, a BaO content of 20% was used. The lower L_p values obtained could be attributed to the low concentration of the basic oxide and also the uncertainties in the analysis of P as well as the dilution of the slag by MnO.

5.1.4 Effect of changing basicity

Increasing the slag basicity ($\%CaO/\%SiO_2$) to 1.3 caused an increase in the slag liquidus temperature to about 1500°C. This caused difficulties in melting the slag and resulted in poor slag separation during the experiment at 1450°C, when alloy was entrained the slag. This had a detrimental effect on the efficiency of the slag to remove P as the reaction occurs in a liquid phase, a lower L_p was obtained from increasing the basicity to 1.3 as shown on Table 22. At the lower $\%CaO/\%SiO_2$ ratio of 0.7, the analytical results reported an undetectable P concentration <0.005% in the slag. L_p at this point could therefore not be calculated. The

results therefore show an initial increase in L_p value from basicity of 0.7 to 0.9, thereafter a slight reduction in the L_p was obtained.

Table 22: Effect of %CaO/%SiO₂ ratio on L_p at 1450°C and 30 minutes retention time for MCFeMn alloy.

%CaO/%SiO ₂	L_p
0.7	-
0.9	0.258
1.3	0.130

∴ P slag analysis <0.005%

5.1.5 Effect of changing temperature

The results obtained from the current experiments show that at higher temperatures, generally lower L_p values were obtained. Slag H however gave slightly higher values at 1450°C. This anomaly may be attributed to the analytical errors at either 1400°C or 1450°C. Lui, et al (Liu, et al., 1995) observed lower L_p was obtained as temperature was increased during dephosphorization of FeMn alloy with BaO-containing slags.

5.1.6 Effect of changing initial alloy composition

Figure 25 and Figure 26 show the L_p values obtained with industry HCFeMn at 1350°C and 1400°C respectively. An observation made from the results is that dephosphorization of HCFeMn by the respective slags was also not significant as lower L_p values of <1 were generally obtained.

Comparison between the results show that at 1350°C, relatively higher L_p values were obtained from MCFeMn and at 1400°C, the opposite was observed. The studies on the effect of initial C, Mn and Si on dephosphorization have shown that high Mn in alloy decreases the activity coefficient of P and L_p increases with increasing initial C contents until the C saturation point.

High initial Si > 0.2% is not favourable for dephosphorization as the element gets oxidised during the dephosphorization leading to increased SiO₂ in slag which consumes the high basic

oxides and ultimately reduces the capacity of the slag to remove P (Chaudary, et al., 2008; Bhardwaj, 2008). During the current study the molten MCFeMn absorbed C from the crucible to become HCFeMn and the final average compositions of the alloys appeared to be similar after the dephosphorization process. The initial Si in both alloys were somewhat similar at about 0.4% which is reported to be undesirable for dephosphorization of FeMn alloys.

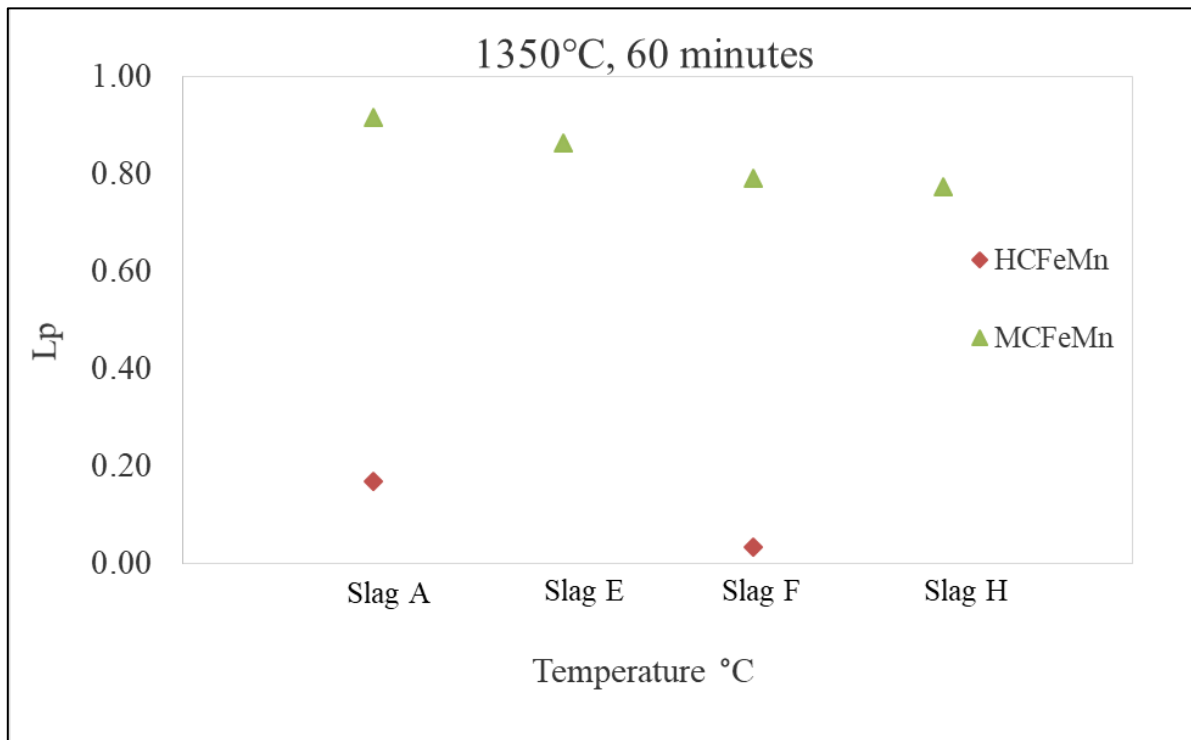


Figure 25: Comparison of phosphorus distribution between MCFeMn and industry HCFeMn and slag, found at 1350°C for 60 minutes reaction time

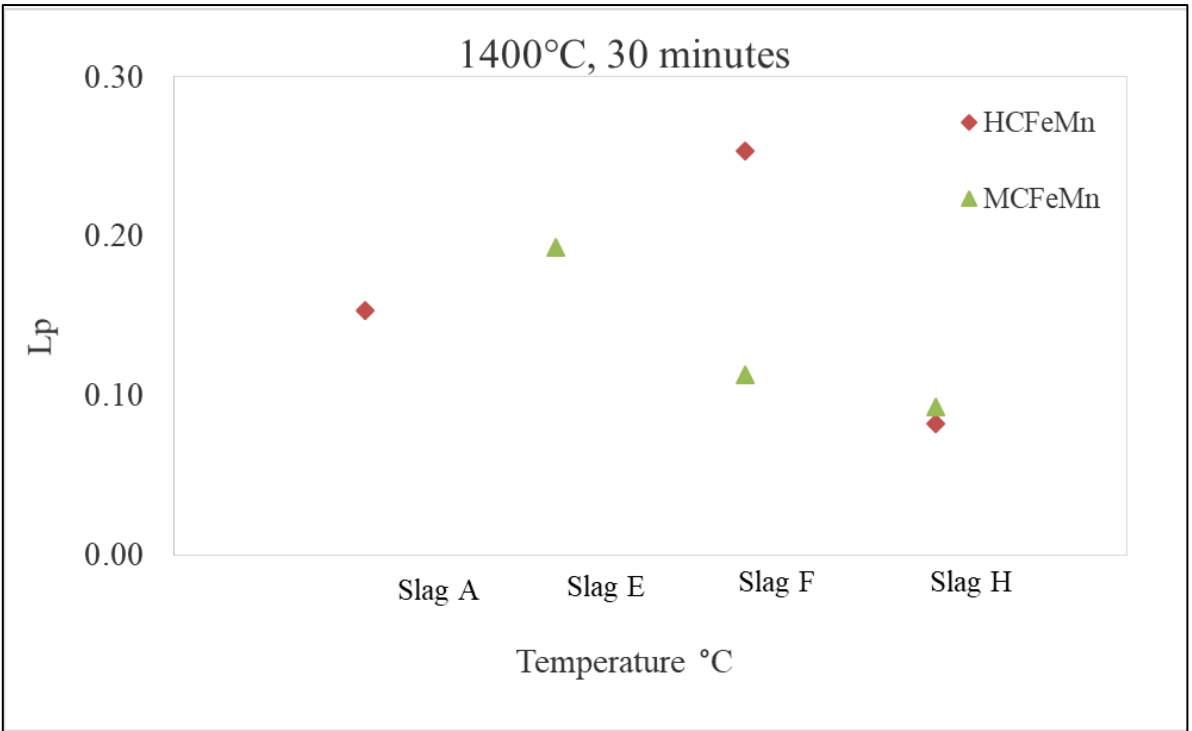


Figure 26: Comparison of phosphorus distribution between MCFeMn and industry HCFeMn and slag, for reaction at 1400°C for 30 minutes.

6 CONCLUSIONS AND RECOMMENDATIONS

The aim of this study was to investigate the suitability of different CaO-based slags systems to dephosphorise MCFeMn alloy by pyrometallurgical means. The tests were conducted at temperatures of 1350°C, 1400°C and 1450°C in a 25 kVA induction furnace at different retention times of 5 minutes, 30 minutes and 60 minutes. The use of HCFeMn alloy was also investigated at few test conditions. However, it is recognized that the alloy picked up carbon from the crucible during the experiments, eliminating the difference between medium-carbon and high-carbon ferromanganese. The end products were characterized to evaluate the P distribution ratio and degree of dephosphorization. The analyses of the low P contents in the slags and alloys proved to be a challenge and at the low concentrations the uncertainties were large.

The following conclusions were made from the experimental data:

6.1 Analytical results

The analytical results of the slags generally showed higher MnO contents than was anticipated when compared to the starting slags. This resulted in dilution of the other major slag components, i.e. SiO₂ and CaO. Generally, low P₂O₅ contents were reported in the slags, this was undesirable and suggested that the removal of P from the alloys was minimal. The alloy results showed C pickup after the tests resulting from dissolution of the graphite from the crucible. The choice of graphite crucible for the experiments was therefore not ideal.

The loss of Mn to the slag was also observed, this resulted in increased Fe alloy contents. The P alloy contents were generally higher than in the feed alloy which was attributed to factors such as the loss of Mn in the alloy which lead to increased P concentration and removal of P from the slag to the alloy as the starting slags contained P.

6.2 P distribution ratio.

1. The results generally showed that the L_p remained small (<1): a significant proportion of P remained in the alloy and thus dephosphorization was not favoured.
2. The CaO-SiO₂-MnO (Slag A) slag system reported relatively higher values of L_p . Addition of Na₂O (Slag E) generally did not show any added benefit. Substituting half of CaO by

BaO, Slag H, resulted similar L_p values to those of Slag A were obtained under a few conditions, namely 1350°C and 1450°C at 30 minutes. Slag A was however not outperformed by slag H under any of the other conditions.

3. Increasing the temperature generally resulted in lower L_p values. This may be attributed to the exothermic nature of the reaction which should be favourable at lower temperatures.
4. Increasing the %CaO/%SiO₂ ratio of the starting slag gave an initial increase in L_p value from basicity of 0.7 to 0.9, thereafter a slight reduction in the partition ratio was obtained. The latter results were not expected as higher basicity is anticipated to improve the P capacity of the slag. Increasing the basicity resulted in increased slag liquidus temperature which apparently negatively affected dephosphorization.
5. In summary, based on the L_p obtained, the conditions investigated are unfavourable for the slags to remove P from the alloy, as significant amounts of the element remained in the alloy.

6.3 Degree of dephosphorization

Based on the analytical results and the low P accountabilities achieved, the degree of dephosphorization suffered a lot of uncertainties. Based on the aforementioned challenges, no plausible conclusion could be made on the degree of dephosphorization achieved for the investigated industry alloys. The BaO-BaF₂-MnO slag however showed potential to dephosphorise HCFeMn master alloy, however the slag posed numerous challenges and the slag should be investigated further.

In summary, based on the L_p obtained, the conditions investigated are unfavourable for the slags to remove P from the MCFeMn and HCFeMn industry alloys under the specified test conditions, as significant amounts of the element remained in the alloy. The experimental results are in line with FactSage predictions that the CaO-slugs are not suitable for dephosphorization of FeMn alloys.

Due to the unsuccessful demonstration to remove P from the ferromanganese alloys by the CaO-based slag systems, the following recommendations can be made:

1. Investigate further the use of BaO-based slags with no CaO addition. A techno-economical study may be required to study the cost implications at an industrial scale.

2. Conduct the dephosphorization testwork with highly pure slag reagents that do not introduce P as an impurity in the master slags. The analytical grade reagents used during the current study appeared to not be free of impurities. For instance the MnO_2 which was used as a source of MnO introduced significant amount of P to the master slag, sourcing of pure MnO which is not readily available should be considered.
3. Investigate various other slags with which higher basicity can be achieved at relatively lower temperatures.

REFERENCES

- Arcelomittal, 2017. *Automotive Arcelomittal*. [Online]
Available at: https://automotive.arcelomittal.com/products/flat/first_gen_AHSS/TRIP
[Accessed 11 February 2020].
- Assis, A. N., 2014. *The Phosphorus Reaction in Oxygen Steelmaking*, Pennsylvania: PhD Thesis Carnegie Mellon University.
- Assis, A. N., Tayeb, M. A., Sridhar, S. & Freuhan, R. J., 2015. Phosphorus Equilibrium Between Liquid Iron and CaO-SiO₂-MgO-Al₂O₃-FeO-P₂O slag Part 1. *Metallurgical and Materials Transaction B*, Volume 46B, pp. 2255-2263.
- Bale, C. et al., 2016. FactSage Thermochemical software and database. In: s.l.:s.n., pp. 35-53.
- Baluch, N., Udin, Z. M. & Abdullah, C. S., 2014. Advanced High Strength Steel in Auto Industry: an Overview. *Engineering Technology and applied Science Research*, 4(4), pp. 686-689.
- Bell, T., 2019. *Steel grades and properties*. [Online]
Available at: <https://www.thoughtco.com/steel-grades-2340174>
[Accessed 08 February 2020].
- Bell, T., 2020. *The balance*. [Online]
Available at: <https://www.thoughtco.com/metal-profile-steel-2340175>
[Accessed 06 February 2020].
- Bhadeshia, H. D. & Suh, D. W., 2015. Is low phosphorus content in steel a product requirement?. *Ironmaking & Steelmaking*, 42(4), pp. 259-267.
- Bhardwaj, B. P., 2008. Production of ferroalloys. In: A. P. B. P. Inc, ed. *The Complete Book on Ferroalloys*. Delhi India: NCPS, pp. 300-309.
- Chaudary, P. N. & Goel, R. P., 2007. Dephosphorization of liquid Ferromanganese. *National Metallurgical Laboratory*, pp. 1-11.
- Chaudary, P. N., Goel, R. P. & Minz, R. K., 2008. *An Improved Process for dephosphorization of High Carbon FerroManganese*. RAFI MARG, NEW DELHI-110001, INDIA, Patent No. 217812.
- Chaudhary, P. N., Minj, R. K. & Goel, R. P., 2007. Development of a process for dephosphorisation of high carbon ferromanganese. In. *11th International Ferroalloys Congress, New Delhi*, pp. 288-295.
- Chaudhary, P. N. & Roy, G. G., 2001. Dephosphorization of HCFeMn using BaCO₃ based fluxes. *Ironmaking & steelmaking*, 29(5), pp. 396-403.

- Clegg, G., 2013. *Chemistry in its element-potassium permanganate..* [Online]
Available at: <http://www.rsc.org/chemistryworld/podcast/CIICompounds/transcripts/po>
[Accessed 24 January 2020].
- Corathers, L. A., 2017. *Mineral commodity summaries 2017*, U.S.: Geological Survey.
- Dashevski, V. Y. et al., 1998. *Desphosphorization of Manganese Ferroalloys with CaO and MnO Based Slag-Forming Mixtures*. Beijin China, INFACON VIII.
- Demeri, M. Y., 2013. Advanced High Strength Steels. In: *Science, Technology and Application*. U.S.A: ASM International.
- Downing, J. H., 2013. *Manganese processing. Encyclopaedic Britannica Online Academic Edition*. [Online]
Available at: <http://www.britannica.com/EBchecked/topic/361933/manganese-processing>
[Accessed 27 April 2020].
- Eramet, 2013. *Eramet*. [Online]
Available at: https://www.eramet.com/sites/default/files/inline-files/eramet_high_carbon_ferromanganese_1.pdf
[Accessed 20 March 2020].
- Fujita, M., Katayama, H., Yamamoto, A. & Mutsuo, M., 1988. Dephosphorization of Fe-Mn-C Alloy with BaCO₃. *Tetsu-to-Hagane*, 74(5), pp. 816-822.
- Goel, R. P. & Srikanth, S., 1992. *A thermodynamic analysis of ferromanganese*, s.l.: paper published at the 46th ATM of IIM.
- Hara, T., Tsukihashi, F. & Sano, N., 1990. *J. Iron and Steel Institute Japan*, 76(3), pp. 46-53.
- ICCT, 2013. *ICCT*. [Online]
Available at: www.theicct.org/chart-library-passenger-vehicle-fuel-economy
[Accessed 02 February 2020].
- ICCT, 2017. *ICCT: Light-duty vehicle greenhouse gas and fuel economy standards..* [Online]
Available at: <https://www.globalfueleconomy.org/media/460866/icct-update-report-summary.pdf>
[Accessed 05 February 2020].
- International Manganese Institute, 2018. *IMnI 2018 Mn Public Report 2018*. [Online]
Available at: www.manganese.org
[Accessed 24 January 2020].
- Karbowiczek, M., Michaliszycz, A., Wcislo, Z. & Slezak, W., 2014. Dephosphorization of Ferromanganese. *Acta Metallurgica Slavaca*, pp. 138-144.

- Kawai, Y., Nakao, R. & Mori, K., 1984. Dephosphorization of Liquid Iron by CaF₂-based Fluxes. *Transactions ISIJ*, Volume 24, pp. 509-514.
- Kolbeinsen, L. & Safarian, J., 2013. *Purity Requirements for Mn-alloys for producing high manganese TRIP and TWIP steels*. Almaty, Kazakhstan, The thirteenth International Ferroalloys Congress, pp. 175-184.
- Kor, G. J., 1977. Effect of fluorspar and other fluxes on slag-metal equilibria involving phosphorus and sulfur. *Metallurgical Transaction B*, Volume 8B, pp. 107-113.
- Lee, B., Pak, J. & You, B., 1999. Manganese loss during the oxygen refining of high-carbon ferromanganese melts. *Metals and materials Vol 5*, 5(497-502), pp. 497-502.
- Lee, Y. E. & Kauser, R. H., 1988. *Dephosphorization Process for Manganese Alloys*. U.S, Patent No. 4752327.
- Liu, X., Wijk, O., Selin, R. & Edstrom, J. O., 1998. Effects of additives in BaO-BaF₂-MnO slags on phosphate and manganese capacities. *ISIJ International*, 38(1), pp. 36-45.
- Liu, X., Wijk, O., Selin, S. R. & Edstrom, J. O., 1995. Phosphorus equilibrium between BaO-BaF₂-MnO fluxes and ferro-manganese melts. *Steel Research*, 66(3), pp. 96-102.
- Lorincz, D. & Greemfelder, J., 2013. *Advanced High-Strength Steels Benefits and Applications*, s.l.: Steel Market Deelopment Institute.
- Manning, C. P. & Fruehan, R. J., 2013. The reta of the Phosphorus reaction between liquid iron and slag. *Metallurgical and Materials Transaction B*, 44(B), pp. 37-44.
- MESU, 2020. *Advanced High Strength Steels*, Johannesburg: Mintek Internal Report.
- Mills, K. C., Hayashi, M., Wang, L. & Watanabe, T., 2014. The Structure and Properties of Silica Slags. In: S. Seetharaman, ed. *Treatise on Process Metallurgy*. Sweden: ELSEVIER, pp. 149-286.
- Mills, K. C. & Keene, B. J., 1987. Physical Properties of BOS slags. *International Materials Reviews*, 32(1-2), p. 44.
- Monaghan, B. J., Coly, K. S. & Pomfret, R. J., 1998. The kinetics of Dephosphorization of carbon-saturated Iron Usig an Oxidizing slag. *Metallurgical and Materials Transactions*, 29B(1), pp. 111-118.
- Mukherjee, T. & Chatterjee, A., 1996. Production of low phosphorus steels from high phosphorus Indian hot metal: Experience at Tata Steel. *Bulletin of Material Science*, 19(6), pp. 893-903.
- Muraki, M., Fukushima, H. & Sano, N., 1966. Phosphorus Distribution between CaO-CaF₂-SiO₂ Melts and Carbon-saturated Iron. *Transactions ISIJ* , Volume 25, pp. 1025-1030.

Nassaralla, C., Fruehan, R. J. & Min, D. J., 1991. A thermodynamic study of dephosphorization using BaO-BaF₂, CaO-CaF₂ and BaO-CaO-CaF₂ systems. *Metallurgical Transactions*, Volume 22B, pp. 33-38.

Nassaralla, C. & Fruehan, R. J., 1992. Phosphate Capacity of CaO-Al₂O₃ Slags Containing CaF₂, BaO, Li₂O, or Na₂O. *Metallurgical Transaction B*, Volume 23B, p. 117.

National Planning commission, 2030. *Our future -make it work*, s.l.: The National Development Plan.

Oliveira, J. R. et al., 2015. *Influence of slag properties in the steel dephosphorization efficiency*. Cleveland, United States, AISTech Conference Proceedings.

Olsen, S. E. & Tangstad, M., 2004. *Silicomanganese Production-Process Understanding*. Cape Town, Tenth International Ferroalloys Congress.

Olsen, S. E., Tangstad, M. & Lindstad, T., 2007. Manganese ores. In: *Production of manganese ferroalloys*. Trondheim, Norway: Tapir Academic Press, pp. 19-26.

Pauling, L., 1960. *Nature of chemical Bond*. 3rd ed. New York: Cornell University .

Raabe, D., 2014. *Dierk Raabe*. [Online]
Available at: <http://www.dierk-raabe.com/dual-phase-steels/>
[Accessed 11 February 2020].

Sano, N. & Katayama, H., 1992. Dephosphorization of stainless steel. *1st International Chromium Steel and Alloys Congress*, Volume 2, pp. 25-33.

Satyendra, 2013. *ispatguru*. [Online]
Available at: <https://www.ispatguru.com/chemistry-of-steelmaking-by-basic-oxygen-furnace/#>
[Accessed 09 February 2020].

SEAISI, 2019. *The making of iron and steel*, Malaysia: South East Asia Iron and Steel Institute.

Shim, S. C., Tsukihashi, F. & Sano, N., 1993. Thermodynamic Properties of the BaO-MnO Flux Systems. *Metallurgical Transactions* , 24(B), pp. 333-337.

Simeonov, S. R. & Sano, N., 1985. Phosphorus Equilibrium Distribution between Slags Containing MnO, CaF₂ and Na₂O and Carbon Saturated Iron Metal Treatment. *Transactions ISIJ*, Volume 25, pp. 1030-1038.

Steenkamp, J. D. & Bam, W. G., 2016. *Working towards an increase in manganese ferroalloy production on South Africa*, Johannesburg: Mintek Internal Report.

Steenkamp, J. D., Bam, W., Ringdalen, E. & Mushwana, M., June 2018. Working towards an increase in manganese ferroalloy production in South Africa-A researchn agenda. *Journal of the Southern African Institute of Mining and Metallurgy*, Volume 118, pp. 645-654.

Steenkamp, J. D. & Basson, J., 2013. The manganese ferroalloys industry in southern Africa. *The Journal of The Southern African Institute of Mining and Metallurgy*, Volume 113, pp. 667-676.

Steenkamp, J. D. & du Preez, L., 2015. Introduction to the production of clean steel. *The Journal of The Southern African Institute of Mining and Metallurgy*, Volume 115, pp. 557-561.

Steenkamp, J. D., Pistorius, P. C. & Tangstad, M., 2015. Chemical wear analysis of a tap-hole on a SiMn production furnace. *The Journal of The Southern African Institute of Mining and Metallurgy*, Volume 115, pp. 199-208.

Steenkamp, J., Maphutha, P. & Mushwana, M., 2019. *Sampling of alloy and slag at SiMn, FeSi, HCFeMn and HCFeMn*, Johannesburg: Mintek Internal Report.

Subramanian, M. & Harman, C. N., 1983. *Problems and prospects of carbonaceous reducing agents in ferroalloys production*. Jamshedpur, Seminar on Problems and Prospects of Ferro-Alloy Industry in India, pp. 133-140.

Suresh, G. & Tyagi, I., 2019. *Automotive AHSS Market Research Report - Global Forecast 2023*, Maharashtra, India: Market Research Future.

Tabuchi, S. & Sano, N., 1985. Thermodynamics of phosphate and phosphide in CaO-CaF₂ melts. *Metallurgical Transactions*, 15(B), pp. 351-356.

Tang, K. & Olsen, S. E., 2006. Computer simulation of equilibrium relations in manganese ferroalloy production. *Metallurgica; ad Materials Transactions B*, Volume 37, pp. 599-606.

Tangstad, M., 2013. Manganese Ferroalloys Technology. In: M. Gasik, ed. *Handbook of Ferroalloys-Theory and Technology*. USA: Elsevier, pp. 221-266.

Total Materia, 2007. *Effect of Phosphorus on the Properties of Carbon Steels: Part One*. [Online]

Available at: <https://www.totalmateria.com/page.aspx?ID=CheckArticle&site=kts&NM=211> [Accessed 23 January 2020].

Total Materia, 2017. *Low Phosphorus Partition Ratio Models*. [Online]

Available at: <http://blog.totalmateria.com/low-phosphorus-partition-ratio-models/> [Accessed 06 January 2020].

USGS, 2020. *USGS*. [Online]

Available at: <https://pubs.usgs.gov/periodicals/mcs2020/mcs2020-manganese.pdf> [Accessed 26 March 2020].

USS, 2015. *United States Steel Corporation*. [Online]

Available at:

<https://www.ussteel.com/uss/portal/home/markets/automotive/advanced%20high-strength/> [Accessed 24 October 2016].

Van Niekerk, W. H. & Dippenaar, R. J., 1998. Phosphorus Distribution Between Carbon-Saturated Iron at 1350°C and Lime-Based Slags Containing Na₂O and CaF₂. *Metallurgical and Materials Transactions*, Volume 29B, pp. 147-153.

Verma, P., 2016. *Slideshare*. [Online]

Available at: <https://www.slideshare.net/poojaverma121/introduction-to-steel-making-processes>

[Accessed 06 February 2020].

Visser, M., Smith, H., Ringdalen, E. & Tangstad, M., 2013. *Properties of Nchwaning and Gloria ores in the production of Mn Ferro-alloys*. Almaty, Kazakhstan, INFACON XIII.

Wagner, C., 1975. The Concept of the Basicity of Slags. *METALLURGICAL TRANSACTIONS B*, Volume 6B, pp. 405-409.

Watanabe, Y. et al., 1993. Thermodynamics of Phosphorus and Sulfur in the BaO-MnO Flux System between 1573 and 1673 K. *Metallurgical Transactions*, Volume 24B, pp. 339-347.

Wente, E. F., Nutting, J. & Wondris, E. F., 2019. *Steel Metallurgy*. [Online]

Available at: <https://www.britannica.com/technology/steel/World-steel-production>

[Accessed 09 February 2020].

Wetlaufer, M. & Kaspar, R., 2000. Effect of phosphorus on the ductility of high strength spring steels. *Steel Research*, 71(0), pp. 357-367.

WorldSteel, 2013. *Worldsteel*. [Online]

Available at: <https://www.worldsteel.org/publications/bookshop/filter-by-year/2013.html>

[Accessed 13 February 2020].

Yuanchi, D., Shangxing, G. & Erbao, C., 1998. *Control of Oxygen Potential and Its Effect on Dephosphorization in Ferromanganese*. Beijing China, INFACON 8.

APPENDIX A

Evaluating the SlagA model versus Slag? model in FactSage (steelmaking conditions). The conclusion is that SlagA gives more reasonable results.

Test of P distribution coefficient: 100 kg slag per tonne Fe. 0.01% P and 0.08% O in Fe to start				
Slag components:				
Species	FeO	MgO	CaO	SiO ₂
Mass (g)	25	8	A	67-A
Slag-A				
1600°C				
Alpha	g-P_FSstel-Liqu#1	g-P_FToxid-SLAGA#1	L _P	
3.50E+01	8.24E-01	1.76E-01	23	
4.00E+01	3.15E-01	6.85E-01	238	
4.00E+01	3.13E-01	6.87E-01	239	
4.22E+01	1.50E-01	8.50E-01	651	
4.30E+01	1.33E-01	8.67E-01	868	
4.50E+01	5.35E-02	3.75E-01	1283	
Slag?				
1600°C				
Alpha	g-P_FSstel-Liqu#1	g-P_FToxid-SLAG?#1	L _P	
3.50E+01	1.01E-04	1.00E+00	1028554	
4.00E+01	2.83E-05	1.00E+00	3792150	
4.05E+01	2.66E-05	1.00E+00	4029127	
4.18E+01	1.88E-05	1.00E+00	5886416	
4.50E+01	2.96E-06	1.00E+00	46373396	

Experimental difficulties

- Equilibration tests

The equilibrium tests were conducted with the aim of investigating the equilibrium phosphorus distribution ratio between the respective slags and the HCFeMn master alloy. The tests were conducted in a drop quench furnace; Figure shows the schematic diagram of the experimental setup. Graphite crucibles were used to contain the feed charge comprising of slag and alloy. A slag to alloy ratio of 0.1 was initially used for the testwork however the ratio was later increased to 1.0 to produce sufficient slag for post analysis. About 10 g of slag was mixed with 10 g of alloy and packed into the graphite crucible, the crucible was then hooked onto molybdenum wire as the support medium. The crucible charge was then inserted into the hot zone of the preheated furnace which already at the operational temperature. The tests were conducted for 20 hrs under inert atmosphere using Argon gas. A bubbler was connected to the furnace off gas pipe to ensure that the gas was gas tight.

Upon completion of the test the crucible was released and quenched into water and allowed to cool. The quenched sample was then retrieved from the crucible and prepared for analysis. A number of challenges were encountered for the tests, the challenges included the MnO-BaO-BaF₂-slag system reacted with the graphite crucible damaging the furnace alumina tube and in certain instances molybdenum wire reacted with the gas/fumes produced from the crucible leading to self-quenching. Figure A2: shows the pictures of the worn-out crucible and damaged furnace tube. Based on the results from the few completed equilibration test, dephosphorization was not achieved.

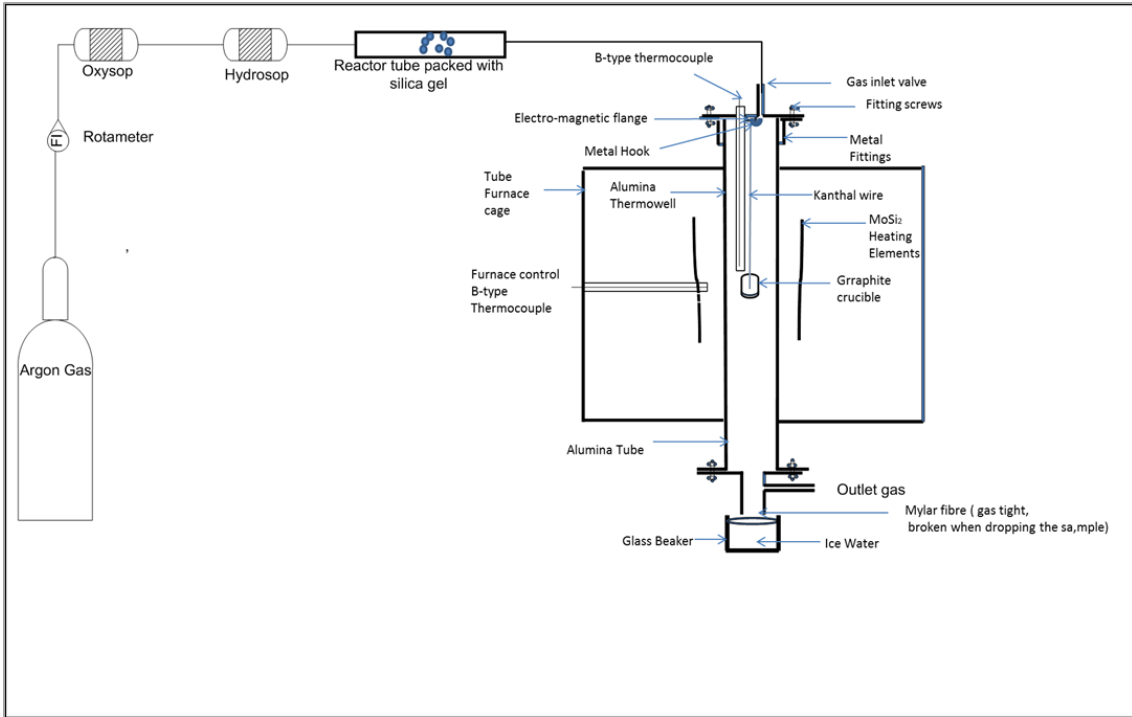


Figure A1: Schematic diagram of a drop quench furnace

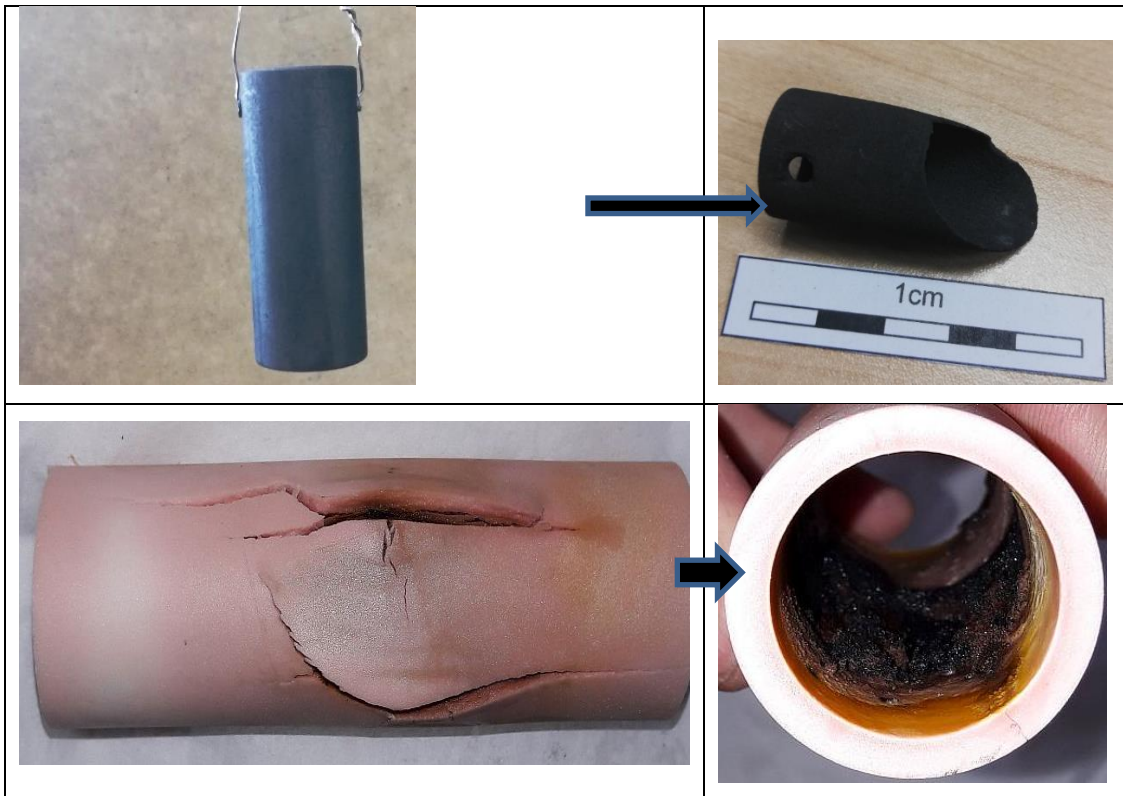


Figure A2: Pictures of the eroded graphite crucible and furnace alumina tube damaged during the equilibration tests

Table A1: L_p values obtained from the equilibration tests

Temperature and time	Alloy	Slag	Alloy					Slag P ₂ O ₅	L_p
			Fe	Mn	Si	C	P		
1400°C 20 hrs	HCFeMn Master alloy	A	17.37	71.83	0.45	7.46	0.10	0.023	0.10
		B	16.87	72.97	1.01	7.61	0.16	0.046	0.11
		C	18.30	69.63	1.48	7.75	0.15	0.092	0.26
		E	22.17	69.27	0.52	6.71	0.10	0.036	0.16
		F	19.60	68.50	0.40	8.48	0.10	0.044	0.19

- Induction furnace sampling tests results.

Table A2: The degree of dephosphorization achieved with HCFeMn master allo

Test	Slag systems	Alloy type	Temperature	Successful sampling times	%P final	%P initial	Degree of dephosphorization
1	20% MnO-40% CaO-40% SiO ₂)	HCFeMn	1400°C			0.082	
				10 min	0.213		0.00
2	20% MnO-20% CaO-40% SiO ₂ -20% Na ₂ O)	HCFeMn	1400°C			0.082	
				5 min	0.130		0.00
				30 min	0.110		0.00
3	(20% MnO-20% CaO-40% SiO ₂ -20% Na ₂ O)	MCFeMn	1400°C			0.067	
				1 hr	0.130		0.00
				4 hr	0.220		0.00
4	(20% MnO-20% CaO-40% SiO ₂ -12.5% Na ₂ O-0.7% CaF ₂)	HCFeMn	1400°C			0.082	
				5 min	0.130		0.00
				30 min	0.166		0.00
				1 hr	0.077		6.07
5	(20% MnO-60% BaO-20% BaF ₂)	HCFeMn	1400°C	5 min	0.063	0.082	26.8
				60 min	0.060		23.2

APPENDIX B

Typical appearance of test product

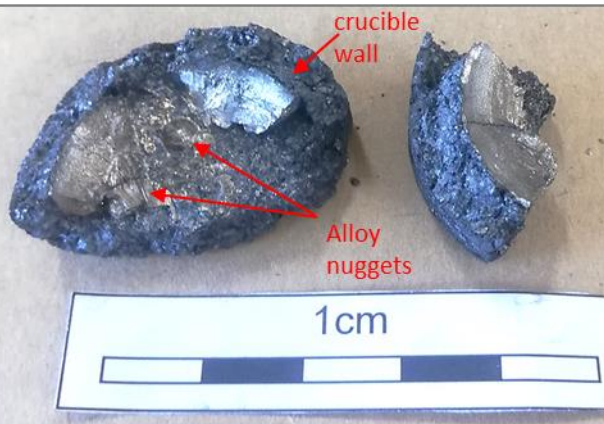
 <p>A photograph of a dark, cylindrical graphite crucible mounted on a metal stand. A small amount of yellowish, crystalline material is visible at the top opening. A red arrow points to this material with the label "Slag". Below the crucible, red text reads "Outside Diameter = 35 mm".</p>	<p>Graphite crucible showing the slag H coating the wall at the top section of the crucible.</p>
 <p>Two cross-sectional views of a crucible containing slag and alloy. The left view shows a dark, porous material labeled "Slag1" above a lighter, more crystalline material labeled "Alloy". The right view shows a similar structure with "Slag2" above "Alloy". A vertical ruler is visible on the right side of the images for scale.</p>	<p>Cross-sectioned slag H (1450°C 30 min) crucible contents.</p>
 <p>A photograph of a broken piece of a dark, porous crucible wall. The interior surface shows several bright, metallic alloy globules. Red arrows point to these globules with the label "Alloy nuggets". Another red arrow points to the dark, porous material with the label "crucible wall". A white ruler with a black scale bar is shown below the crucible, labeled "1cm".</p>	<p>Broken crucible showing the alloy globules distributed at the base of the crucible. Slag A. 1450°C 60 min test.</p>

Figure B1: Typical appearance of test product

Masses of the starting slags and alloys

Table B1: Initial slag and alloy masses

Test	Slag	Before	
		Alloy, g	Slag, g
1350°C,30 min	Slag A	10.00	10.66
	Slag E	10.00	11.72
	Slag F	10.00	11.29
	Slag H	10.00	10.58
1350°C, 1 hr	Slag A	10.00	10.27
	Slag E	10.00	11.66
	Slag F	10.00	11.56
	Slag H	10.00	11.29
1400°C5 min	Slag A	10.00	10.27
	Slag E	10.00	11.27
	Slag F	10.00	11.50
	Slag H	10.00	11.29
1400°C, 30 min	Slag A	10.00	10.01
	Slag E	10.00	11.54
	Slag F	10.00	11.57
	Slag H	10.00	11.66
1400°C60 min	Slag A	10.00	10.66
	Slag E	10.00	11.97
	Slag F	10.00	11.29
	Slag H	10.00	11.30
1450°C 5 min	Slag A	10.00	10.75
	Slag E	10.00	11.98
	Slag F	10.00	12.22
	Slag H	10.00	10.14
1450°C, 30 min	Slag A	10.00	10.90
	Slag E	10.00	12.05
	Slag F	10.00	12.04
	Slag H	10.00	11.36
1450°C, 60 min	Slag A	10.00	10.12
	Slag E	10.00	10.81
	Slag F	10.00	11.46
	Slag H	10.00	11.06
HCFeMn 1350°C, 1 hr	Slag A	10.00	10.47
	Slag E	10.00	12.17
	Slag F	10.00	11.38
	Slag H	10.00	11.35

Test	Slag	Before	
		Alloy, g	Slag, g
HCFeMn 1400°C, 30 min	Slag A	10.00	12.50
	Slag E	10.00	14.70
	Slag F	10.00	13.10
	Slag H	10.00	12.70
MCFMN B 1450°C 30 min	Slag B	10.00	10.83
MCFMN C 1450°C 30 min	Slag C	10.00	10.71
MCFMN A basicity 1.3 1450°C 30 min	Slag A	10.00	10.96
MCFMN slag A basicity 0.7 1450°C 30 min	Slag A	10.00	10.75

Bulk chemical compositions of the alloys and slags before corrections were done.

Table B2: Chemical compositions of alloys

		C	S	P	Al	Si	Ca	Mn	Fe	Mg	Total
1350°C,30 min	Alloy A	7.990	0.007	0.091	0.011	0.440	0.300	66.400	22.700	0.008	97.939
	Alloy E	4.000	0.015	0.059	0.161	7.130	2.730	58.000	22.100	0.063	94.195
	Alloy F	7.800	0.000	0.104	0.018	0.290	0.150	59.300	26.400	0.006	94.062
	Alloy H	7.050	0.007	0.108	0.017	0.610	0.200	66.400	23.000	0.010	97.392
1350°C, 1 hr	Alloy A	5.740	0.000	0.056	0.240	0.470	1.030	67.400	24.000		98.936
	Alloy E	6.800	0.000	0.062	0.020	0.567	2.800	64.000	23.162		97.411
	Alloy F	7.700	0.006	0.111	0.017	1.290	0.075	61.000	27.400		97.599
	Alloy H	6.690	0.008	0.091	0.001	2.570	0.130	63.200	27.000		99.690
1400°C5 min	Alloy A										
	Alloy E	6.986	0.007	0.130	0.269	0.531	0.168	63.596	26.300		97.986
	Alloy F	6.111	0.007	0.141	0.279	0.887	0.235	63.296	26.970		97.925
	Alloy H	6.281	0.006	0.131	0.248	0.327	0.188	66.363	25.500		99.043
1400°C, 30 min	Alloy A										
	Alloy E	6.730	0.007	0.078	0.010	0.430	0.340	62.900	27.900		98.395
	Alloy F	7.650	0.008	0.076	0.008	0.330	0.320	64.300	26.400		99.092
	Alloy H	7.490	0.000	0.072	0.000	0.550	0.180	64.960	26.430		99.682
1400°C60 min	Alloy A	7.890		0.103		0.480	0.160	66.600	25.700	0.008	99.933
	Alloy E	7.240		0.112	0.009	0.400	0.100	64.700	27.400	0.006	98.201
	Alloy F	7.300		0.140		0.560	0.150	65.700	23.500	0.006	97.350
	Alloy H	8.770		0.117		0.540	0.100	65.300	26.800	0.007	99.627
1450°C 5 min	Alloy A	6.890		0.096		0.190	0.060	65.900	23.400	≤ 0.005	96.536
	Alloy E										
	Alloy F	6.700		0.119	0.014	0.270	0.080	60.800	26.600	0.009	94.583
	Alloy H	6.500		0.097		0.390	0.080	64.700	24.000	0.006	95.767
1450°C, 30 min	Alloy A	6.860		0.053		0.300	0.680	70.200	21.600		99.693
	Alloy E	5.970		0.089	0.006	0.450	0.720	74.100	17.500		99.690
	Alloy F	6.900	0.000	0.078	0.007	0.230	0.210	63.800	27.500		98.725
	Alloy H	6.540	0.003	0.077	0.045	0.380	0.420	65.500	26.650		99.603

		C	S	P	Al	Si	Ca	Mn	Fe	Mg	Total
1450°C, 60 min	Alloy A	7.890	0.005	0.083	0.315	0.235	0.375	68.400	22.600		99.903
	Alloy E	6.910	0.006	0.093	0.011	0.600	0.520	66.700	22.900		97.740
	Alloy F	7.390	0.000	0.085	0.008	0.000	0.470	68.300	22.200		98.951
	Alloy H	7.580	0.004	0.096	0.055	0.470	0.620	64.450	26.400		99.675
HCFeMn 1350°C, 1 hr	Alloy A	6.990	0.006	0.075	0.009	0.290	0.190	68.500	21.700	0.007	97.760
	Alloy E	7.360	0.007	0.110		0.310	0.100	61.300	26.900	0.006	96.087
	Alloy F	7.170	0.007	0.086		0.370	0.160	65.200	23.300	0.009	96.293
	Alloy H	7.830	0.007	0.090		0.380	0.120	64.800	24.100	0.008	97.327
HCFeMn 1400°C, 30 min	Alloy A	7.390	0.008	0.061		0.690	0.230	65.100	22.100	0.014	95.579
	Alloy E	7.084		0.096		0.560	0.150	66.800	23.900	0.011	98.590
	Alloy F	7.510		0.091		0.500	0.130	65.600	23.000	0.011	96.831
	Alloy H	7.390		0.068		0.550	0.120	67.000	22.800	0.011	97.928
MCFMN B 1450°C 30min	Slag B	7.690		0.105		0.140	0.050	64.500	26.900	0.006	99.385
MCFMN C 1450°C 30min	Slag C	7.600		0.090		0.260	0.060	67.700	22.800	0.006	98.510
MCFMN A basicity 1.3 1450°C 30min	Slag A	6.990		0.085		0.270	0.100	67.250	22.550	0.007	97.245
MCFMN slagA basicity 0.7 1450°C 30min	Slag A	7.830	0.013	0.110	0.000	0.530	0.130	67.600	23.300	0.020	99.513

Table B3: Chemical compositions of slags

T.	Reaction time		Slag compositions (%)										Total	
			C	S	P ₂ O ₅	Al ₂ O ₃	SiO ₂	CaO	MnO	FeO	BaO	MgO		CaF ₂
MCFeMn 1350°C	30 min	Slag A	0.100	0.038	0.110	0.420	30.600	25.900	39.500	0.740		0.400		97.808
		Slag E	0.800	0.018	0.058	0.480	31.400	12.300	50.600	2.720		0.560		98.936
		Slag F	0.740	0.021	0.062	0.571	28.300	17.200	49.300	2.810		0.350	4.150	103.504
		Slag H	0.570	0.031	0.140	0.480	29.400	19.800	44.700	0.840	10.500	0.260		106.721
	60 min	Slag A	1.010	0.029	0.1100	0.240	30.600	25.900	39.500	0.740		0.400		98.529
		Slag E	2.850	0.008	0.126	0.480	31.900	21.600	36.200	4.875		0.540		98.579
		Slag F	2.140	0.000	0.247	0.610	36.200	21.900	31.600	4.810		1.150	3.800	102.531
		Slag H	1.060	0.018	0.164	0.590	32.800	15.800	39.600	3.480	8.500	0.570		102.582
MCFeMn 1400°C	5 min	Slag A												
		Slag E	0.170	0.032	0.000	0.450	28.600	13.400	50.900	1.150		0.310		95.012
		Slag F	0.810	0.031	0.028	0.460	28.200	15.800	50.900	3.700		0.350	3.130	101.160

		Slag compositions (%)														
T.	Reaction time		C	S	P ₂ O ₅	Al ₂ O ₃	SiO ₂	CaO	MnO	FeO	BaO	MgO	CaF ₂	Total		
MCFeMn 1450°C	30 min	Slag H	0.210	0.046	0.009	0.540	30.700	24.400	42.600	0.750	10.000	0.400		109.655		
		Slag A														
		Slag E	1.690	0.032	0.081	0.360	23.300	11.600	53.800	9.490			0.300		100.653	
		Slag F	0.570	0.035	0.027	0.450	28.000	16.600	42.400	1.940			0.320	4.10	91497	
	60 min	Slag H	0.460	0.048	0.015	0.470	30.300	14.700	39.000	0.100	10.000	0.350			95.443	
		Slag A	0.089	0.034	0.096	0.850	30.500	20.900	40.200	0.260			0.860		93.789	
		Slag E	3.900	0.020	0.086	0.730	25.900	10.000	50.600	6.680			0.480		98.396	
		Slag F	0.850	0.029	0.015	0.640	29.200	14.500	51.600	2.270			0.600	2.940	100.500	
	MCFeMn 1450°C	5 min	Slag H	0.100	0.021	0.011	0.400	31.100	11.900	44.800	0.190	12.950	0.530		102.002	
			Slag A	0.450	0.066	0.046	0.520	31.500	26.500	37.000	2.220		0.450		98.752	
			Slag E													
			Slag F	0.300	0.038	0.025	0.480	30.600	17.900	45.200	1.330			0.360	4.500	97.500
30 min		Slag H	0.890	0.031	0.016	0.480	31.500	14.900	37.900	0.210	12.200	0.620			98.747	
		Slag A	0.180	0.037	0.030	0.590	35.500	25.800	32.700	0.110		0.480			94.309	
		Slag E	0.560	0.042	0.018	0.430	26.600	12.100	51.400	2.750			0.280		94.180	
		Slag F	0.130	0.047	0.000	0.560	33.100	17.900	48.100	0.160			0.390	3.620	101.406	
60 min		Slag H	0.170	0.042	0.042	0.680	31.100	13.900	42.950	0.140	11.200	0.382			100.606	
		Slag A	0.250	0.069	0.049	0.695	29.700	26.050	38.800	1.315		0.460			97.423	
		Slag E	0.730	0.035	0.011	0.470	29.100	20.000	46.600	0.510			0.300		97.756	
		Slag F	0.390	0.034	0.017	0.470	29.200	16.400	49.900	2.210			0.390	2.770	99.791	
HCFeMn	1350°C, 1 hr	Slag H	0.725	0.034	0.061	0.565	26.700	12.100	53.200	5.900	10.500	0.480		110.264		
		Slag A	0.510	0.019	0.037	0.900	33.200	27.500	31.300	1.300		0.540		95.306		
		Slag E												0.000		
		Slag F	0.310	0.013	0.016	0.360	32.900	13.731	46.500	1.440			0.630	2.880	98.780	
	1400°C, 30 min	Slag H	2.340	0.019	0.039	0.517	24.800	10.600	50.600	9.403	9.200	0.480			107.998	
		Slag A	0.460	0.008	0.026	0.570	40.500	31.900	23.000	0.830		0.370			97.664	
		Slag E	0.470	0.011	0.000	0.480	33.000	14.700	45.000	0.840			0.420		94.921	
		Slag F	0.660	0.021	0.065	0.420	32.900	15.282	44.100	1.910			0.440	2.530	98.328	
	MCFeMn 1450°C	1450°C 30min	Slag H	1.780	0.021	0.015	0.460	32.200	14.500	47.800	0.370	10.800	0.530		108.476	
			Slag B	0.440	0.033	0.051	0.380	29.500	26.400	40.600	1.310		0.770		99.484	
			Slag C	0.390	0.022	0.023	0.290	25.900	23.000	22.400	0.310		0.410		72.745	
			Slag A	0.360	0.029	0.085	0.240	18.800	21.700	53.000	8.900*		0.400		103.514	
		Slag A	0.320	0.033	0.000	0.370	35.100	18.800	43.500	0.210		0.760		99.093		

*: high alloy entrainment

Effect of MnO content

Table B4: Corrected bulk chemical compositions of alloys obtained from varying the initial MnO slag contents

Initial %MnO	C	S	P	Al	Si	Ca	Mn	Fe	Mg	Total
12	7.60	0.00	0.09	0.00	0.22	0.00	67.64	22.80	0.01	98.35
17	6.85	0.00	0.05	0.00	0.00	0.00	69.28	21.60	0.00	97.78
22	7.69	0.00	0.10	0.00	0.10	0.00	64.42	26.90	0.00	99.23

Elemental accountability

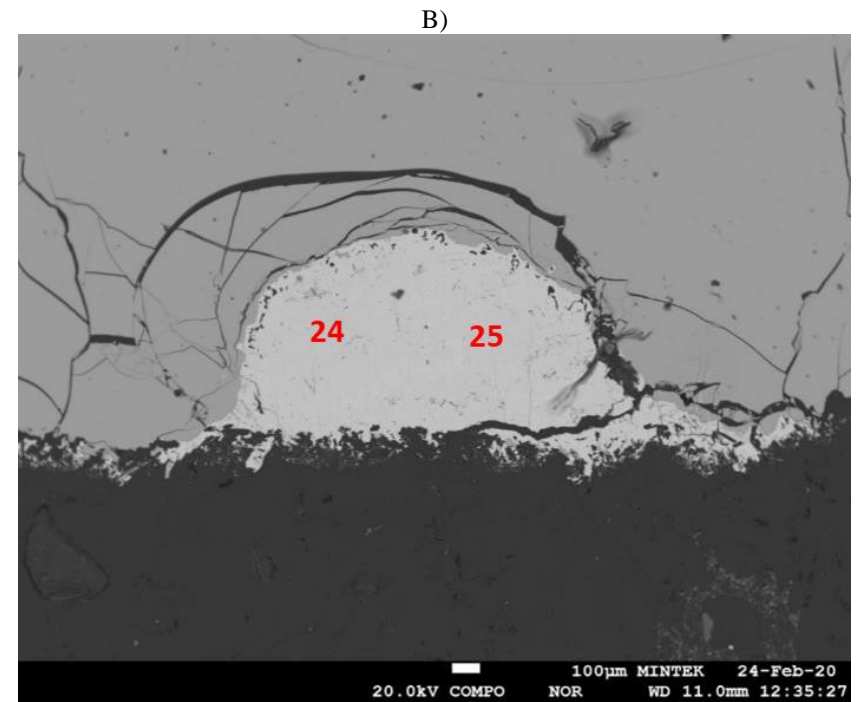
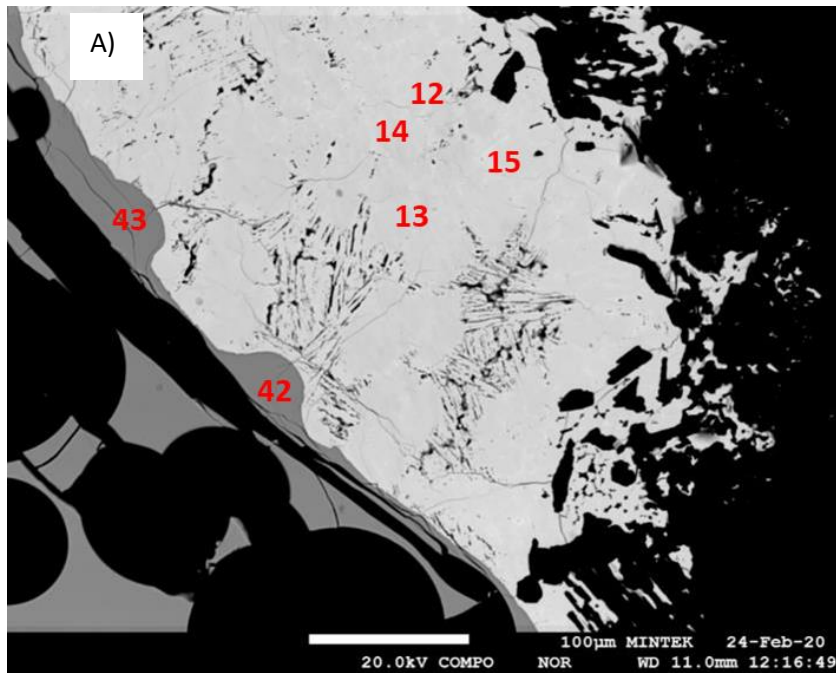
Table B5: Elemental accountabilities

		Accountability				
		P	Al	Si	Mn	Mg
1350°C,30 min	Alloy A	137.956	78.262	96.751	112.970	91.024
	Alloy E	82.710	220.733	125.220	110.081	193.949
	Alloy F	87.664	166.489	106.336	108.460	110.920
	Alloy H	166.418	96.055	68.588	102.329	56.519
1350°C, 1 hr	Alloy A	103.834	94.014	95.785	107.901	90.048
	Alloy E	90.684	107.352	66.286	79.047	106.499
	Alloy F	118.865	83.828	66.553	58.423	166.260
	Alloy H	173.090	162.212	114.750	94.340	170.711
	Alloy E	106.228	260.106	96.880	113.360	98.551
	Alloy F	86.241	205.535	122.025	118.294	125.526
	Alloy H	117.090	151.527	55.430	88.701	65.196
	Alloy E	83.854	150.243	90.134	97.782	110.171
	Alloy F	57.122	138.908	112.954	110.517	108.513
	Alloy H	71.399	131.110	101.893	108.079	106.355
1400°C60 min	Alloy A	145.028	192.191	119.669	119.342	240.446
	Alloy E	118.580	353.726	116.764	113.500	204.758
	Alloy F	71.497	214.343	128.903	115.415	221.353
	Alloy H	102.045	129.299	121.075	115.945	187.445
1450°C 5 min	Alloy A	97.223	92.730	97.006	102.294	99.010

	Alloy F	79.706	132.648	109.098	108.963	108.902
	Alloy H	101.583	126.708	100.104	104.351	179.320
1450°C, 30 min	Alloy A	64.711	108.067	111.691	114.925	108.476
	Alloy E	60.241	171.818	98.773	104.920	98.843
	Alloy F	46.025	139.106	107.614	110.807	106.500
	Alloy H	82.659	194.206	101.366	110.116	113.844
1450°C, 60 min	Alloy A	95.100	195.366	92.402	110.222	102.959
	Alloy E	62.589	114.114	65.539	73.513	63.899
	Alloy F	48.276	138.332	111.797	106.813	125.542
	Alloy H	101.227	204.603	111.787	117.476	183.852
HCFeMn 1350°C, 1 hr	Alloy A	83.068	326.499	99.004	101.767	113.865
	Alloy F	63.066	108.476	131.055	115.084	206.447
	Alloy H	79.919	258.996	148.677	120.323	257.610
HCFeMn 1400°C, 30 min	Alloy A	70.231	84.439	105.838	99.283	69.543
	Alloy E	73.643	157.718	102.651	112.961	121.586
	Alloy F	86.737	120.273	125.366	118.083	138.414
	Alloy H	83.873	112.240	95.823	123.541	141.008
MCFMN B 1450°C 30min	Slag B	116.669	161.377	103.579	94.346	92.297
MCFMN C 1450°C 30min	Slag C	102.569	164.850	107.376	104.475	69.399
MCFMN A basicity 1.3 1450°C 30min	Slag A	102.892	79.918	110.647	108.484	78.397
MCFMN slagA basicity 0.7 1450°C 30min	Slag A	92.735	93.005	153.070	139.212	239.364

APPENDIX C

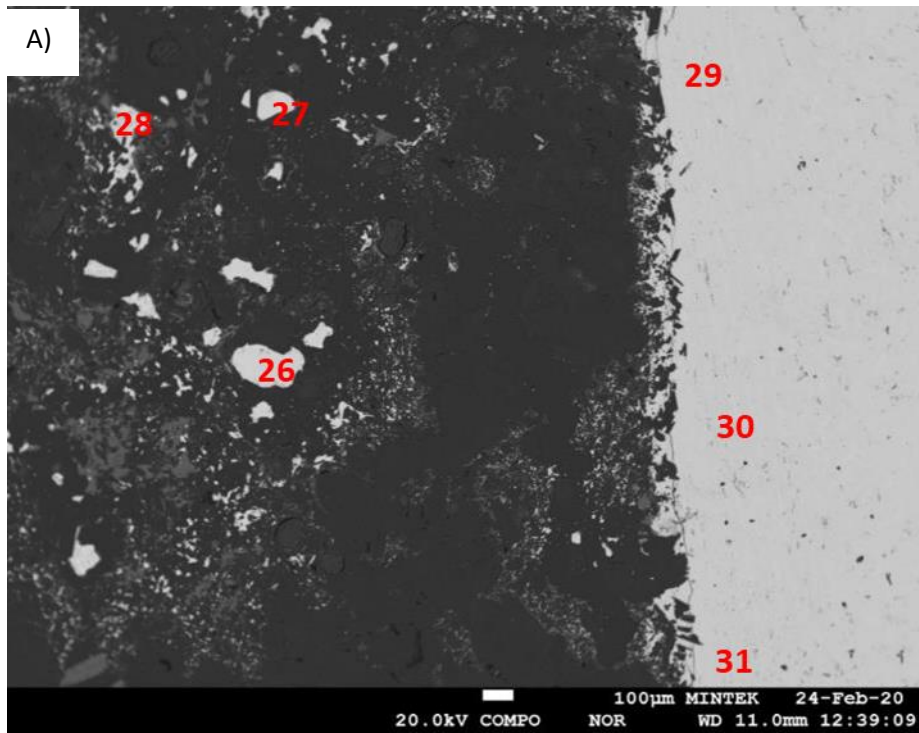
EMPA analysis of other sections of the crucible, Slag H 1400°C, 30 min.



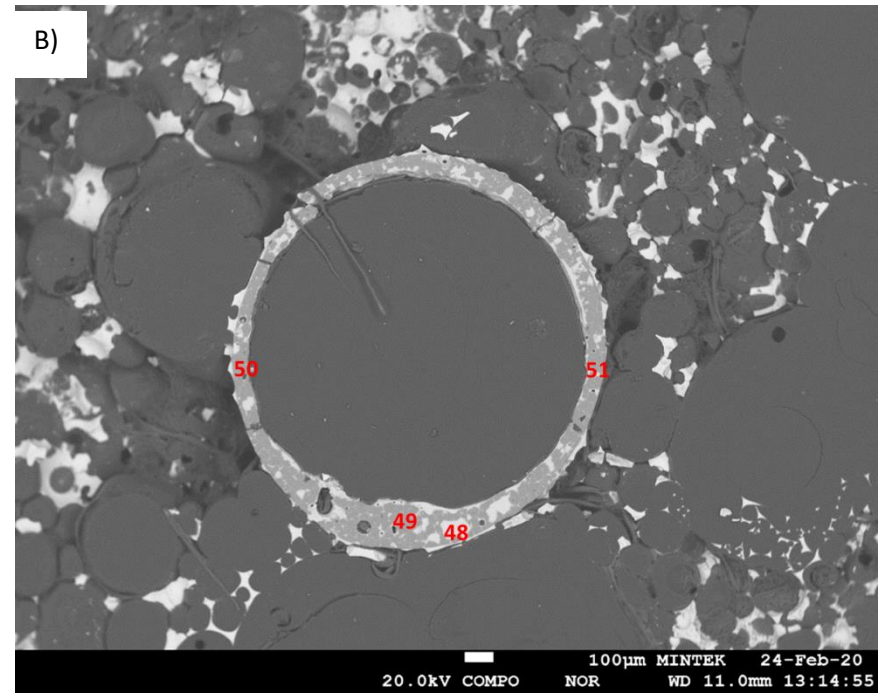
Point	SiO ₂	S	P ₂ O ₅	BaO	CaO	MnO	FeO	Total
42	37.48	0.14	-	10.33	13.00	39.35	0.04	100.29
43	37.38	0.03	-	10.62	13.29	39.06	0.02	100.44
Position	Si	Ca	C	P	Fe	Mn	Total	
12	0.13	-	8.39	-	18.31	71.65	98.49	
13	0.20	-	8.64	0.05	20.20	70.21	99.29	
14	0.76	-	7.77	0.19	22.53	68.84	100.10	
15	0.22	-	8.65	0.06	19.99	71.46	100.37	

Point	Si	C	P	Fe	Mn	Total
25	0.03	9.16	-	23.27	67.60	100.06

Figure C1: Electron Backscattered images and analysis of A) Metal and slag on right edge of crucible B) Bottom left of crucible section



Point	Si	Ca	C	P	Fe	Mn	Total
28	1.46	-	-	-	90.63	8.60	100.70
29	-	-	10.07	-	21.54	69.76	101.36
30	0.68	-	7.77	0.29	28.69	63.67	101.10
31	0.14	-	8.54	0.08	25.74	67.00	101.50



Point	SiO ₂	S	P ₂ O ₅	BaO	CaO	MnO	Total
48	35.97	0.03	-	11.10	13.33	39.13	99.61
49	36.57	0.03	-	11.09	13.33	39.14	100.21
50	36.06	0.07	0.01	11.05	13.42	39.45	100.06
51	36.67	0.08	-	11.08	13.31	39.46	100.60

Figure C2: Electron Backscattered images and analysis of A) Lower left edge of the crucible B) Low density slag - upper part of crucible.